

Precision studies of observables in $pp \rightarrow W \rightarrow l\nu_l$ and $pp \rightarrow \gamma, Z \rightarrow l^+l^-$ processes at the LHC

S. Alioli¹, A. B. Arbuzov^{2,3}, D. Yu. Bardin², L. Barzè^{4,6}, C. Bernaciak⁵, S. G. Bondarenko^{2,3}, C. M. Carloni Calame⁶, M. Chiesa⁶, S. Dittmaier⁷, G. Ferrera⁸, D. de Florian^{9,10}, M. Grazzini¹¹, S. Höche¹², A. Huss¹³, S. Jadach¹⁴, L. V. Kalinovskaya², A. Karlberg¹⁵, F. Krauss¹⁶, Y. Li¹⁷, H. Martinez^{4,6}, G. Montagna^{4,6}, A. Mück¹⁸, P. Nason¹⁹, O. Nicrosini⁶, F. Petriello^{20,21}, F. Piccinini⁶, W. Płaczek²², S. Prestel¹², E. Re²³, A. A. Saproinov², M. Schönherr¹¹, C. Schwinn¹⁸, A. Vicini^{8,a}, D. Wackerroth^{5,b}, Z. Was¹⁴, G. Zanderighi^{1,15}

- ¹ TH Division, Physics Department, CERN, 1211 Geneva 23, Switzerland
² Dzhelapov Laboratory for Nuclear Problems, JINR, Joliot-Curie 6, 141980 Dubna, Russia
³ Bogoliubov Laboratory of Theoretical Physics, JINR, Joliot-Curie 6, 141980 Dubna, Russia
⁴ Dipartimento di Fisica, Università di Pavia, Via A. Bassi 6, 27100 Pavia, Italy
⁵ Department of Physics, University at Buffalo, The State University of New York, Buffalo, NY 14260, USA
⁶ INFN, Sezione di Pavia, Via A. Bassi 6, 27100 Pavia, Italy
⁷ Physikalisches Institut, Albert-Ludwigs-Universität Freiburg, 79104 Freiburg, Germany
⁸ Tif Lab, Dipartimento di Fisica, Università di Milano and INFN, Sezione di Milano, Via Celoria 16, 20133 Milan, Italy
⁹ Departamento de Física and IFIBA, FCEyN, Universidad de Buenos Aires, Pabellon 1 Ciudad Universitaria, Capital Federal, 1428 Buenos Aires, Argentina
¹⁰ International Center for Advanced Studies (ICAS), UNSAM, Campus Miguelete, 25 de Mayo y Francia, 1650 Buenos Aires, Argentina
¹¹ Physik-Institut, Universität Zürich, 8057 Zürich, Switzerland
¹² SLAC National Accelerator Laboratory, Menlo Park, CA 94025, USA
¹³ Institute for Theoretical Physics, ETH, 8093 Zürich, Switzerland
¹⁴ Institute of Nuclear Physics, Polish Academy of Sciences, ul. Radzikowskiego 152, 31-342 Kraków, Poland
¹⁵ Rudolf Peierls Centre for Theoretical Physics, University of Oxford, 1 Keble Road, Oxford, UK
¹⁶ Physics Department, Institute for Particle Physics Phenomenology, Durham University, Durham DH1 3LE, UK
¹⁷ Fermilab, P.O. Box 500, Batavia, IL 60510, USA
¹⁸ Institute for Theoretical Particle Physics and Cosmology, RWTH Aachen University, 52056 Aachen, Germany
¹⁹ INFN, Sezione di Milano Bicocca, 20126 Milan, Italy
²⁰ Department of Physics and Astronomy, Northwestern University, Evanston, IL 60208, USA
²¹ High Energy Physics Division, Argonne National Laboratory, Argonne, IL 60439, USA
²² Marian Smoluchowski Institute of Physics, Jagiellonian University, ul. Łojasiewicza 11, 30-348 Kraków, Poland
²³ LAPTh, Université Savoie Mont Blanc, CNRS, B.P.110, Annecy-le-Vieux 74941, France

Received: 21 December 2016 / Accepted: 13 April 2017 / Published online: 3 May 2017
© The Author(s) 2017. This article is an open access publication

Abstract This report was prepared in the context of the LPPC *Electroweak Precision Measurements at the LHC WG* (<https://lppc.web.cern.ch/lppc/index.php?page=electroweak-wg>) and summarizes the activity of a subgroup dedicated to the systematic comparison of public Monte Carlo codes, which describe the Drell–Yan processes at hadron colliders, in particular at the CERN Large Hadron Collider (LHC). This work represents an important step towards the definition of an accurate simulation framework necessary for very high-precision measurements of electroweak (EW) observables such as the W boson mass and the weak mixing angle. All the codes considered in this report share at least next-

to-leading-order (NLO) accuracy in the prediction of the total cross sections in an expansion either in the strong or in the EW coupling constant. The NLO fixed-order predictions have been scrutinized at the technical level, using exactly the same inputs, setup and perturbative accuracy, in order to quantify the level of agreement of different implementations of the same calculation. A dedicated comparison, again at the technical level, of three codes that reach next-to-next-to-leading-order (NNLO) accuracy in quantum chromodynamics (QCD) for the total cross section has also been performed. These fixed-order results are a well-defined reference that allows a classification of the impact of higher-order sets of radiative corrections. Several examples of higher-order effects due to the strong or the EW interaction are discussed in this common framework. Also the combination

^a e-mail: alessandro.vicini@mi.infn.it

^b e-mail: dow@ubpheno.physics.buffalo.edu

of QCD and EW corrections is discussed, together with the ambiguities that affect the final result, due to the choice of a specific combination recipe. All the codes considered in this report have been run by the respective authors, and the results presented here constitute a benchmark that should be always checked/reproduced before any high-precision analysis is conducted based on these codes. In order to simplify these benchmarking procedures, the codes used in this report, together with the relevant input files and running instructions, can be found in a repository at <https://twiki.cern.ch/twiki/bin/view/Main/DrellYanComparison>.

1 Introduction

Precision electroweak (EW) measurements in Drell–Yan-like processes at the Fermilab Tevatron and CERN Large Hadron Collider (LHC), $pp(p\bar{p}) \rightarrow W^\pm \rightarrow l^\pm \nu_l$ and $pp(p\bar{p}) \rightarrow \gamma, Z \rightarrow l^+l^-$ ($l = e, \mu$), require the development of sophisticated simulation tools that should include the best theoretical knowledge available (for recent reviews see, e.g., [1–3]). Several different theoretical effects enter in the accurate evaluation of total cross sections and kinematic distributions: higher-order QCD corrections, higher-order EW corrections, the interplay between EW and QCD effects, matching of fixed-order results with QCD/QED Parton Showers (PS), tuning of QCD PS to reproduce non-perturbative low-energy effects, and effects of Parton Distribution Functions (PDF) and their uncertainties. The usage of different Monte Carlo (MC) programs that implement some or all of the above mentioned effects is not trivial.

As an explicit example of the need for the best theoretical predictions, we can consider for instance the measurement of the W boson mass (M_W), which is extracted from the transverse mass distribution of the $l\nu$ pair in $pp(p\bar{p}) \rightarrow W^\pm \rightarrow l^\pm \nu_l$ by means of a template fit to the experimental data. The inclusion of different subsets of radiative corrections in the preparation of the templates modifies the final result of the fit. Having in mind an accuracy target of $\mathcal{O}(10 \text{ MeV})$, it is important to include the $\mathcal{O}(\alpha)$ QED final-state radiation effects which yield a shift of M_W of about 100–200 MeV (depending on the precise definition of the final state), but also final-state multiple photon radiation to all orders, which induces an additional shift of up to $\mathcal{O}(-10\%)$ of the $\mathcal{O}(\alpha)$ [4]. One may thus also wonder about the size of the shift in M_W induced by weak or mixed QCD-EW corrections. Different subsets of corrections became available separately in the past years in codes that simulate purely QCD or purely EW effects. The combination of QCD and EW corrections is an important step in the development of the MC programs that will be used in high-precision measurements and is one of the main topics of the present report.

The combination of results produced by different MC simulation codes can be quite difficult and should satisfy some basic requirements:

1. Two codes that have the same perturbative approximation, the same input parameters (couplings, masses, PDFs), the same setup (choice of scales, acceptance cuts), should yield exactly the same results, within the accuracy of the numerical integration.
2. The results of different codes can be meaningfully combined only if they satisfy the previous point.

The size of the mismatches which occur if the first point is not satisfied may have a larger effect on predictions for EW precision observables than the anticipated experimental uncertainties. For this reason it is important to produce a collection of benchmark results for total cross sections and kinematic distributions with the most used, publicly available tools to describe Drell–Yan (DY) processes. These results should serve

1. to verify at any time that a given code works properly according to what its authors have foreseen,
2. to demonstrate explicitly the level of agreement of different codes which include identical subsets of radiative corrections, and
3. to expose the impact of different subsets of higher-order corrections and of differences in their implementations.

In this report, the authors of the MC codes DYNLO [5], DYNLOPS [6], FEWZ [7,8], HORACE [4,9–11], PHOTOS [12], POWHEG [13], POWHEG_BMNNP [14], POWHEG_BMNNPV [15], POWHEG_BW [16], RADY [17,18], SANC [19,20], SHERPA NNLO+PS [21], WINHAC [22–24], and WZGRAD [25–27], provide predictions for a number of observables relevant to the study of charged (CC) and neutral-current (NC) Drell–Yan processes at the LHC and LHCb.¹ Most of these codes first have been compared, using a common choice of input parameters, PDFs, renormalization and factorization scales, and acceptance cuts (tuned comparison), to test the level of technical agreement at leading order (LO), NLO EW and QCD and NNLO QCD, before studying the impact of higher-order effects.

The report is structured as follows: In Sect. 2.1 we describe the common setup for the tuned comparison and the observables under study in this report. The choice of observables was guided by the relevance to the study of Drell–Yan processes at the LHC, in particular to a precise measurement

¹ For recent W/Z physics results from the LHC see: ATLAS: <https://twiki.cern.ch/twiki/bin/view/AtlasPublic/StandardModelPublicResults> CMS: <https://twiki.cern.ch/twiki/bin/view/CMSPublic/PhysicsResultsSMP> LHCb: <https://lhcb.web.cern.ch/lhcb/Physics-Results/LHCb-Physics-Results.html>.

of the W boson mass. In Sects. 2.2 and 2.3 we present the results of the tuned comparison at NLO: in Sect. 2.2 we show the predictions of NLO-EW and NLO-QCD total cross sections, and in Sect. 2.3 we show the results at NLO EW and NLO QCD for a sample of kinematic distributions listed in Sect. 2.1.

In Sect. 3 we discuss the impact of higher-order QCD and EW corrections, i.e. corrections beyond NLO accuracy, on a selected set of W and Z boson observables. For each code used in this study we consider all the subsets of available corrections which are beyond NLO. To compute the results presented in this section, we adopted an EW input scheme, described in Sect. 3.1, which absorbs known higher-order corrections already in the (N)LO predictions, thus minimizing the impact of neglected orders in perturbation theory. All results obtained in this *benchmark* setup can serve as a benchmark for future studies. For completeness we provide the results for the total cross sections at NLO EW and NLO QCD obtained in this *benchmark* setup in Sect. 3.2. In Sect. 3.3 we discuss the effects of purely QCD corrections: after a short introduction in Sect. 3.3.1 on the impact of the $\mathcal{O}(\alpha_s)$ corrections on the observables under study, we consider in Sects. 3.3.2 and 3.3.3 exact results at $\mathcal{O}(\alpha_s^2)$ respectively for the total cross sections and for some differential distributions; in Sect. 3.3.4 we briefly introduce the problem of matching fixed- and all-order results in perturbation theory; we present results of (NLO+PS)-QCD matching in Sect. 3.3.5 and of (NNLO+PS)-QCD matching in Sect. 3.3.6. In Sect. 3.4 we discuss the effects of purely EW corrections: after a short introduction in Sect. 3.4.1 on the role of the $\mathcal{O}(\alpha)$ corrections on the observables under study, we compare in Sect. 3.4.2 the predictions for the partonic subprocesses induced by photons, which are naturally part of the NLO EW results. We discuss different EW input scheme choices in Sect. 3.4.3 and the impact of different gauge boson mass definitions in Sect. 3.4.4. In Sects. 3.4.5–3.4.7, we describe respectively the impact of higher-order corrections introduced via the ρ parameter or via the definition of effective couplings or due to multiple photon radiation described with a QED PS properly matched to the NLO EW calculation. The effect of light fermion-pair emission is discussed in Sect. 3.4.8.

In Sect. 4 we consider the combination of QCD and EW corrections and discuss some possibilities which are allowed by our presently incomplete knowledge of the $\mathcal{O}(\alpha\alpha_s)$ corrections to the DY processes. In Sect. 4.1 we compare the results that can be obtained with the codes presently available and discuss the origin of the observed differences. In Sect. 4.2 the results of a first calculation of $\mathcal{O}(\alpha\alpha_s)$ corrections in the pole approximation are used to assess the validity of simple prescriptions for the combination of EW and QCD corrections.

In Appendix A we provide a short description of the MC codes used in this study. In Appendix B we present a tuned

comparison of the total cross sections at NLO EW and NLO QCD for W^\pm and Z production with LHCb cuts.

1.1 Reproducibility of the results: a repository of the codes used in this report

The goal of this report is to provide a quantitative assessment of the technical level of agreement of different codes, but also a classification of the size of higher-order radiative corrections.

The usage of modern MC programs is quite complex and it is not trivial to judge whether the numerical results “out-of-the-box” of a code are correct. The numbers presented here, computed by the respective authors, should be considered as benchmarks of the codes; every user should thus be able to reproduce them, provided that he/she uses the same inputs and setup and runs with the appropriate amount of statistics.

In order to guarantee the reproducibility of the results presented in this report, we prepared a repository that contains a copy of all the MC codes used in this study, together with the necessary input files and the relevant instructions to run them. The repository can be found at the following URL: <https://twiki.cern.ch/twiki/bin/view/Main/DrellYanComparison> It should be stressed that simulation codes may evolve in time, because of improvements but also of bug fixes.

2 Tuned comparison of the codes

2.1 Setup for the tuned comparison

For the numerical evaluation of the cross sections at the LHC ($\sqrt{s} = 8$ TeV) we choose the following set of Standard Model input parameters [28]:

$$\begin{aligned}
 G_\mu &= 1.1663787 \times 10^{-5} \text{ GeV}^{-2}, & \alpha &= 1/137.035999074, \\
 \alpha_s &\equiv \alpha_s(M_Z^2) = 0.12018 \\
 M_Z &= 91.1876 \text{ GeV}, & \Gamma_Z &= 2.4952 \text{ GeV} \\
 M_W &= 80.385 \text{ GeV}, & \Gamma_W &= 2.085 \text{ GeV} \\
 M_H &= 125 \text{ GeV}, \\
 m_e &= 0.510998928 \text{ MeV}, & m_\mu &= 0.1056583715 \text{ GeV}, \\
 m_\tau &= 1.77682 \text{ GeV} \\
 m_u &= 0.06983 \text{ GeV}, & m_c &= 1.2 \text{ GeV}, \\
 m_t &= 173.5 \text{ GeV} \\
 m_d &= 0.06984 \text{ GeV}, & m_s &= 0.15 \text{ GeV}, \\
 m_b &= 4.6 \text{ GeV} \\
 |V_{ud}| &= 0.975, & |V_{us}| &= 0.222 \\
 |V_{cd}| &= 0.222, & |V_{cs}| &= 0.975 \\
 |V_{cb}| &= |V_{ts}| = |V_{ub}| = |V_{td}| = |V_{tb}| = 0.
 \end{aligned} \tag{1}$$

We work in the constant width scheme and fix the weak mixing angle by $c_w = M_W/M_Z, s_w^2 = 1 - c_w^2$. The Z and W boson decay widths given above are used in the LO, NLO and NNLO evaluations of the cross sections. The fermion masses only enter through loop contributions to the vector-boson self energies and as regulators of the collinear singularities which arise in the calculation of the QED contribution. The light quark masses are chosen in such a way, that the value for the hadronic five-flavour contribution to the photon vacuum polarization, $\Delta\alpha_{had}^{(5)}(M_Z^2) = 0.027572$ [29], is recovered, which is derived from low-energy e^+e^- data with the help of dispersion relations.

To compute the hadronic cross section we use the MSTW2008 [30] set of parton distribution functions, and take the renormalization scale, μ_r , and the QCD factorization scale, μ_{QCD} , to be the invariant mass of the final-state lepton pair, i.e. $\mu_r = \mu_{QCD} = M_{l\bar{l}}$ in the W boson case and $\mu_r = \mu_{QCD} = M_{l+l-}$ in the Z boson case.

All numerical evaluations of EW corrections require the subtraction of QED initial-state collinear divergences, which is performed using the QED DIS scheme. It is defined analogously to the usual DIS [31] scheme used in QCD calculations, i.e. by requiring the same expression for the leading and next-to-leading order structure function F_2 in deep inelastic scattering, which is given by the sum of the quark distributions. Since F_2 data are an important ingredient in extracting PDFs, the effect of the $\mathcal{O}(\alpha)$ QED corrections on the PDFs should be reduced in the QED DIS scheme. The QED factorization scale is chosen to be equal to the QCD factorization scale, $\mu_{QED} = \mu_{QCD}$. The QCD factorization is performed in the \overline{MS} scheme. The subtraction of the QED initial state collinear divergences is a necessary step to obtain a finite partonic cross section. The absence of a QED evolution in the PDF set MSTW2008 has little phenomenological impact on the kinematic distributions as discussed in Sect. 3.4.2. However, to be consistent in the order of higher order corrections in a *best* EW prediction, modern PDFs which include QED corrections, such as NNPDF2.3QED [32] and CT14QED [33], should be used.

For NLO EW predictions, we work in the on-shell renormalization scheme and use the following Z and W mass renormalization constants:

$$\delta M_Z^2 = \text{Re}\Sigma^Z(M_Z^2), \quad \delta M_W^2 = \text{Re}\Sigma^W(M_W^2), \quad (2)$$

where Σ^V denotes the transverse part of the unrenormalized vector-boson self energy.

For the sake of simplicity and to avoid additional sources of discrepancies in the tuned comparison we use the fine-structure constant $\alpha(0)$ throughout in both the calculation of CC and NC cross sections. We will discuss different EW input schemes in Sect. 3.4.3.

In the course of the calculation of radiative corrections to W boson observables the Kobayashi–Maskawa mixing has

Table 1 Two-loop and three-loop running of $\alpha_s(\mu_r^2)$

μ_r [GeV]	α_s (NLO)	α_s (NNLO)
91.1876	0.1201789	0.1170699
50	0.1324396	0.1286845
100	0.1184991	0.1154741
200	0.1072627	0.1047716
500	0.0953625	0.0933828

been neglected, but the final result for each parton level process has been multiplied with the square of the corresponding physical matrix element V_{ij} . From a numerical point of view, this procedure does not significantly differ from a consideration of the Kobayashi–Maskawa matrix in the renormalisation procedure as it has been pointed out in [34].

We choose to evaluate the running of the strong coupling constant at the two-loop level, with five flavours, for LO, NLO and NLO+PS predictions using as reference value $\alpha_s^{NLO}(M_Z) = 0.12018$, which is consistent with the choice made in the NLO PDF set of MSTW2008. NNLO QCD predictions use the NNLO PDF set and correspondingly the three-loop running of $\alpha_s(\mu_r)$, with reference value $\alpha_s^{NNLO}(M_Z) = 0.117$. In Table 1 we provide $\alpha_s(\mu_r^2)$ for several choices of the QCD renormalization scale μ_r , which are consistent with the results provided by the LHAPDF function `alphasPDF(μ_r)` when called in conjunction with MSTW2008.

The detector acceptance is simulated by imposing the following transverse momentum (p_\perp) and pseudo-rapidity (η) cuts:

$$\begin{aligned} \text{LHC: } & p_\perp^\ell > 25 \text{ GeV}, \quad |\eta(\ell)| < 2.5, \quad p_\perp^\nu > 25 \text{ GeV}, \\ & \ell = e, \mu, \\ \text{LHCb: } & p_\perp^\ell > 20 \text{ GeV}, \quad 2 < \eta(\ell) < 4.5, \\ & p_\perp^\nu > 20 \text{ GeV}, \quad \ell = e, \mu, \end{aligned} \quad (3)$$

where p_\perp^ν is the missing transverse momentum originating from the neutrino. These cuts approximately model the acceptance of the ATLAS, CMS, and LHCb detectors at the LHC. In addition to the separation cuts of Eq. (3) we apply a cut on the invariant mass of the final-state lepton pair of $M_{l+l-} > 50 \text{ GeV}$ and $M(l\nu) > 1 \text{ GeV}$ in the case of γ/Z production and W production respectively,

Results are provided for the *bare* setup, i.e. when only applying the acceptance cuts of Eq. (3), and the *calo* setup, which is defined as follows: In addition to the acceptance cuts, for muons we require that the energy of the photon is $E_\gamma < 2 \text{ GeV}$ for $\Delta R(\mu, \gamma) < 0.1$. For electrons we first recombine the four-momentum vectors of the electron and photon to an effective electron four-momentum vector when $\Delta R(e, \gamma) < 0.1$ and then apply the acceptance cuts to the recombined momenta. For both electrons and muons we

Table 2 Summary of lepton identification requirements in the *calo* setup

Electrons	Muons
Combine e and γ momentum four vectors, if $\Delta R(e, \gamma) < 0.1$	Reject events with $E_\gamma > 2 \text{ GeV}$ for $\Delta R(\mu, \gamma) < 0.1$
Reject events with $E_\gamma > 0.1 E_e$ for $0.1 < \Delta R(e, \gamma) < 0.4$	Reject events with $E_\gamma > 0.1 E_\mu$ for $0.1 < \Delta R(\mu, \gamma) < 0.4$

reject the event for $E_\gamma > 0.1 E_{\mu,e}$ for $0.1 \leq \Delta R(e, \gamma) \leq 0.4$, where

$$\Delta R(l, \gamma) = \sqrt{(\Phi_l - \Phi_\gamma)^2 + (\eta_l - \eta_\gamma)^2}.$$

We summarize the lepton identification requirements in the *calo* setup in Table 2.

Since we consider predictions inclusive with respect to QCD radiation, we do not impose any jet definition.

We use the Pythia version 6.4.26, Perugia tune (PYTUNE(320)). When producing NLO QCD+EW results with Pythia, the QED showering effects are switched off by setting $\text{MSTJ}(41) = \text{MSTP}(61) = \text{MSTP}(71) = 1$.

In the following we list the observables considered in this study for charged (CC) and neutral current (NC) processes: $pp \rightarrow W^\pm \rightarrow l^\pm \nu_l$ and $pp \rightarrow \gamma, Z \rightarrow l^+ l^-$ with $l = e, \mu$.

2.1.1 W boson observables

- σ_W : total inclusive cross section of W boson production.
- $\frac{d\sigma}{dM_\perp(l\nu)}$: transverse mass distribution of the lepton lepton-neutrino pair. The transverse mass is defined as

$$M_\perp = \sqrt{2p_\perp^\ell p_\perp^\nu (1 - \cos \phi^{\ell\nu})}, \tag{4}$$

where p_\perp^ν is the transverse momentum of the neutrino, and $\phi^{\ell\nu}$ is the angle between the charged lepton and the neutrino in the transverse plane.

- $\frac{d\sigma}{dp_\perp^\ell}$: charged lepton transverse momentum distribution.
- $\frac{d\sigma}{dp_\perp^W}$: missing transverse momentum distribution.
- $\frac{d\sigma_W}{dp_\perp^W}$: lepton-pair (W) transverse momentum distribution.

2.1.2 Z boson observables

- σ_Z : total inclusive cross section of Z boson production.
- $\frac{d\sigma}{dM_{l+l^-}}$: invariant mass distribution of the lepton pair.
- $\frac{d\sigma}{dp_\perp^l}$: transverse lepton momentum distribution (l is the positively charged lepton).
- $\frac{d\sigma_Z}{dp_\perp^Z}$: lepton-pair (Z) transverse momentum distribution.

Finally, for the case of Z boson production we add the distribution in ϕ^* to our list of observables. This observable is defined, e.g., in Ref. [35] as follows:

$$\phi^* = \tan\left(\frac{\pi - \Delta\Phi}{2}\right) \sin(\theta_\eta^*),$$

with $\Delta\Phi = \Phi^- - \Phi^+$ denoting the difference in the azimuthal angle of the two negatively/positively charged leptons in the laboratory frame, and

$$\cos(\theta_\eta^*) = \tanh\left(\frac{\eta^- - \eta^+}{2}\right).$$

η^\pm denote the pseudo rapidity of the positively/negatively charged lepton.

2.2 Tuned comparison of total cross sections at NLO EW and NLO QCD with ATLAS/CMS cuts

In this section we provide a tuned comparison of the total cross sections computed at fixed order, namely LO, NLO EW and NLO QCD, using the setup of Sect. 2.1 for the choice of input parameters and ATLAS/CMS acceptance cuts.

All codes can provide LO results, but different codes may include different sets of higher-order corrections. We use the symbol \times in the tables to indicate that a particular correction is not available in the specified code. Note that even when working at the same, fixed order and using the same setup, there can be slight differences in the implementation of higher-order corrections, resulting in small numerical differences in the predictions of different codes. In Tables 3, 5, and 7, we present the results obtained in the *bare* treatment of real photon radiation. The photon-lepton recombination procedure described in Sect. 2.1, which is only relevant for the codes that include NLO EW corrections, modifies the total cross section, as shown in Tables 4, 6, and 8. The total cross section results computed with LHCb acceptance cuts can be found in Appendix B.

2.3 Tuned comparison of kinematic distributions at NLO EW and NLO QCD with ATLAS/CMS cuts

In Sects. 2.3.1 and 2.3.2 we provide a sample of the kinematic observables calculated for this report including either NLO EW or NLO QCD corrections. The results have been obtained with different codes, using exactly the same setup as described in Sect. 2.1. While in earlier studies [36,37]² relative corrections have been compared, i.e. predictions for

² See also a recent study in Ref. [38].

Table 3 Tuned comparison of total cross sections (in pb) for $pp \rightarrow W^+ \rightarrow l^+ \nu_l + X$ at the 8 TeV LHC, with ATLAS/CMS cuts and *bare* leptons. (×) indicates that although POWHEG_BW provides NLO EW results also for *bare* electrons, due to the smallness of the electron mass

Code	LO	NLO QCD	NLO EW μ	NLO EW e
HORACE	2897.38(8)	×	2988.2(1)	2915.3(1)
WZGRAD	2897.33(2)	×	2987.94(5)	2915.39(6)
RADY	2897.35(2)	2899.2(4)	2988.01(4)	2915.38(3)
SANC	2897.30(2)	2899.9(3)	2987.77(3)	2915.00(3)
DYNNLO	2897.32(5)	2899(1)	×	×
FEWZ	2897.2(1)	2899.4(3)	×	×
POWHEG-w	2897.34(4)	2899.41(9)	×	×
POWHEG_BMNNP	2897.36(5)	2899.0(1)	2988.4(2)	2915.7(1)
POWHEG_BW	2897.4(1)	2899.2(3)	2987.7(4)	(×)

Table 4 Tuned comparison of total cross sections (in pb) for $pp \rightarrow W^+ \rightarrow l^+ \nu_l + X$ at the 8 TeV LHC, with ATLAS/CMS cuts and *calorimetric* leptons

Code	LO	NLO EW μ calo	NLO EW e calo
HORACE	2897.38(8)	2899.0(1)	3003.5(1)
WZGRAD	2897.33(2)	2898.33(5)	3003.33(6)
RADY	2897.35(2)	2898.37(4)	3003.36(4)
SANC	2897.30(2)	2898.18(3)	3003.00(4)

NLO/LO ratios of different codes, we expose here any effects of slight differences in the implementation of these corrections by comparing the ratios of different NLO EW and NLO QCD predictions to HORACE and POWHEG, respectively. Although technically the codes under consideration calculate the same quantity, in practice there are different possible ways to implement these higher-order corrections in a Monte Carlo integration code, which may result in ratios slightly different from one. This tuned comparison is thus a non-trivial test of these different implementations. The observed differences can be interpreted as a technical limit of agreement one can reach, and thus as a lower limit on the theoretical uncertainty.

The corresponding total cross sections can be found in Sect. 2.2.

It is important to note that NLO QCD is not sufficient for the description of certain observables and kinematic regimes where the resummation of logarithmic enhanced contributions and/or the inclusion of NNLO corrections is required, as discussed in detail in Sect. 3.3. In these cases, the NLO QCD results presented in this section are only used for technical checks.

2.3.1 Tuned comparison of W^\pm boson observables

In the following we present a tuned comparison of results for the M_\perp , p_\perp^W and p_\perp^l , p_\perp^ν distributions for W^\pm production

it would require very high-statistics to obtain per-mille level precision. Thus, we recommend to use the *bare* setup in POWHEG_BW only for muons

Table 5 Tuned comparison of total cross sections (in pb) for $pp \rightarrow W^- \rightarrow l^- \bar{\nu}_l + X$ at the 8 TeV LHC, with ATLAS/CMS cuts and *bare* leptons. (×) indicates that although POWHEG_BW provides NLO EW results also for *bare* electrons, due to the smallness of the electron mass it would require very high-statistics to obtain per-mille level precision. Thus, we recommend to use the *bare* setup in POWHEG_BW only for muons

Code	LO	NLO QCD	NLO EW μ	NLO EW e
HORACE	2008.84(5)	×	2076.48(9)	2029.15(8)
WZGRAD	2008.95(1)	×	2076.51(3)	2029.26(3)
RADY	2008.93(1)	2050.5(2)	2076.62(2)	2029.29(2)
SANC	2008.926(8)	2050.3(3)	2076.56(2)	2029.19(3)
DYNNLO	2008.89(3)	2050.2(9)	×	×
FEWZ	2008.9(1)	2049.97(8)	×	×
POWHEG-w	2008.93(3)	2050.14(5)	×	×
POWHEG_BMNNP	2008.94(3)	2049.9(1)	2076.9(1)	2029.71(6)
POWHEG_BW	2009.2(4)	2050.2(4)	2076.0(3)	(×)

in $pp \rightarrow \mu^\pm \nu_\mu + X$ at the 8 TeV LHC with ATLAS/CMS cuts in the *bare* setup. To compare the results of different codes at NLO EW we show in Figs. 1, 2, 3 and 4 the ratios $R = \text{code}/\text{HORACE}$, where code=HORACE, POWHEG_BMNNP, POWHEG_BW, RADY, SANC, WZGRAD, and at NLO QCD we show in Figs. 5, 6, 7, 8, 9 and 10 the ratios $R = \text{code}/\text{POWHEG}$, where code=DYNNLO, FEWZ, POWHEG, RADY, SANC.

We observe that the agreement between different codes that include NLO EW corrections is at the five per mill level or better in the transverse mass of the lepton pair, M_\perp , and in the lepton transverse momentum, p_\perp^l , in the relevant kinematic range under study. Some codes exhibit larger statistical fluctuations at larger values of the lepton transverse momenta, for instance, which can be improved by performing dedicated higher-statistics runs. For very small values of the transverse momentum of the lepton pair, p_\perp^W , the agreement is only at the one percent level and there are large statistical uncertainties

Table 6 Tuned comparison of total cross sections (in pb) for $pp \rightarrow W^- \rightarrow l^- \bar{\nu}_l + X$ at the 8 TeV LHC, with ATLAS/CMS cuts and calorimetric leptons

Code	LO	NLO EW μ calo	NLO EW e calo
HORACE	2008.84(5)	2013.67(7)	2085.42(8)
WZGRAD	2008.95(1)	2013.42(3)	2085.26(3)
RADY	2008.93(1)	2013.49(2)	2085.37(2)
SANC	2008.926(8)	2013.48(2)	2085.24(4)

Table 7 Tuned comparison of total cross sections (in pb) for $pp \rightarrow \gamma, Z \rightarrow l^+ l^- + X$ at the 8 TeV LHC, with ATLAS/CMS cuts and bare leptons. (×) indicates that FEWZ provides NLO EW results only in the G_μ scheme, and thus no results are available for the setup of the tuned comparison (see Sect. 2.1)

Code	LO	NLO QCD	NLO EW μ	NLO EW e
HORACE	431.033(9)	×	438.74(2)	422.08(2)
WZGRAD	431.048(7)	×	439.166(6)	422.78(1)
RADY	431.047(4)	458.16(3)	438.963(4)	422.536(5)
SANC	431.050(2)	458.27(3)	439.004(5)	422.56(1)
DYNNLO	431.043(8)	458.2(2)	×	×
FEWZ	431.00(1)	458.13(2)	(×)	(×)
POWHEG-z	431.08(4)	458.19(8)	×	×
POWHEG_BMNNPV	431.046(9)	458.16(7)	438.9(1)	422.2(2)

Table 8 Tuned comparison of total cross sections (in pb) for $pp \rightarrow \gamma, Z \rightarrow l^+ l^- + X$ at the 8 TeV LHC, with ATLAS/CMS cuts and calorimetric leptons

Code	LO	NLO EW μ calo	NLO EW e calo
HORACE	431.033(9)	407.67(1)	439.68(2)
WZGRAD	431.048(7)	407.852(7)	440.29(1)
RADY	431.047(4)	407.568(6)	440.064(5)
SANC	431.050(2)	407.687(5)	440.09(1)

at larger values of p_\perp^W . We consider this level of agreement to be sufficient, since there is only a very small p_\perp^W kick due to photon radiation, and it is not worthwhile to perform dedicated higher statistics runs for higher values of p_\perp^W to improve the statistical uncertainty. Only the POWHEG_BW result for the p_\perp^W distribution in the W^- case shows a systematic difference, and its origin is presently under study. In any case, these results should be considered just for technical checks, since p_\perp^W receives large contributions from QCD radiation. The combined effects of EW and QCD corrections in p_\perp^W can be studied for instance by using a calculation of NLO EW corrections to $W + j$ production [39] and the implementation of NLO EW corrections in POWHEG [14, 16] as discussed in Sect. 4.

2.3.2 Tuned comparison of Z boson observables

In Figs. 11 and 12 and in Figs. 13 and 14 we present a tuned comparison of results for NLO EW and QCD predictions, respectively, for the M_{l+l^-} , p_\perp^Z and p_\perp^l distributions in $pp \rightarrow \gamma, Z \rightarrow \mu^+ \mu^- + X$ at the 8 TeV LHC with ATLAS/CMS cuts in the bare setup of Sect. 2.1. The agreement of different

codes providing NLO EW predictions for these distributions in the kinematic regions under study are at the five per mill level or better, apart from a difference at the one per cent level in the transverse momentum distribution of the lepton pair for small values of p_\perp^Z . As it is the case for CC DY, these results should be considered just for technical checks, since p_\perp^Z receives large contributions from QCD radiation. The combined effects of EW and QCD corrections in p_\perp^Z can be studied for instance by using a calculation of NLO EW corrections to $Z + j$ production [40] and the implementation of NLO EW corrections in POWHEG [41] as discussed in Sect. 4.

3 Impact of higher-order radiative corrections

The setup described in Sect. 2.1, and used to perform the tuned comparison of the codes participating in this study, has been chosen with two main practical motivations: (1) the simplicity to implement the renormalization of the NLO EW calculation and (2) the possibility to rely and easily reproduce the results of previous similar studies [36, 37], where technical agreement between different codes had already been demonstrated.

On the other hand, the setup of Sect. 2.1 suffers for two reasons, relevant from the phenomenological but also from the theoretical point of view: (1) the choice of the fine-structure constant as input parameter in the EW Lagrangian introduces an explicit dependence on the value of the light-quark masses via the electric charge renormalization; these masses are not well defined quantities and introduce a non-negligible parametric dependence of all the results; (2) the strength of the coupling of the weak currents is best expressed

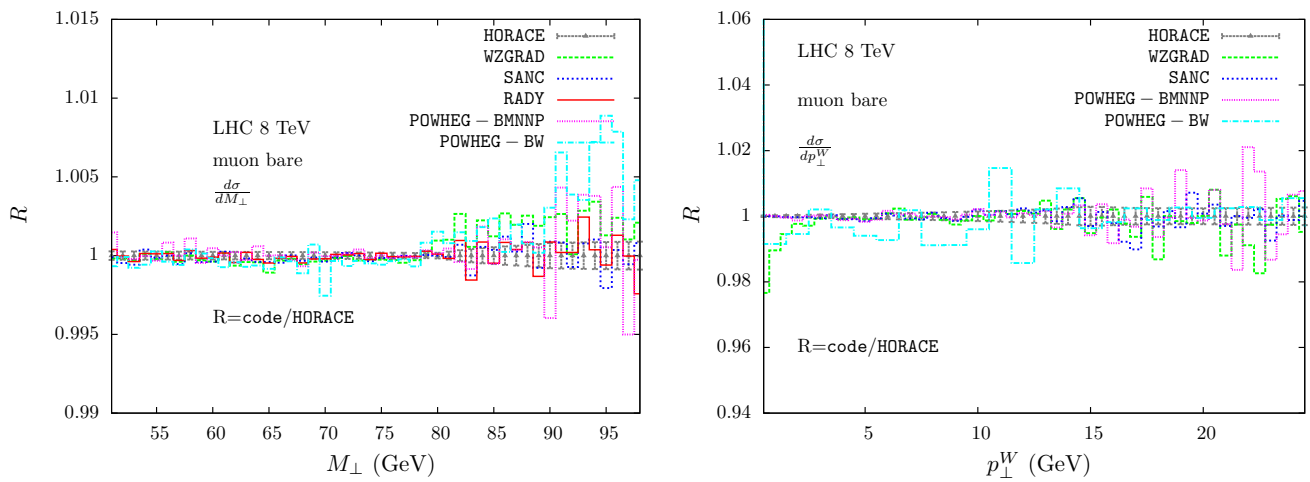


Fig. 1 Tuned comparison of the lepton-pair transverse mass and transverse momentum distributions in $pp \rightarrow W^+ \rightarrow \mu^+ \nu_\mu + X$ at the 8 TeV LHC with ATLAS/CMS cuts in the *bare* setup, including NLO EW corrections

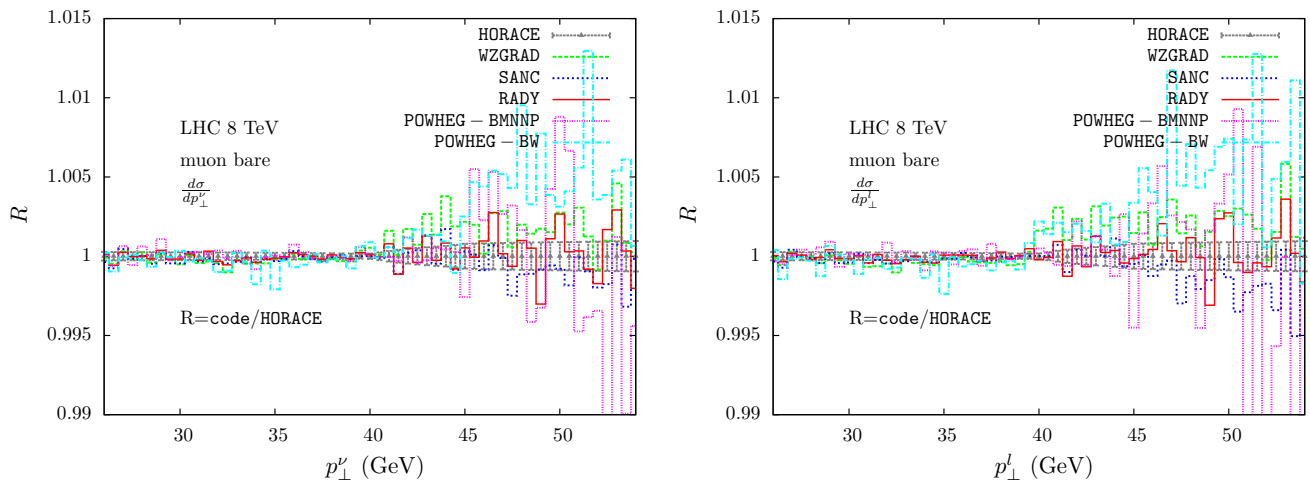


Fig. 2 Tuned comparison of the muon and muon neutrino transverse momentum distributions in $pp \rightarrow W^+ \rightarrow \mu^+ \nu_\mu + X$ at the 8 TeV LHC with ATLAS/CMS cuts in the *bare* setup, including NLO EW corrections

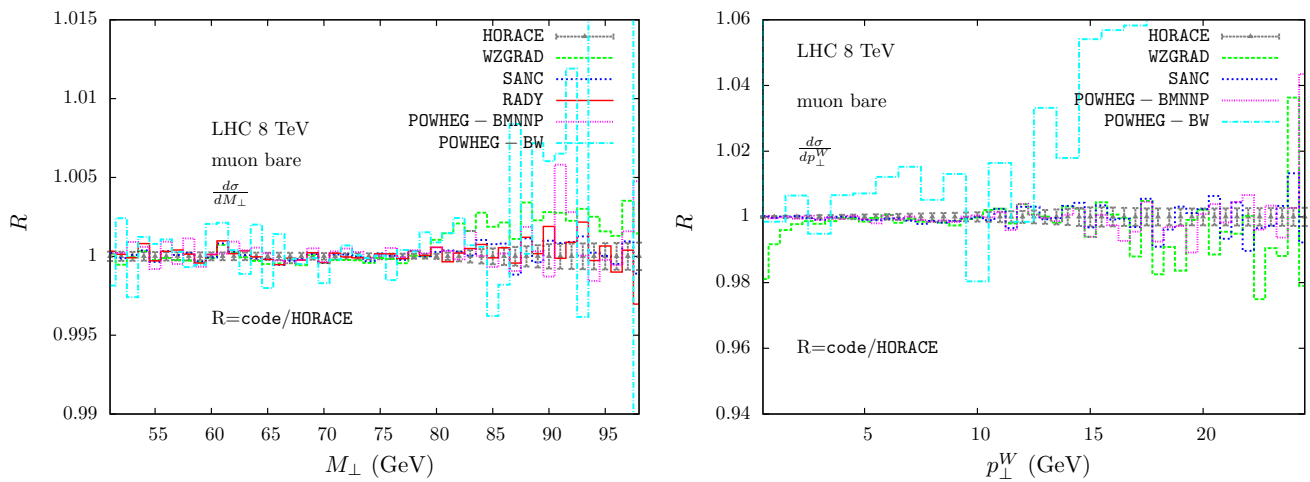


Fig. 3 Tuned comparison of the lepton-pair transverse mass and transverse momentum distributions in $pp \rightarrow W^- \rightarrow \mu^- \nu_\mu + X$ at the 8 TeV LHC with ATLAS/CMS cuts in the *bare* setup, including NLO EW corrections

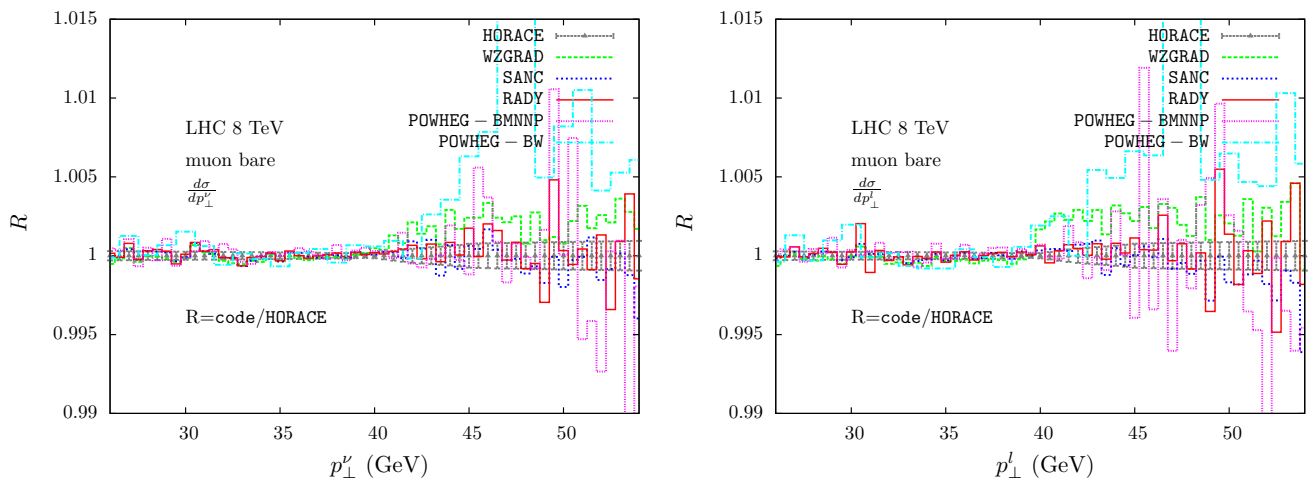


Fig. 4 Tuned comparison of the muon and muon neutrino transverse momentum distributions in $pp \rightarrow W^- \rightarrow \mu^- \nu_\mu + X$ at the 8 TeV LHC with ATLAS/CMS cuts in the *bare* setup, including NLO EW corrections

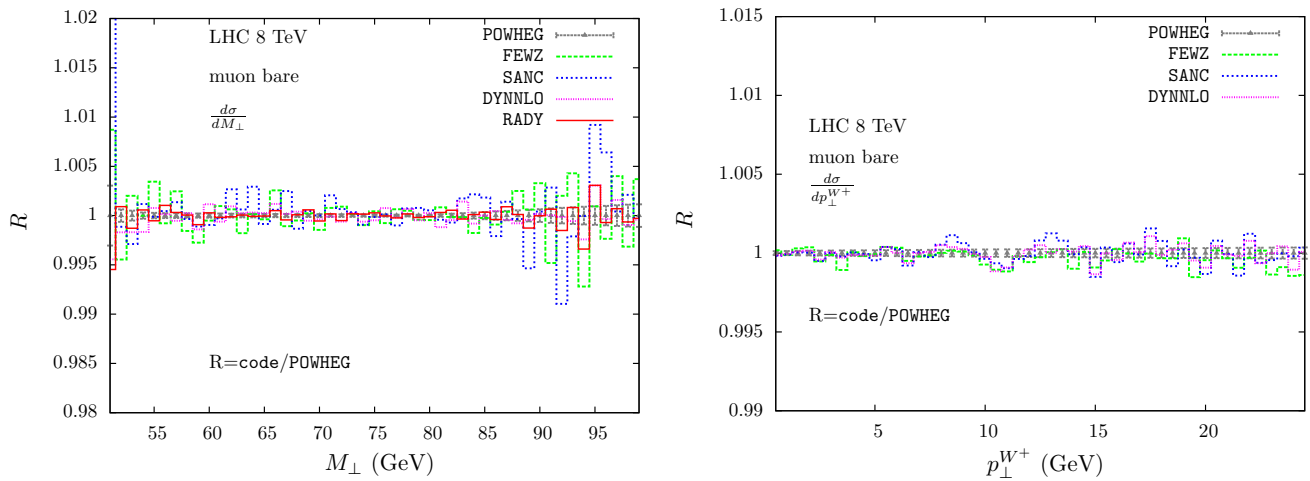


Fig. 5 Tuned comparison of the lepton-pair transverse mass and transverse momentum distribution in $pp \rightarrow W^+ \rightarrow \mu^+ \nu_\mu + X$ at the 8 TeV LHC with ATLAS/CMS cuts in the *bare* setup, including NLO QCD corrections

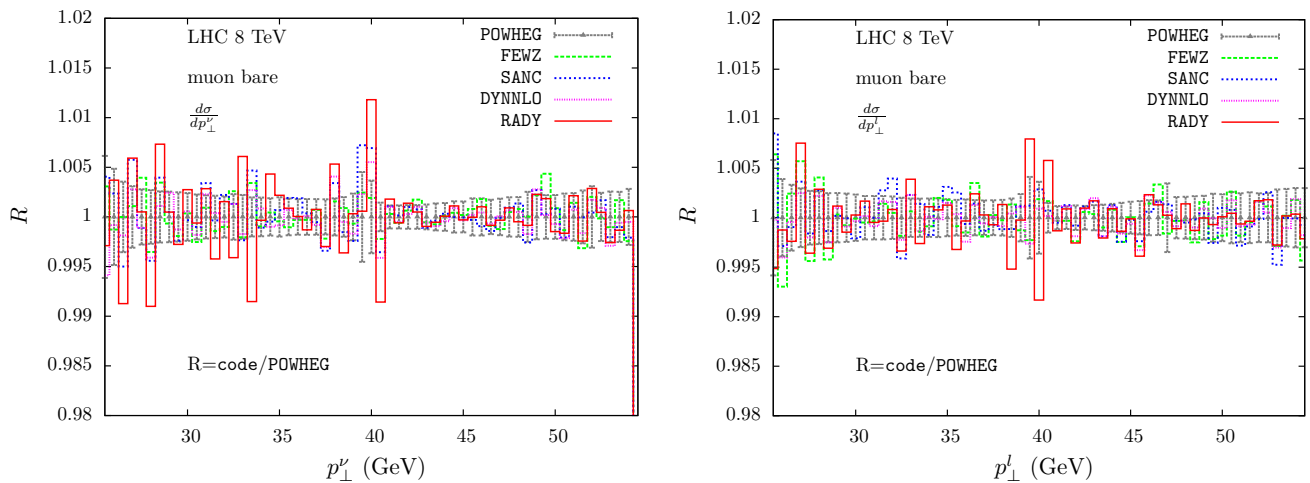


Fig. 6 Tuned comparison of the muon and muon neutrino transverse momentum distributions in $pp \rightarrow W^+ \rightarrow \mu^+ \nu_\mu + X$ at the 8 TeV LHC with ATLAS/CMS cuts in the *bare* setup, including NLO QCD corrections

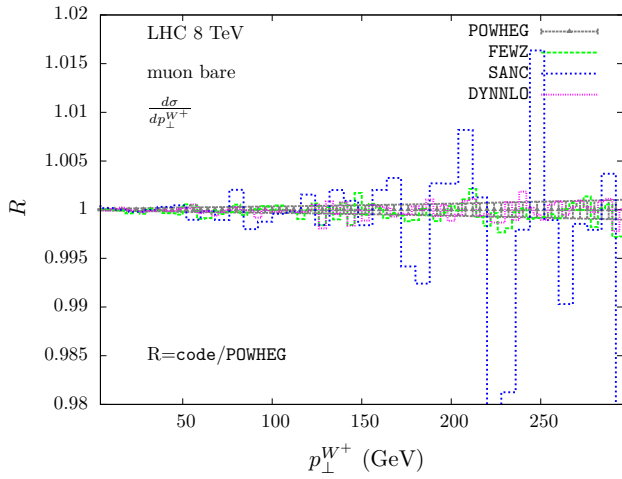


Fig. 7 Tuned comparison of the lepton-pair transverse momentum distribution in $pp \rightarrow W^+ \rightarrow \mu^+ \nu_\mu + X$ at the 8 TeV LHC with ATLAS/CMS cuts in the *bare* setup at high p_\perp^W , including NLO QCD corrections

in terms of the Fermi constant, whose definition reabsorbs to all orders various classes of large radiative corrections; when using the Fermi constant, the impact of the remaining, process dependent corrections is thus reduced in size with respect to other input schemes, like, e.g., the one of Sect. 2.1.

We propose here to use a different input scheme, which absorbs known higher-order corrections already in the (N)LO predictions, thus minimalizing the impact of neglected orders in perturbation theory. This scheme will be called *benchmark* and the corresponding numbers at NLO EW will be considered as our benchmark results, relevant in particular for the discussion of the impact of higher-order corrections.

3.1 Setup for *benchmark* predictions

We provide *benchmark* predictions for the 8 TeV LHC for muons in the *bare* setup, i.e. when only applying acceptance cuts, and for electrons in the *calo* setup as defined in the setup for the tuned comparison in Sect. 2.1. For the *benchmark* results we made the following changes to the setup described in Sect. 2.1:

1. In the case of W boson production, in addition to the acceptance cuts we apply $M_\perp(l\nu) > 40$ GeV.
2. To account for the fact that we are using the constant width approach, we have to adjust the W, Z mass and width input parameters that have been measured in the s -dependent width approach accordingly, as follows [18, 42] ($\gamma_V = \Gamma_V/M_V$):

$$M_V \rightarrow \frac{M_V}{\sqrt{1 + \gamma_V^2}}; \quad \Gamma_V \rightarrow \frac{\Gamma_V}{\sqrt{1 + \gamma_V^2}}.$$

Consequently, the input values for the W, Z masses and widths change to

$$\begin{aligned} M_Z &= 91.1535 \text{ GeV}, & \Gamma_Z &= 2.4943 \text{ GeV} \\ M_W &= 80.358 \text{ GeV}, & \Gamma_W &= 2.084 \text{ GeV}. \end{aligned} \quad (5)$$

3. We use the following EW input scheme:
In the calculation of the tree-level couplings we replace $\alpha(0)$ by the effective coupling $\alpha_{G_\mu} = \sqrt{2}G_\mu M_W^2(1 - M_W^2/M_Z^2)/\pi$. The relative $\mathcal{O}(\alpha)$ corrections are calculated with the fine structure constant $\alpha(0)$. At NLO EW this replacement implies an additional contribution of Δr to the relative $\mathcal{O}(\alpha)$ corrections. The one-loop result

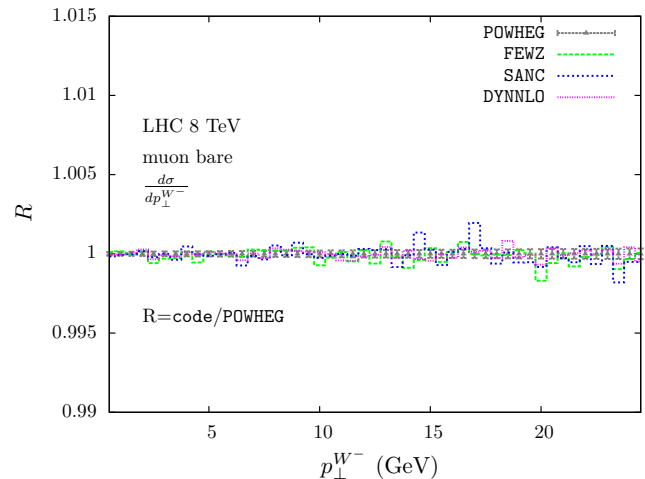
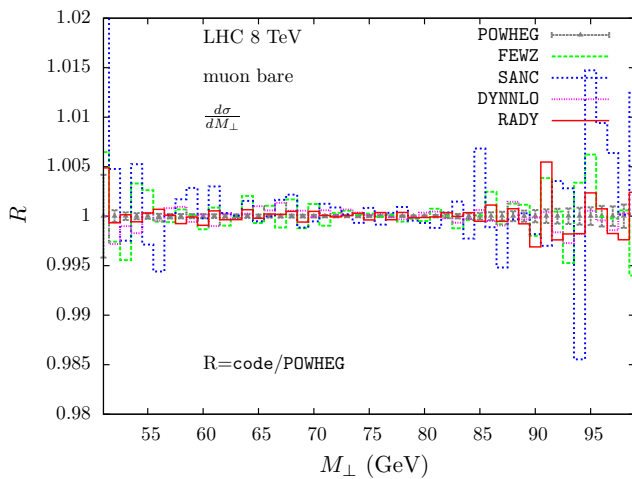


Fig. 8 Tuned comparison of the lepton-pair transverse mass and transverse momentum distribution in $pp \rightarrow W^- \rightarrow \mu^- \bar{\nu}_\mu + X$ at the 8 TeV LHC with ATLAS/CMS cuts in the *bare* setup, including NLO QCD corrections

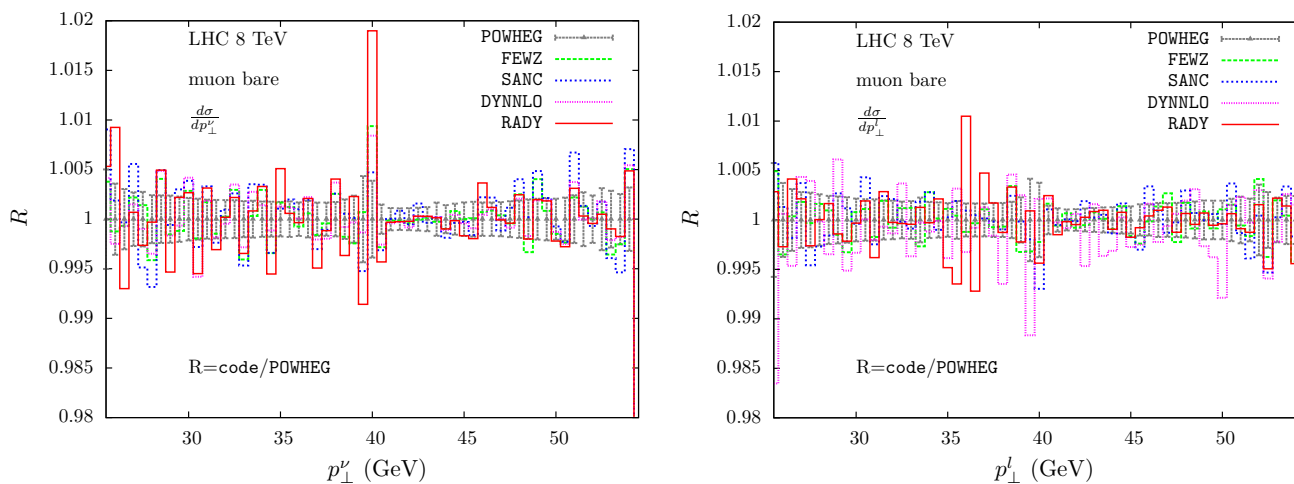


Fig. 9 Tuned comparison of the muon and muon neutrino transverse momentum distributions in $pp \rightarrow W^- \rightarrow \mu^- \bar{\nu}_\mu + X$ at the 8 TeV LHC with ATLAS/CMS cuts in the *bare* setup, including NLO QCD corrections

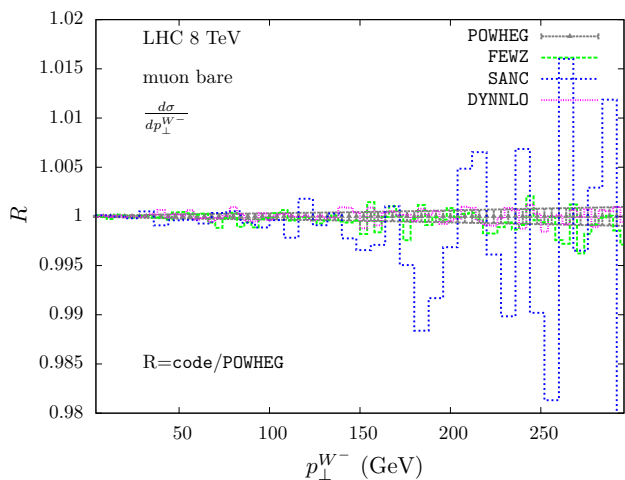


Fig. 10 Tuned comparison of the lepton-pair transverse momentum distributions in $pp \rightarrow W^- \rightarrow \mu^- \bar{\nu}_\mu + X$ at the 8 TeV LHC with ATLAS/CMS cuts in the *bare* setup at high p_\perp^W , including NLO QCD corrections

for Δr has been calculated in Refs. [43,44] and can be decomposed as follows:

$$\Delta r(1 - \text{loop}) = \Delta\alpha - \frac{c_w^2}{s_w^2} \Delta\rho + \Delta r_{rem}(M_H).$$

When using the input values of Eq. (1) and the values for M_W and M_Z given in item (2) $\Delta r(1 - \text{loop}) = 0.0295633444$ ($\Delta r = 0.0296123554$ for the unshifted W/Z masses of Eq. (1)).

To be able to discuss the impact of higher order correction beyond NLO in this setup, we successively included higher-order corrections, i.e. we start with the NLO result using the

changed setup as described above, successively add different sources of higher order corrections, such as multiple photon radiation and two-loop corrections to $\Delta\rho$, and compare the resulting observables to the NLO results.

3.1.1 Setup for the evaluation of photon-induced contributions

For the comparison of predictions for the photon-induced processes $\gamma\gamma \rightarrow l^+l^-$ and $\gamma q^{(-)} \rightarrow l^+l^- q^{(-)}$ in NC DY, and $\gamma q^{(-)} \rightarrow l\nu_l q^{(-)}$ in CC DY we make the following additional changes to the *benchmark* setup:

- In order to have a modern parametrization of the photon density, we used the central NNPDF2.3_10_as_130_qed PDF set [32].
- We use as input parameters $(\alpha(0), M_W, M_Z)$ for all photon-induced processes.

In the NC DY case, we compute separately the contribution of the LO $\gamma\gamma \rightarrow l^+l^-$ process and those of the $\gamma q^{(-)} \rightarrow l^+l^- q^{(-)}$ processes. To express the percentage effect of these subprocesses, we present their ratio to the LO $q\bar{q}$ -initiated cross sections.

3.2 Total cross sections in the benchmark setup at NLO EW and NLO QCD with ATLAS/CMS cuts

In Tables 9, 10, and 11 we provide a tuned comparison of the total cross sections for W^+ , W^- and Z boson production, respectively, computed at fixed order, namely LO, NLO EW and NLO QCD, using the *benchmark* setup of Sect. 3.1 for

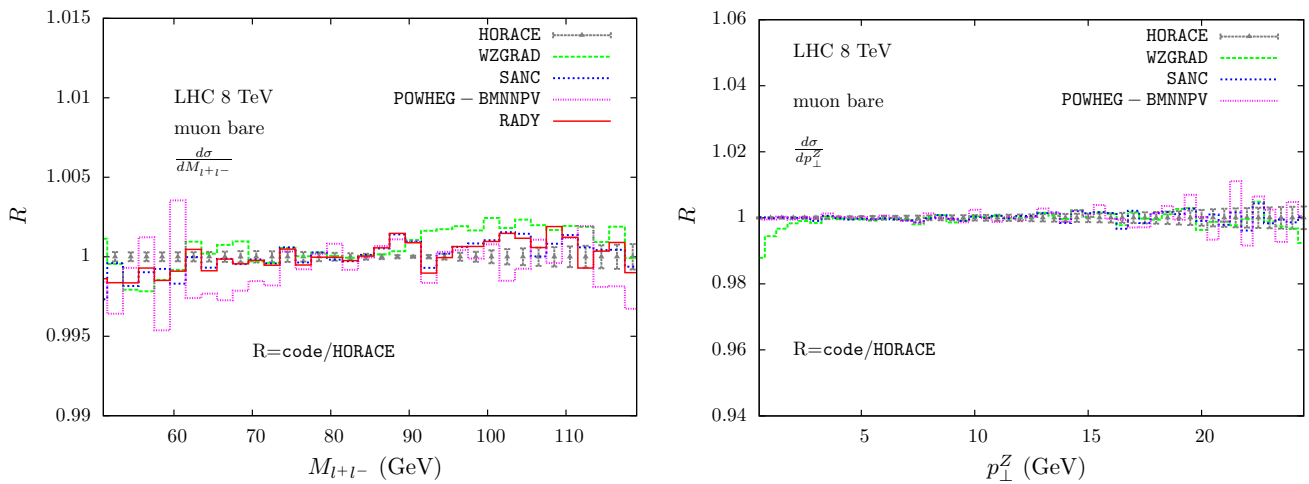


Fig. 11 Tuned comparison of the lepton-pair invariant mass and transverse momentum distributions in $pp \rightarrow \gamma, Z \rightarrow \mu^+ \mu^- + X$ at the 8 TeV LHC with ATLAS/CMS cuts in the *bare* setup, including NLO EW corrections

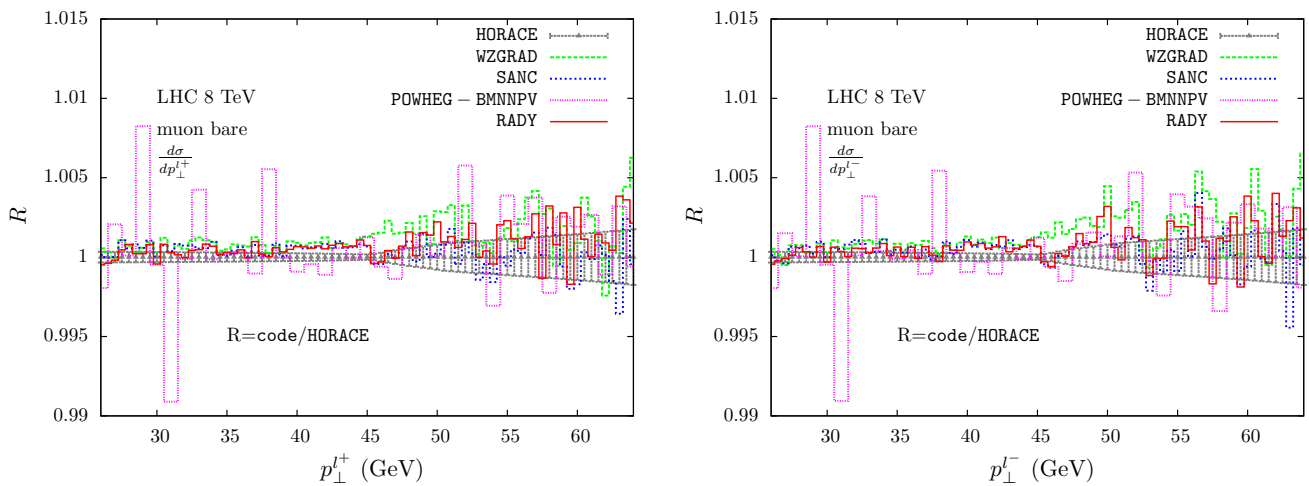


Fig. 12 Tuned comparison of the μ^+ and μ^- transverse momentum distributions in $pp \rightarrow \gamma, Z \rightarrow \mu^+ \mu^- + X$ at the 8 TeV LHC with ATLAS/CMS cuts in the *bare* setup, including NLO EW corrections

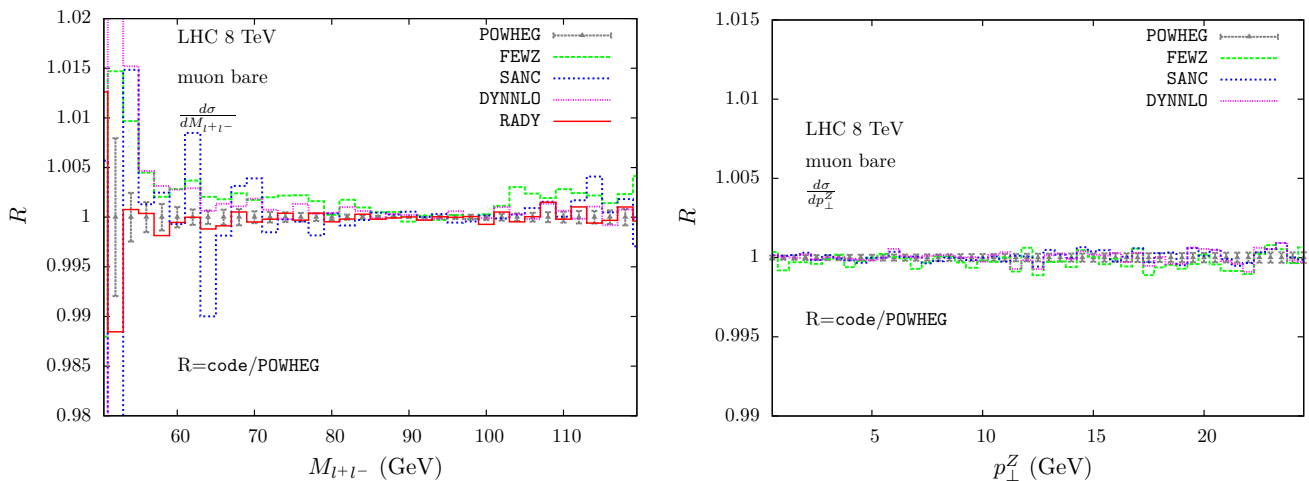


Fig. 13 Tuned comparison of the lepton-pair invariant mass and transverse momentum distributions in $pp \rightarrow \gamma, Z \rightarrow \mu^+ \mu^- + X$ at the 8 TeV LHC with ATLAS/CMS cuts in the *bare* setup, including NLO QCD corrections

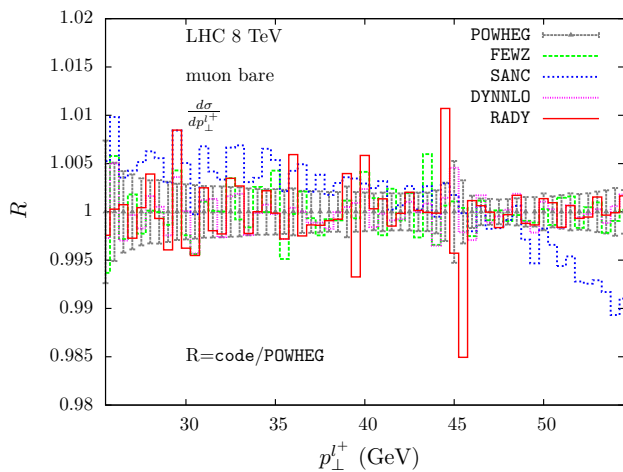


Fig. 14 Tuned comparison of the muon transverse momentum distributions in $pp \rightarrow \gamma, Z \rightarrow \mu^+\mu^- + X$ at the 8 TeV LHC with ATLAS/CMS cuts in the *bare* setup, including NLO QCD corrections

the choice of input parameters and ATLAS/CMS acceptance cuts. We use the symbol \times in the tables to indicate that a particular correction is not available in the specified code, and (\times) in cases where the result can be produced with the specified code but has not been provided for this report.

3.3 Impact of QCD corrections on W and Z boson observables in the *benchmark* setup

3.3.1 NLO QCD corrections

At LO the DY processes are described in terms of quark-antiquark annihilation subprocesses.³ The NLO QCD corrections are due to real and virtual corrections to the incoming quark-antiquark line, but they receive a contribution also from the (anti)quark-gluon scattering subprocesses.

Some observables, such as the lepton-pair transverse momentum, the ϕ^* variable or the single-lepton transverse momentum, are strongly sensitive to the details of real QCD radiation. The lepton-pair transverse momentum or the ϕ^* distributions are indeed absent at LO ($p_{\perp}^V = 0$ and $\phi^* = \pi$), so that for these quantities NLO QCD is the first perturbative non-vanishing order. In the single-lepton transverse momentum case, the distribution receives, on top of the LO value, a large contribution from the recoil of the intermediate gauge boson against initial-state QCD radiation, enhanced by its collinearly divergent behaviour. Even if this is not formally the case, NLO QCD is numerically the lowest perturbative order which can be used to assess the impact of higher order corrections. On the contrary the (pseudo)-rapidity distribu-

tions and the invariant/transverse mass distributions receive a milder, slowly varying NLO QCD correction, close in size to the value of the total NLO K-factor.

3.3.2 NNLO QCD corrections: total cross section

We study the predictions for DY processes with the inclusion of QCD next-to-next-to-leading order (NNLO) corrections in the strong coupling constant using⁴ the following three MC codes, DYNLO [5], FEWZ [7,46], and SHERPA-NNLO-FO [21].

These three codes have the same perturbative accuracy, in the sense that they include the same set of radiative corrections, but differ in the explicit implementation of the combination of real and virtual corrections, in particular for what concerns the cancellation of soft and collinear divergences. In principle the differences between these codes are at the technical level and should not affect physical predictions. The comparison of their results should thus be understood as a tuned comparison at NNLO QCD level. The results for the evaluation of the total cross section in the *benchmark* setup described in Sect. 3.1 are reported in Table 12. The agreement between the three codes is at the 0.5% level, for the three processes (NC and CC) under consideration.

The impact of NNLO QCD corrections on the total cross section of the DY processes depends on the corrections to the lower-order processes but also on a small contribution from new partonic channels. The second order corrections reduce the renormalization/factorization scale dependence of the final result, with respect to NLO QCD, and bring it down to the 1% level [5,46].

The small differences between the results of Table 12 can be partially understood by an analysis of the behavior of the subtraction methods implemented in the three codes in the setup of the report. The integrated cross section in presence of symmetric cuts on the transverse momentum of lepton and missing energy suffers from the pathological behavior first described in [47]. Let us assume staggered cuts, where $p_{T,l} \geq E_T^{\text{cut}}$ and $E_{T,miss} \geq E_T^{\text{cut}} + \Delta$, i.e. the difference in the minimum transverse momentum is parametrized as Δ . The real-emission contribution to the integrated NLO cross section then behaves as [47]

$$\sigma^{(r)} = A(\Delta, \delta) + B \log \delta - C(\Delta + \delta) \log(\Delta + \delta). \quad (6)$$

Here, δ denotes the regulator in a phase-space slicing method. In subtraction methods, δ is zero. $A(\Delta, \delta)$ and its first derivative with respect to Δ are regular in $\Delta = 0$ for any δ , including $\delta = 0$ [47]. B and C are coefficients, with B identifying the collinear singularity, which is canceled by

³ We discuss separately the NC DY LO contribution given by $\gamma\gamma \rightarrow l^+l^-$ scattering, which receives a non-trivial QCD correction only starting from third perturbative order.

⁴ Recently, an implementation of NNLO QCD corrections to $pp \rightarrow Z$ and $pp \rightarrow W$ including the decays of the unstable gauge bosons became also available in MCFM [45].

Table 9 $pp \rightarrow W^+ \rightarrow l^+ \nu_l$ total cross sections (in pb) at LO, NLO EW and NLO QCD at the 8 TeV LHC with ATLAS/CMS cuts in the benchmark setup

Code	LO	NLO QCD	NLO EW μ bare	NLO EW e calo
HORACE	3109.65(8)	×	3022.8(1)	3039.5(2)
WZGRAD	3109.62(2)	×	3022.68(4)	3039.13(5)
SANC	3109.66(2)	(×)	3022.53(4)	3038.94(4)
DYNNLO	3109.5(2)	3092.3(9)	×	×
FEWZ	3109.20(8)	3089.1(3)	×	×
POWHEG-w	(×)	3090.4(2)	×	×
POWHEG_BMNNP	3109.68(7)	3089.6(2)	3022.8(2)	(×)

Table 10 $pp \rightarrow W^- \rightarrow l^- \bar{\nu}_l$ total cross sections (in pb) at LO, NLO EW and NLO QCD at the 8 TeV LHC with ATLAS/CMS cuts in the benchmark setup

Code	LO	NLO QCD	NLO EW μ bare	NLO EW e calo
HORACE	2156.36(6)	×	2101.17(8)	2111.1(2)
WZGRAD	2156.46(2)	×	2101.23(2)	2110.65(4)
SANC	2156.46(2)	(×)	2101.31(4)	2110.69(4)
DYNNLO	2156.38(2)	2189.3(7)	×	×
FEWZ	2156.09(4)	2187.1(1)	×	×
POWHEG-w	(×)	2187.72(6)	×	×
POWHEG_BMNNP	2156.44(4)	2187.5(1)	2101.5(1)	(×)

Table 11 $pp \rightarrow \gamma, Z \rightarrow l^- l^+$ total cross sections (in pb) at LO, NLO EW and NLO QCD at the 8 TeV LHC with ATLAS/CMS cuts in the benchmark setup

Code	LO	NLO QCD	NLO EW μ bare	NLO EW e calo
HORACE	462.663	×	443.638	
WZGRAD	462.677(4)	×	443.950(6)	445.178(7)
SANC	462.675(2)	(×)	443.794(4)	444.963(4)
DYNNLO	(×)	491.94(5)	×	×
FEWZ	462.631(9)	491.62(4)	443.84(2)	444.67(2)
POWHEG-z	(×)	491.744(4)	×	×
POWHEG_BMNNPV	462.67(1)	491.3(8)	443.4(1)	(×)

Table 12 Tuned comparison of NNLO QCD total cross sections (in pb) at the 8 TeV LHC in the benchmark setup with ATLAS/CMS cuts

Process	DYNNLO	FEWZ	SHERPA-NNLO-FO
$pp \rightarrow l^+ \nu_l + X$	3191(7)	3207(2)	3204(4)
$pp \rightarrow l^- \bar{\nu}_l + X$	2243(6)	2238(1)	2252(3)
$pp \rightarrow l^+ l^- + X$	502.4(4)	504.6(1)	502.0(6)

the corresponding singular terms in the two-body contribution to the total cross section. The term of interest is therefore $-C(\Delta + \delta) \log(\Delta + \delta)$. It is possible to verify numerically that it describes the behavior of the NLO cross section in the Drell–Yan process as a function of Δ . The maximal deviation of the cross section from the expected behavior based on phase-space considerations is $\mathcal{O}(1\%)$. The important point to notice, however is the dependence on the slicing parameter δ . Its value must be chosen small enough to suppress any residual effect on the total cross section as $\Delta \rightarrow 0$, i.e. in the presence of symmetric cuts. The relevance to the present comparison arises from the fact that both SHERPA NNLO+PS and DYNNLO use a phase-space

slicing technique at NNLO, while FEWZ employs a subtraction method. The NNLO calculation shows a feature similar to Eq. (6), although the magnitude and functional dependence on Δ and δ cannot be predicted due to the intricate interplay between real-virtual and double-real corrections. A variation of the q_T slicing parameter in SHERPA NNLO+PS in the range 0.15...1 GeV, yields a residual effect on the total cross section of $\mathcal{O}(0.2\%)$, which is of the same order as the numerical accuracy in the NNLO calculations. The SHERPA-NNLO-FO results shown in Table 12 are obtained with a q_T slicing parameter of 0.01 GeV. When changing the q_T slicing parameter to 0.1 GeV, the total NNLO

QCD cross section for the NC DY process obtained with SHERPA-NNLO-FO is 502.2(5) pb.

3.3.3 NNLO QCD corrections: kinematic distributions

The NNLO QCD predictions for kinematic distributions are compared for a subset of observables in Figs. 15 and 16, where the ratio to the SHERPA-NNLO-FO prediction is shown. As it can be seen, the predictions agree within the statistical uncertainties of the MC integration.

The impact of NNLO QCD corrections on the kinematic distributions of the DY processes depends on the observable under study. Since some observables such as the lepton-pair transverse momentum, the single-lepton transverse momentum or the ϕ^* variable are strongly sensitive to the details of real QCD radiation at NLO, they are significantly modified by the second order QCD corrections. On the contrary the (pseudo-)rapidity distributions and the invariant/transverse mass distributions receive a milder corrections, closer in size to the value of the total NNLO K-factor.

To illustrate the impact of the NNLO QCD corrections we compute for a given observable \mathcal{O} the ratio $R_{\mathcal{O}} = \left(\frac{d\sigma^{NNLO}}{d\mathcal{O}}\right) / \left(\frac{d\sigma^{NLO}}{d\mathcal{O}}\right)$ with the same distribution evaluated respectively with NNLO QCD and NLO QCD accuracy. We consider the distributions at NLO QCD as perfectly tuned and neglect here the differences introduced by the choice in the denominator of one NLO QCD code with respect to another one. We present the results in Figs. 17, 18 and 19.

We observe in Figs. 17 and 19 that the NNLO corrections have a mild impact on the invariant-mass (NC DY) or transverse-mass (CC DY) distributions; the correction is almost flat over the entire mass range considered. The more pronounced corrections that appear at the lower end of the distributions can be understood as an effect of the acceptance cuts.

Figures 17 and 19 show the relative correction to the lepton and to the neutrino transverse momentum distributions. The NNLO QCD corrections, expressed in terms of the NLO QCD result, are quite flat and moderate (smaller than 10%) below the Jacobian peak, they have a sharply peaked behaviour about the Jacobian peak, where fixed order perturbation theory breaks down, while they are of $\mathcal{O}(20\%)$ and are growing for increasing transverse momentum above the Jacobian peak. Again, the pronounced corrections that appear at the lower end of the distributions can be understood as an effect of the acceptance cuts.

In Figs. 18 and 19 we show the relative corrections to the lepton-pair transverse momentum distributions, for the three processes (NC and CC) under consideration, in two ranges of transverse momentum ($p_{\perp}^V \in [0, 25]$ GeV and $p_{\perp}^V \in [0, 250]$ GeV). In fixed-order perturbation theory the distribution is divergent in the limit of vanishing transverse

momentum; the sign of the first bin and the slope of the distributions in this limit depend on the perturbative order, so that a comparison between NLO QCD and NNLO QCD predictions is merely of technical interest. At large lepton-pair transverse momentum, where the perturbative regime of QCD allows to study the convergence of the perturbative expansion, the NNLO QCD corrections are large, of $\mathcal{O}(40\%)$, and quite flat in the range $50 \leq p_{\perp}^V \leq 300$ GeV.

The relative correction to the lepton-pair ϕ^* distribution in the NC DY process is shown in Fig. 19. Since in the limit $\phi^* \rightarrow 0$ we probe the same phase-space region where the lepton-pair has small transverse momentum, the distribution suffers of the break-down of perturbation theory, so that the comparison between the NNLO QCD and the NLO QCD predictions is again merely of technical interest in this region.

3.3.4 Higher-order QCD corrections to all orders: generalities

As already mentioned in Sect. 3.3.1, there are observables whose description in fixed-order QCD is not adequate, so that the resummation to all orders of logarithmically enhanced contributions is necessary to obtain a physically sensible prediction. The solution of this problem requires a certain number of choices, which can be understood as potential sources of uncertainty.

- Matching a resummed and a (N)NLO fixed-order expressions requires a procedure that avoids double countings and possibly allows for the MC simulation of events with a probabilistic interpretation. The solution of this problem at NLO was developed in [48, 49] and more recently in [21, 50, 51] also for the inclusion of NNLO partonic results. Each approach solves the matching problem in a different way, yielding predictions that respect the nominal perturbative accuracy for observable that are stable under the inclusive evaluation of radiative effects, but differ in the treatment of higher-order terms. The matching ambiguity, parametrized in different ways, should be considered as an additional source of theoretical uncertainty, together with the one usually expressed by the choice of the renormalization/factorization scales.
- In the MC codes the resummation to all orders of some classes of contributions is done by means of a Parton Shower (PS) approach, with leading logarithmic (LL) accuracy in the log of the gauge boson transverse momentum. There are differences of subleading logarithmic order in the available PS algorithms, which yield a difference in the final predictions.
- The PS codes are usually interfaced with models that describe non-perturbative effects of the strong interaction at low energy scales; the parameters of these models are usually tuned to reproduce some relevant distribution,

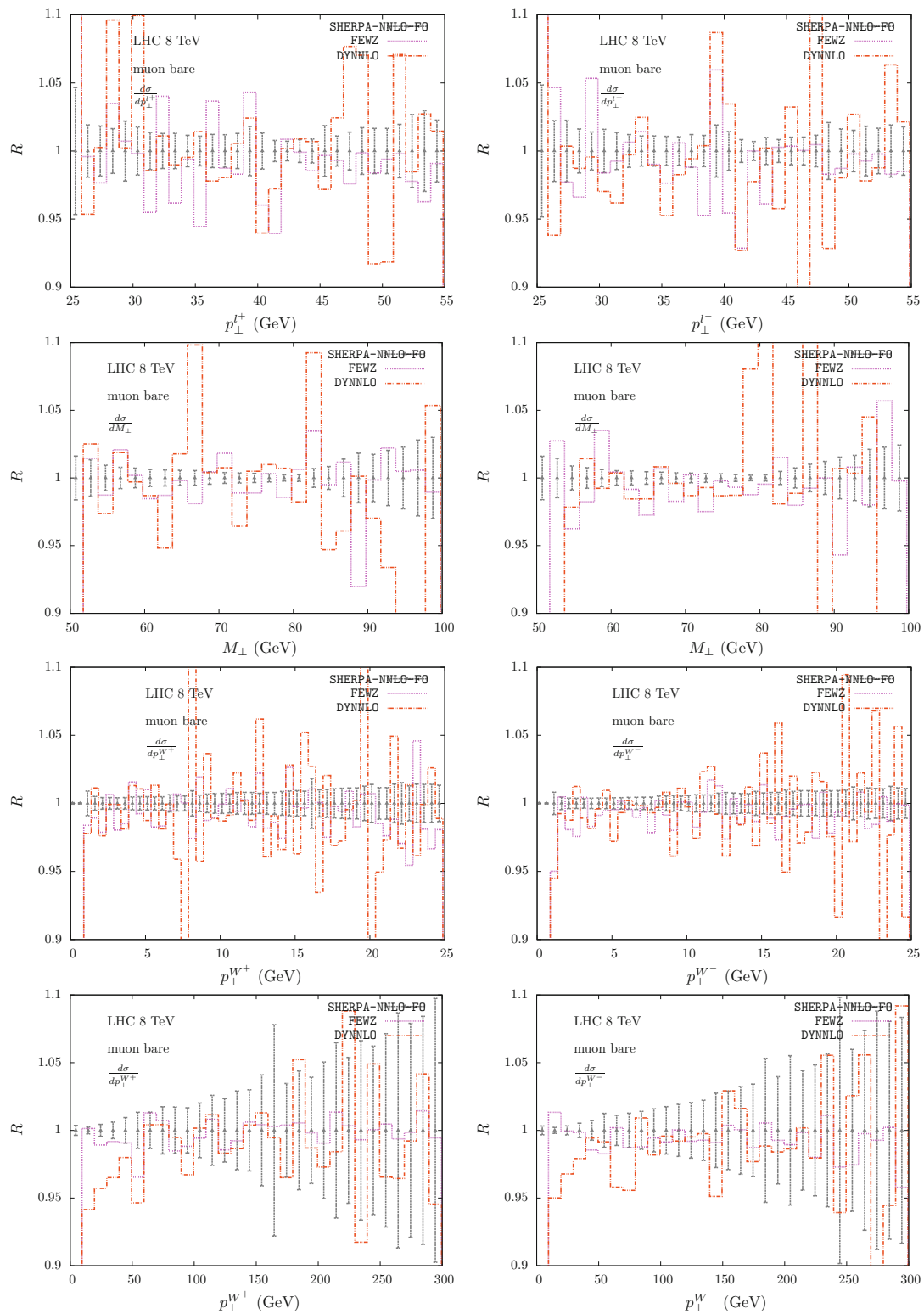


Fig. 15 Comparison of NNLO QCD predictions by DYNLLO, FEWZ and SHERPA-NNLO-FO for $pp \rightarrow W^\pm \rightarrow \mu^\pm \nu_\mu + X$ for $\mu^+ \nu_\mu$ (left plots) and $\mu^- \bar{\nu}_\mu$ (right plots) final states. Comparison of the lepton

transverse momentum (upper plots), transverse mass (middle plots) and lepton-pair transverse momentum (lower plots) distributions, obtained in the benchmark setup with ATLAS/CMS cuts at the 8 TeV LHC

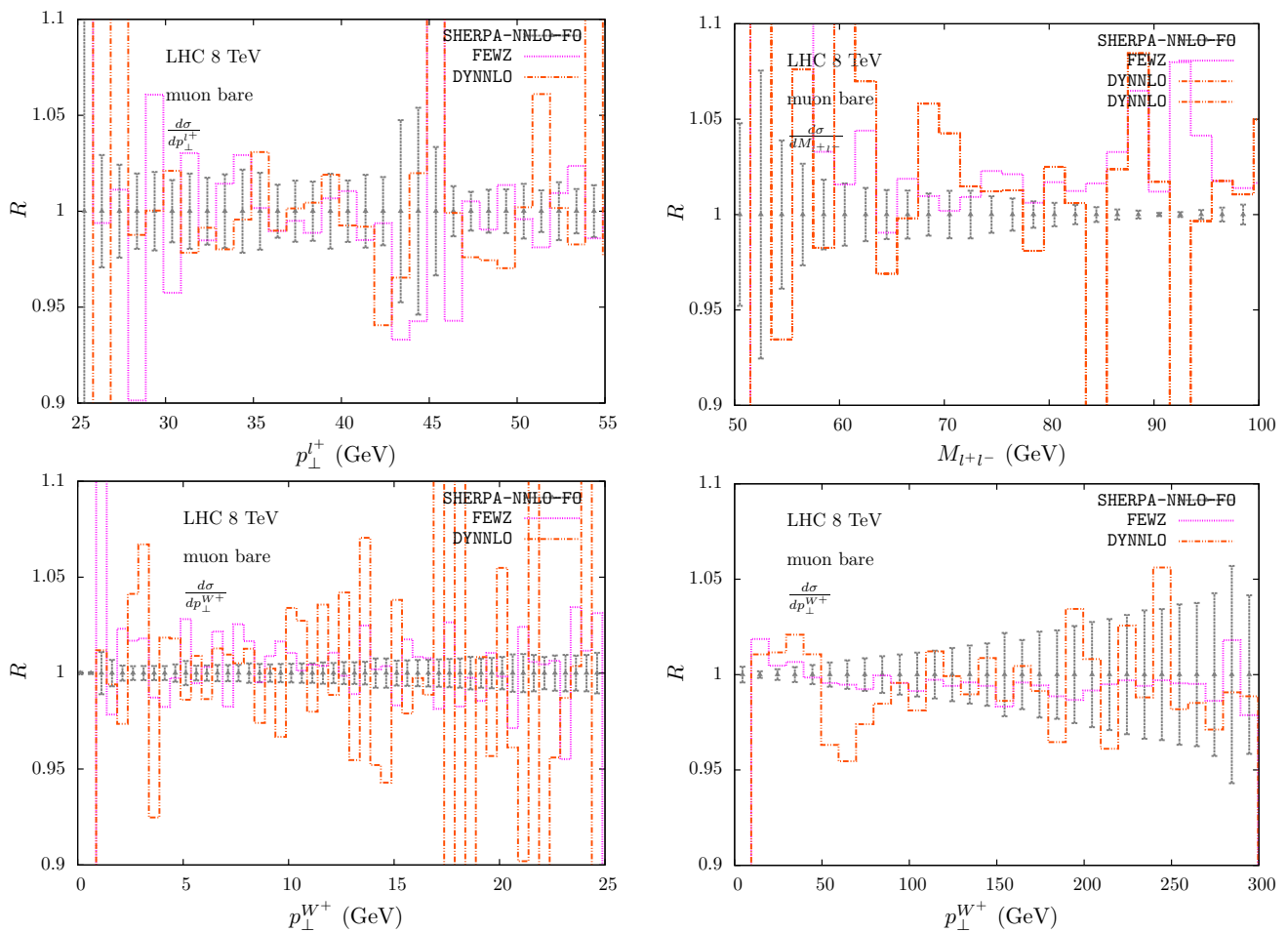


Fig. 16 Comparison of NNLO QCD predictions by DYNLO, FEWZ and SHERPA-NNLO-FO for $pp \rightarrow \gamma, Z \rightarrow \mu^+\mu^- + X$. Comparison of the lepton transverse momentum (*upper left*), lepton-

pair invariant mass (*upper right*) and lepton-pair transverse momentum (*lower plots*) distributions, obtained in the *benchmark* setup with ATLAS/CMS cuts at the 8 TeV LHC

but their choice (and the corresponding quality of the description of the data) represents an additional source of ambiguity in the predictions.

In the study of the codes which match resummed and fixed-order results,⁵ the presence of the entangled sources of differences listed above does not allow a tuned comparison of ‘central’ values, as done with fixed order results, and requires a careful interpretation of observed differences.

In Figs. 20, 21, 22 and 23 we expose the impact of higher-order corrections, $\mathcal{O}(\alpha_s^2)$ and higher, in units of the NLO QCD results. In this way we appreciate where the higher orders play a crucial role, how well the NNLO QCD results

are approximated by a NLO+PS formulation (Figs. 20, 21), and the impact of matching the NNLO QCD fixed-order calculation and a QCD-PS (Figs. 22, 23). The disadvantage of this choice of presenting the results is that for some observables the NLO QCD is not a sensible lowest order approximation.

3.3.5 Comparison of (NLO+PS)-QCD vs NNLO QCD results

The POWHEG +PYTHIA and the SHERPA NLO+PS NLO+PS predictions are based on the same exact matrix elements present in all the codes that have NLO QCD accuracy for the total cross section, but they add the higher-order effects due to multiple parton emissions to all orders via a QCD-PS, with two different matching procedures. At $\mathcal{O}(\alpha_s^2)$ they both have a partial overlap with those by the fixed-order NNLO results, because of the inclusion of the LL terms.

⁵ We note that the public codes RESBOS [52–54] and MC@NLO [48] also provide predictions for matched NLO QCD+resummed initial-state contributions for DY processes but are not used in this study.

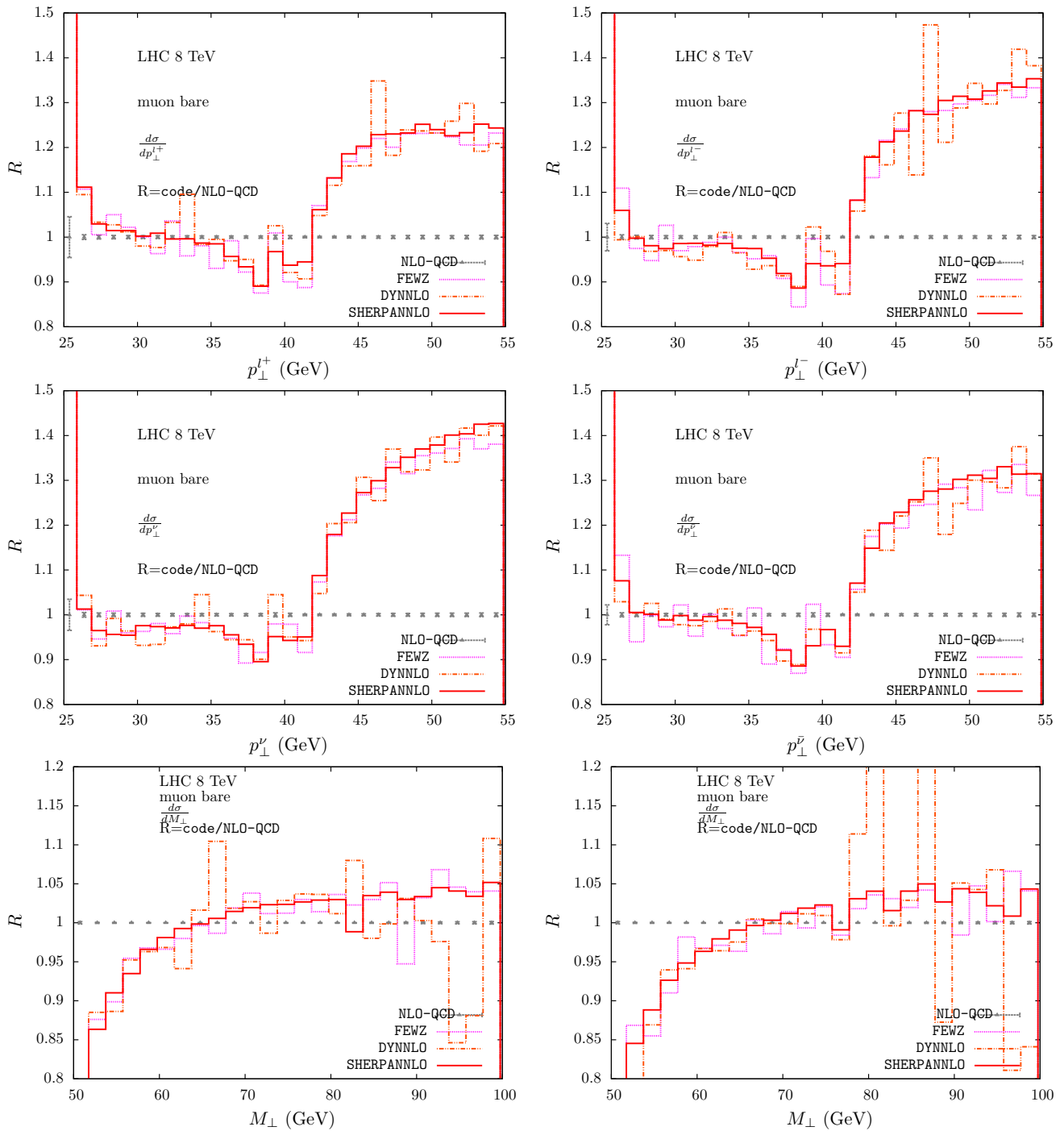


Fig. 17 NNLO QCD effects, expressed in units of NLO QCD, in $pp \rightarrow \mu^\pm \nu_\mu + X$ in the benchmark setup with ATLAS/CMS cuts at the 8 TeV LHC, for $\mu^+ \nu_\mu$ (left plots) and $\mu^- \bar{\nu}_\mu$ (right plots) final states. Comparison of the lepton transverse momentum (upper plots), neutrino

transverse momentum (middle plots) and transverse mass (lower plots) distributions, as predicted by SHERPA-NNLO-FO (red), FEWZ (pink) and DYNLNLO (orange dashed)

It should be stressed that the POWHEG+PYTHIA and the SHERPANLO+PS NLO+PS codes do not have NNLO QCD accuracy for the total cross section nor do they have an accurate description of the large lepton-pair transverse momen-

tum region, where exact matrix element effects for the second emission are important. On the other hand, they include the resummation to all orders of multiple parton emissions, which is important to yield a sensible description of the

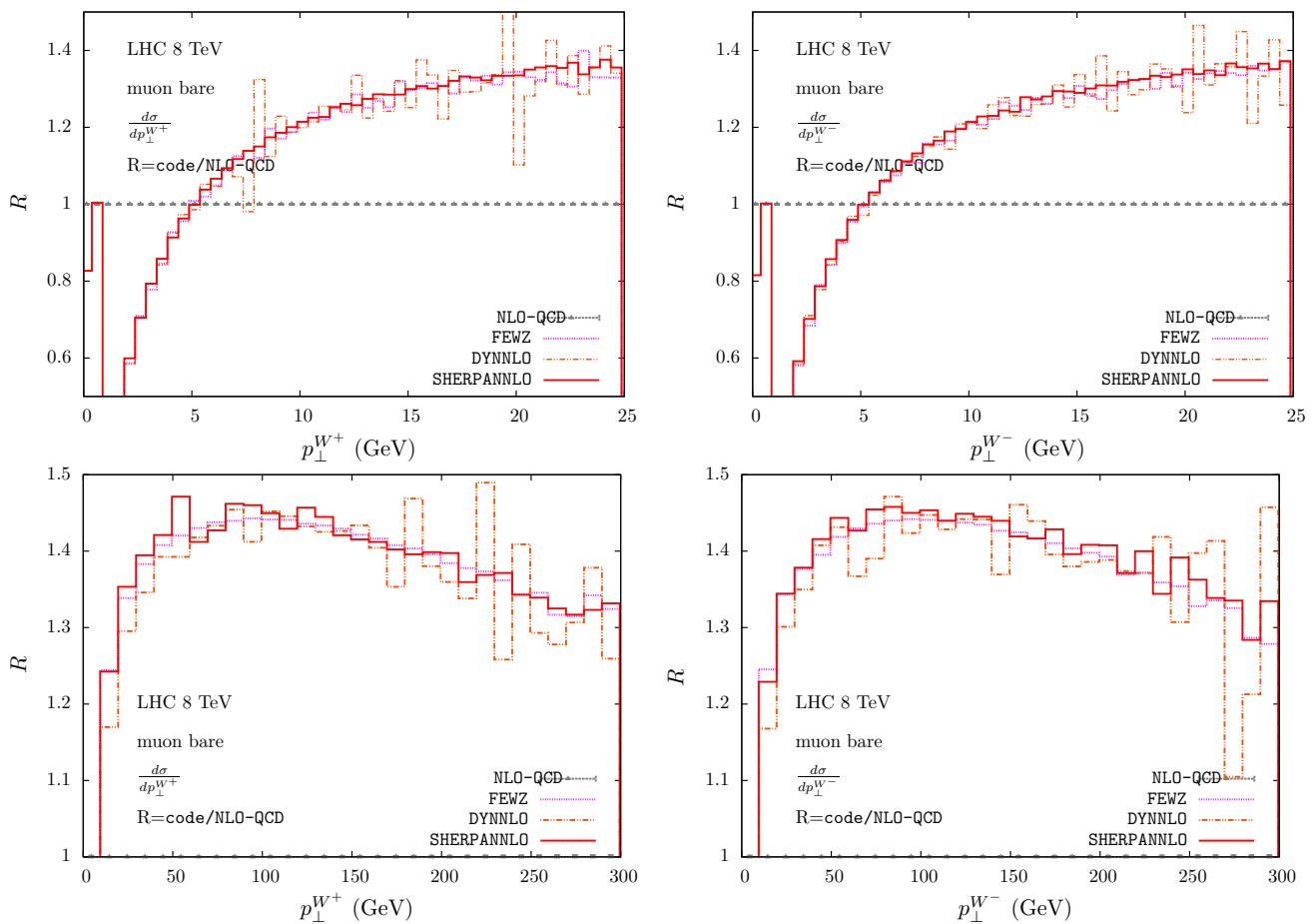


Fig. 18 NNLO QCD effects, expressed in units of NLO QCD, in $pp \rightarrow \mu^\pm \nu_\mu + X$, in the benchmark setup with ATLAS/CMS cuts at the 8 TeV LHC, for $\mu^+ \nu_\mu$ (left plots) and $\mu^- \bar{\nu}_\mu$ (right plots) final states. Comparison of the lepton-pair transverse momentum distributions in

the range $[0, 25]$ GeV (upper plots) and in the range $[0, 300]$ GeV (lower plots), as predicted by SHERPA-NNLO-FO (red), FEWZ (pink) and DYNNLO (orange dashed)

small lepton-pair transverse momentum region, of the low- ϕ^* region of the ϕ^* distribution or of the Jacobian peak of the single lepton transverse momentum distribution.

We observe in Figs. 20 and 21 that the QCD-PS corrections in POWHEG +PYTHIA have a small impact on the invariant-mass (NC DY) or transverse-mass (CC DY) distributions (middle plots); the correction is slowly varying over the entire mass range, with the exception of the lower end of the distribution, where the acceptance cuts yield a distinction between one-emission and multiple-emissions final states.

In the same figures, we show the corrections to the lepton transverse momentum distribution (upper plots). We observe at the jacobian peak the distortion due to the fact that in this region a fixed order description is not sufficient to describe this observable. Below the jacobian peak the corrections of $\mathcal{O}(\alpha_s^2)$ and higher become smaller for decreasing values of the transverse momentum, before reaching the acceptance cut. Above the jacobian peak, the QCD-PS effects follow those obtained at NNLO QCD. This result can be interpreted

by observing that the lepton transverse momentum has two components, one from the gauge boson decay at LO and one due to the gauge-boson recoil against QCD radiation; immediately above the jacobian peak, the recoil component is characterized by a small value of the lepton-pair transverse momentum; in this region the collinear approximation on which the PS is based is quite accurate, and thus the second real emission in the PS approximation is close to the exact result. For larger values of the lepton-pair transverse momentum the QCD-PS becomes inadequate to describe the spectrum; the role of the first and second order exact matrix element corrections is shown in the lower plots of Figs. 20 and 21. The difference between the two approximations vary between zero and 40% in the interval $p_\perp^V \in [70, 300]$ GeV.

The resummation of multiple parton emissions to all orders via the PS makes the distribution vanish in the limit of vanishing lepton-pair transverse momentum, as it is physically expected (Sudakov suppression). The size of the QCD-PS correction in units NLO QCD is infinitely negative when

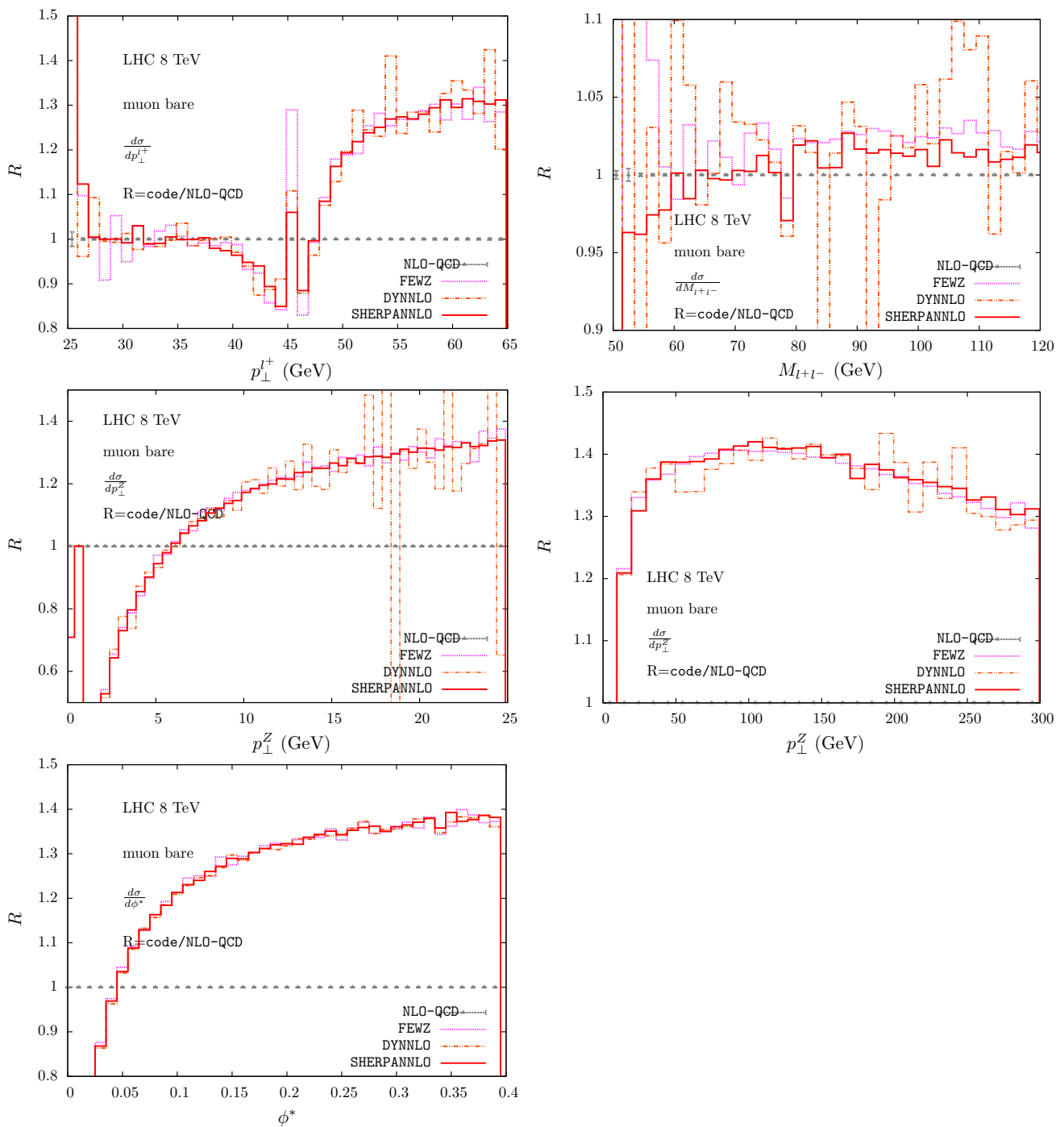


Fig. 19 NNLO QCD effects, expressed in units of NLO QCD, in $pp \rightarrow \mu^+\mu^- + X$, in the benchmark setup with ATLAS/CMS cuts at the 8 TeV LHC. Comparison of the lepton transverse momentum (upper left), lepton-pair invariant mass (upper right), lepton-

pair transverse momentum (middle plots), ϕ^* (lower plot) distributions, as predicted by SHERPA-NNLO-FO (red), FEWZ (pink) and DYNMLO (orange dashed)

$p_{\perp}^V \rightarrow 0$; this peculiar result is a consequence of the choice of the NLO QCD prediction as unit to express the higher-order effects, which is inappropriate in this specific corner of the phase-space. This comment is at variance with respect

to the one for the NNLO QCD corrections: also in that case the size of the correction is infinitely large, but only because at each fixed order the distribution diverges, each time with a different coefficient.

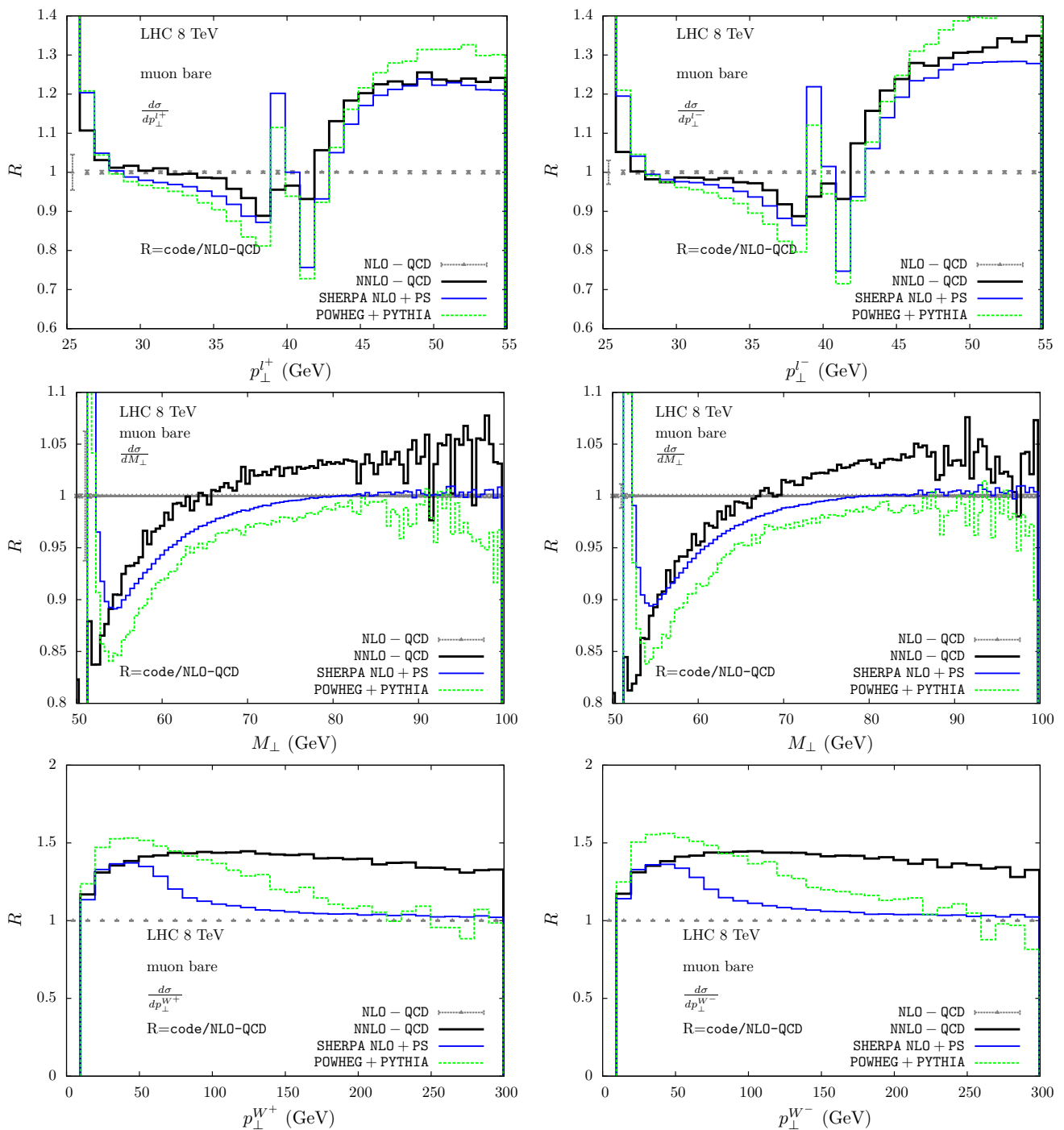


Fig. 20 Higher-order QCD effects, expressed in units of NLO QCD, in $pp \rightarrow \mu^\pm \nu_\mu + X$, due to the matching of resummed and fixed order results, in codes with NLO accuracy: POWHEG + PYTHIA (green) and SHERPA NLO+PS (blue). The fixed-order NNLO QCD results are shown in black. Comparison of results for the lepton transverse momen-

tum (upper plots), lepton-pair transverse mass (middle plots) and transverse momentum (lower plots) distributions, for $\mu^+ \nu_\mu$ (left plots) and $\mu^- \bar{\nu}_\mu$ (right plots) final states, obtained with ATLAS/CMS cuts at the 8 TeV LHC

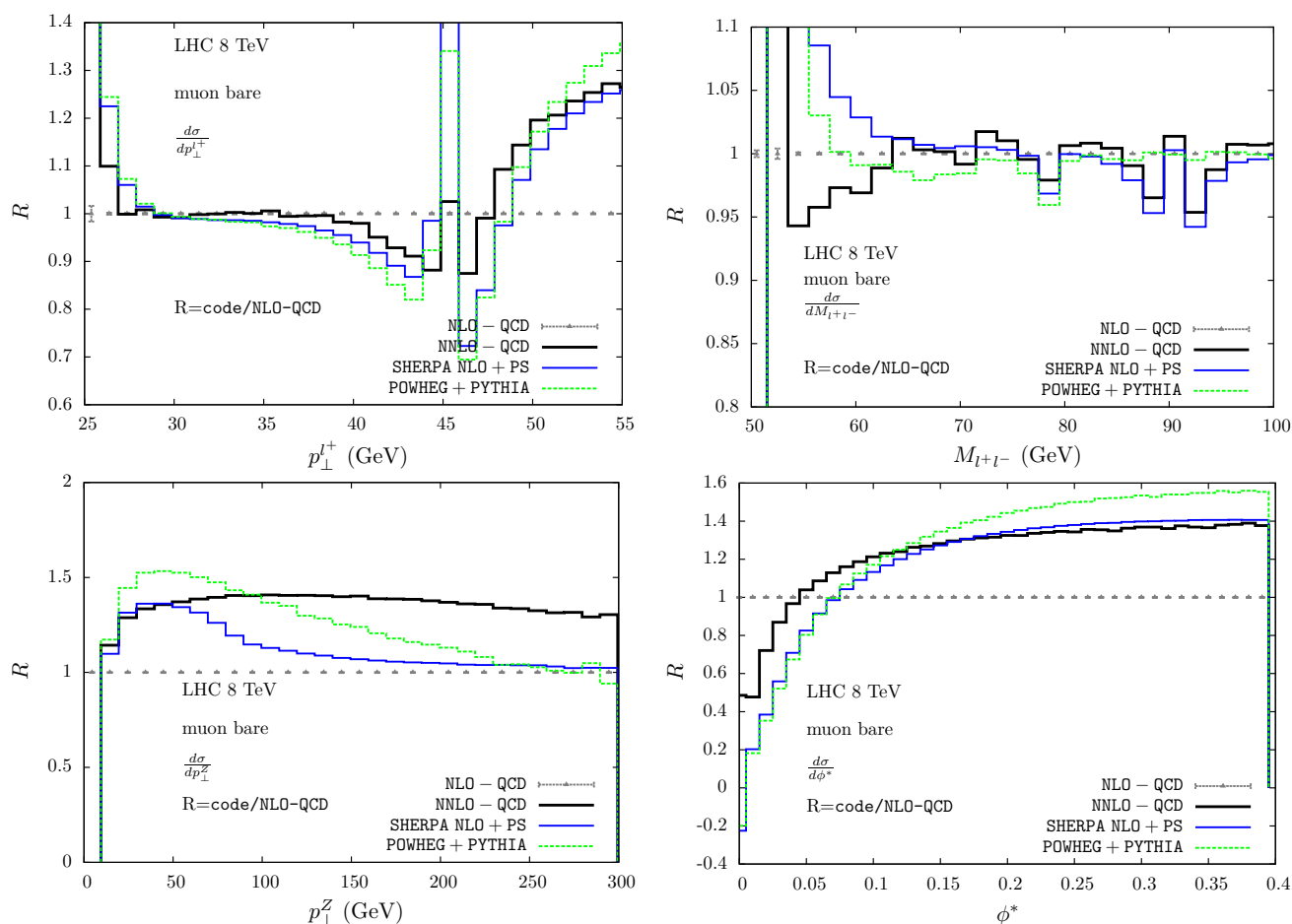


Fig. 21 Higher-order QCD effects, expressed in units of NLO QCD, in $pp \rightarrow \mu^+\mu^- + X$, due to the matching of resummed and fixed order results, in codes with NLO accuracy: POWHEG+PYTHIA (green) and SHERPA NLO+PS (blue). The fixed-order NNLO QCD results are

shown in black. Comparison of results for the lepton transverse momentum (upper left), lepton-pair invariant mass (upper right), transverse momentum (lower left) and ϕ^* (lower right) distributions, obtained with ATLAS/CMS cuts at the 8 TeV LHC

3.3.6 Comparison of different (NNLO+PS)-QCD matching schemes

The matching of NNLO QCD results with a QCD-PS has been achieved first in the `MINLO` approach [50,51,55]. In the DY case the calculation has been implemented in a code based on POWHEG+MINLO combined with DYNLO, and henceforth denoted DYNLOPS [6]. This method is based on the NLO+PS formulation of the original hard process plus one-jet, and supplements it with Sudakov form factors that lead to finite predictions as the additional jet becomes unresolved. The NNLO accuracy is achieved by reweighing via a pre-tabulated phase-space dependent K-factors.

Another NNLO+PS matching approach is called UN2LOPS [21,56] and it is a variant of the UNLOPS [57] method. UNLOPS is one of the unitary merging techniques recently developed to merge multi-jet NLO calculations while preserving the inclusive cross section of the process with the lowest jet multiplicity. In UN2LOPS, by only keep-

ing events with resolvable QCD emissions, which are available as part of the NNLO calculation, the description of the DY processes at large transverse momentum becomes equivalent to the study of $W(Z)$ plus one additional jet at NLO. The remainder of the phase space is filled by a calculation at NNLO, with a corresponding veto on any QCD activity, forming the zero jet bin. This is essentially the phase space slicing method, and the goal of the UN2LOPS approach is to merge the two parts after the PS is added. Only the part of $W(Z)$ plus one jet at NLO is matched with PS, where any standard methods could be used. Events in the zero jet bin should not be showered to avoid double counting because QCD radiation has already been described by the PS matched $W(Z)$ plus one jet process at NLO.⁶ The merging is done by suppressing the divergence in $W(Z)$ plus one jet via the shower veto algorithm in which the vetoed events are added

⁶ Except for the pure two-loop virtual contribution, which contributes to $W(Z)$ plus one jet at NNLO if showered.

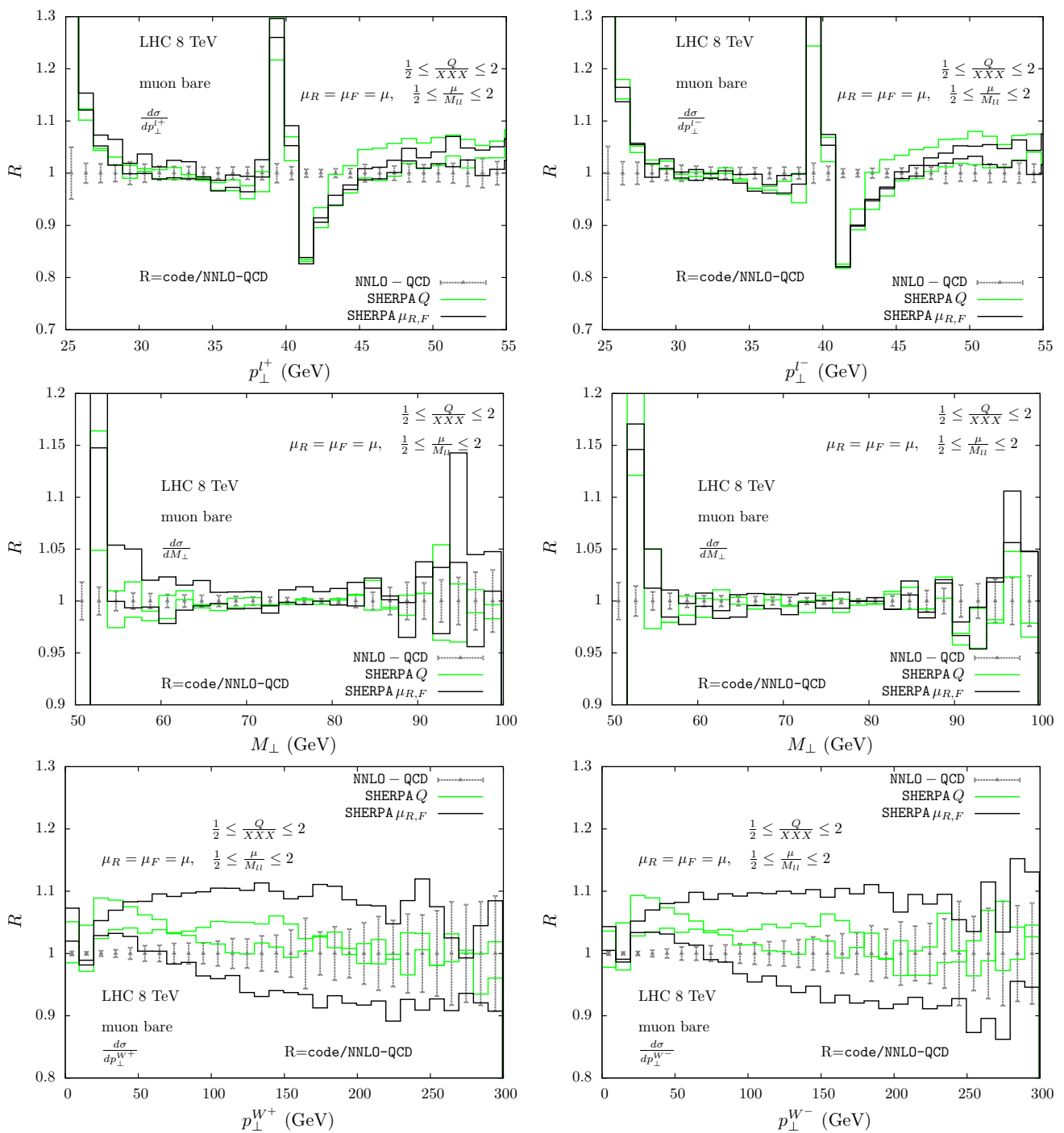


Fig. 22 Higher-order QCD effects, expressed in units of NNLO QCD, due to the matching of resummed and fixed order results, in codes with NNLO accuracy, for the processes $pp \rightarrow \mu^+ \nu_\mu + X$ (left plots) and $pp \rightarrow \mu^- \bar{\nu}_\mu + X$ (right plots), obtained with ATLAS/CMS cuts at the 8 TeV LHC. The SHERPA NNLO+PS uncertainty bands due to renor-

malization/factorization scales (black) and shower scale (green) variations are shown for the lepton transverse momentum (upper plots), neutrino transverse momentum (middle plots) and transverse mass (lower plots) distributions

back to the zero jet bin to preserve the inclusive cross section. In order to generate physically meaningful results, the separation cut scale q_\perp must be smaller than the terminating scale of the parton shower. In contrast to the $\overline{\text{MiNLO}}$ method,

real-emission configurations do not receive a contribution from the NNLO calculation because two-loop virtual contributions in the 0-jet bin are not showered. The resulting difference is beyond NNLO accuracy for the original hard process.

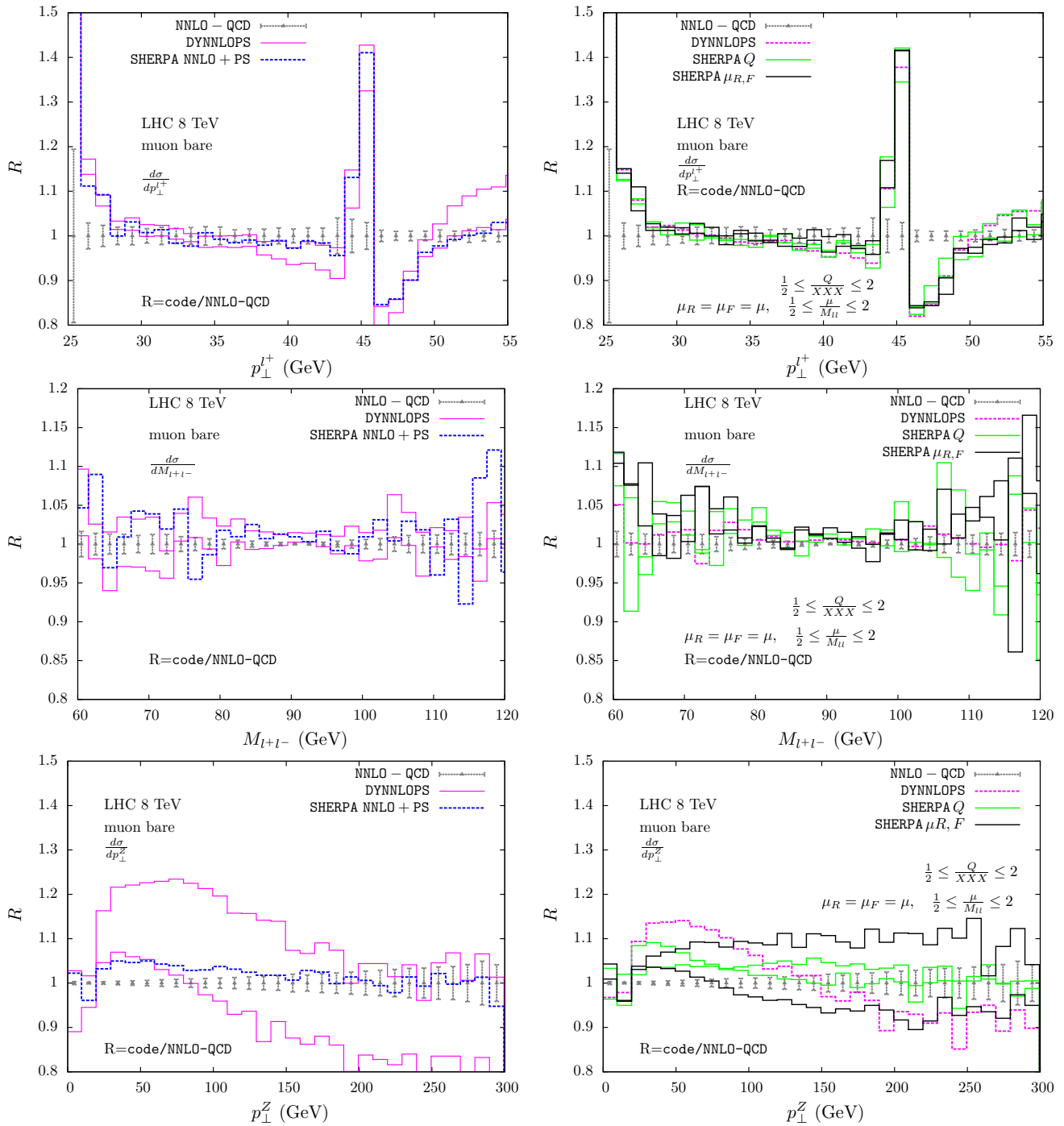


Fig. 23 Higher-order QCD effects, expressed in units of NNLO QCD, due to the matching of resummed and fixed order results, in codes with NNLO accuracy, for the process $pp \rightarrow \mu^+\mu^- + X$, obtained with ATLAS/CMS cuts at the 8 TeV LHC. The SHERPA NNLO+PS uncertainty bands for renormalization/factorization scales (black) and shower scale (green) variations are shown in the right plots. The DYNLNLOPS (pink) uncertainty bands are

shown in the left plots. Cfr. the text for details about the definition of the bands. The central scales results are presented with dashed lines for SHERPA NNLO+PS (blue) and DYNLNLOPS (pink). Results are shown for the lepton transverse momentum (upper plot), lepton-pair invariant mass (middle plots) and transverse momentum (lower plot) distributions

Formally the resummation of UN2LOPS is limited by the accuracy of the parton shower, while in the `MINLO` method, a higher logarithmic accuracy of the first emission can be achieved with analytic Sudakov form factor for the corresponding observable.⁷ Nevertheless, for other observables or subsequent emissions, resummation in `MINLO` is only as accurate as the parton shower can provide. The calculation of the DY processes in the UN2LOPS approach has been implemented in the code `SHERPA NNLO+PS`.

Both these two matching approaches should not be considered as a final answer to the problem of matching NNLO fixed order with PS results, but rather as a first step towards more general methods.

We note that results for Drell–Yan production at NNLL'+NNLO matched to a PS in the `GENEVA` Monte-Carlo framework are presented in Ref. [58], but not included in this study.

In Fig. 22 we show the results obtained with the `SHERPA NNLO+PS` code, in the case of CC DY, and compare them to the corresponding NNLO fixed-order predictions. We present two different uncertainty bands: the first one, in black in the plots, is obtained by varying the renormalization μ_R and factorization μ_F scales of the underlying fixed order calculation, with $\mu_R = \mu_F$ and $1/2 \leq \mu_R/M_H \leq 2$; the second one, in green in the plots, is obtained by varying the shower scale Q of the QCD-PS in the interval $1/2 \leq Q/M_H \leq 2$.

In Fig. 23 we show the results obtained with the two codes `SHERPA NNLO+PS` and `DYNNLOPS`, in the case of NC DY, and compare them with each other and with the corresponding NNLO fixed-order predictions. The `SHERPA NNLO+PS` uncertainty bands have been computed as described above, while in the `DYNNLOPS` case the band is obtained by varying by a factor 2 up and down independently all renormalization and factorization scales appearing in the underlying `MINLO` procedure (at variance with the report setup, in the `MINLO` approach both renormalization and factorization scales are set equal to the gauge boson transverse momentum), keeping their ratio between 1/2 and 2. This leads to seven different scale choices. Independently of this we vary by a factor 2 up and down the renormalization and factorization scale in the underlying `DYNNLO` calculation keeping the two equal. This leads to three different scale choices. As these scale choices are taken to be independent, this leads to $3 \cdot 7 = 21$ scale choices of which the envelope is taken as the uncertainty band. The procedure is described in more detail in [6]. Since the procedures used to evaluate the uncertainty bands are different for the two codes, we present separately in the two columns: the `DYNNLOPS` band and

the central scales `SHERPA NNLO+PS` prediction (left plots) and the two `SHERPA NNLO+PS` bands and the central scales `DYNNLOPS` prediction (right plots).

As expected, for the invariant mass distribution of the lepton pair, in Fig. 23, all predictions agree very well. In particular in the central region, closer to the peak, the large statistics allow us to appreciate that also uncertainty bands are very similar among the two NNLO+PS results, and that the central line of one lies well within the (very narrow) uncertainty band of the other tool. For smaller and larger invariant masses, the conclusions are similar, although the limited statistics do not allow such a precise comparison.

Turning to the lepton transverse momentum, p_{\perp}^l , spectrum, in Fig. 23 one observes that in the range where this distribution is NNLO accurate (i.e. where p_{\perp}^l is less than half the mass of the Z boson), the results of the two NNLO+PS codes are again in good agreement with each other and with the NNLO QCD reference line. The uncertainty band is very thin, as expected, until one approaches the Jacobian peak region. As explained in the previous section, in this region resummation effects are important. Although the two NNLO+PS results are obtained with very different approaches, the mutual agreement is very good. One should notice however, that to the left of the Jacobian peak, the NNLO+PS result from `DYNNLOPS` seems to depart from the pure fixed-order results a few bins earlier than the one from `SHERPA NNLO+PS`. These differences are likely to be due to the differences in how events are generated close to the Sudakov peak in p_{\perp}^Z , which is a phase-space region where resummation is crucial, and the two NNLO+PS calculations perform it using very different approaches. Therefore differences at the few percent level are not unexpected. The differences between the NNLO+PS and the fixed-order results at the lower end of the p_{\perp}^l spectrum have already been noticed and commented on earlier in this chapter. For transverse momenta larger than $M_Z/2$, the two NNLO+PS results rapidly start to re-approach the fixed-order line, which in this region is NLO QCD accurate. However, towards the end of the plotted range, some differences among the results can be observed: firstly, the `DYNNLOPS` result exhibits a moderately harder spectrum, which would probably be more evident at higher p_{\perp}^l values. Secondly, the uncertainty band of the two NNLO+PS results (the one due to the μ_R, μ_F scale variation only) is larger in the `DYNNLOPS` result than in the `SHERPA NNLO+PS` one. Both these differences can be understood by looking at the differences amongst the results for the vector-boson transverse momentum in the medium to low range ([0, 50] GeV), which is the phase space region where the bulk of the events with p_{\perp}^l approximately equal to [55, 60] GeV are generated.

The transverse momentum spectrum p_{\perp}^Z of the lepton pair is the observable that exposes most clearly the differences between the two results. For the purpose of this comparison,

⁷ The analytic Sudakov form factor is generally observable-dependent (not fully differential); in the application to DY here, the relevant observable used by `MINLO` is the $W(Z)$ transverse momentum p_{\perp}^V .

the more relevant difference to explain is the difference in shape (and absolute value) for $p_{\perp}^Z \in [20, 100]$ GeV, that we will address in the next paragraph. At very high p_{\perp}^Z , differences are also fairly large, but in that region they can be mostly attributed to the `MINLO` scale choice: when p_{\perp}^Z is large (above M_Z), the `MINLO` Sudakov form factor switches off, but the strong coupling is evaluated at p_{\perp}^Z , whereas in `SHERPA NNLO+PS` and in the fixed-order calculation it is evaluated at the dilepton invariant mass m_{ll} .

The range $p_{\perp}^Z \in [20, 50]$ GeV is a “transition” region, since it is the region where higher-order corrections (of fixed-order origin as well as from resummation) play a role, but none of them is dominant. Due to Sudakov suppression, in `DYNNLOPS` the first two bins of the p_{\perp}^Z distribution are suppressed compared to the fixed-order results; in turn, the unitarity fulfilled by the matching procedure, in order to respect the total cross section normalization, spreads part of the cross section close to the singular region across several bins in p_{\perp}^Z , including those to the right of the Sudakov peak.

The `SHERPA NNLO+PS` results instead are closer to the fixed-order prediction in the first bins, which is may be a consequence of the PS not being applied to the events of the 0-jet bin.

Since the first bins are the region where most of the cross-section is sitting, a relatively small difference among the two NNLO+PS results in the peak region will show up, greatly amplified, in the transition region (to preserve the total cross section). At, say, 50 GeV, both the NNLO+PS results have a cross section larger than the pure fixed-order, with `DYNNLOPS` larger than `SHERPA NNLO+PS`. Moreover, although at large p_{\perp}^Z the cross section is small, the `DYNNLOPS` result is, by construction, below the others, as explained previously. This difference must also be compensated, and this takes place in the transition region too.

For the `DYNNLOPS` results, the scale choice in the transition region is inherited from the underlying `MINLO` simulation. This means that the conventional factor 1/2 or 2 is applied to a dynamical scale choice ($\mu = p_{\perp}^Z$), and this fact helps in explaining why not only the result is larger than the fixed order and the `SHERPA NNLO+PS` distributions, but it also exhibits a different shape and uncertainty band. In the `SHERPA NNLO+PS` approach, effects similar to the latter in the transition region are mainly taken into account by the variation of the resummation scale, as the corresponding plot supports. In fact, this is the dominant uncertainty of the `SHERPA NNLO+PS` result in the transition region.

In spite of all the aforementioned details, one should also notice that for p_{\perp}^Z , the two NNLO+PS results are mutually compatible over almost all the entire spectrum, once the uncertainty bands are considered.

3.4 Impact of EW corrections on W and Z boson observables in the *benchmark* setup

In Sect. 3.3 we presented the impact of higher-order QCD corrections, using the fixed-order NLO QCD results (which have been demonstrated to be fully under control) as unit to express the relative effect of different subsets. We follow the same approach now to discuss the EW corrections.

We discuss in Sect. 3.4.1 the main features of the NLO EW corrections, with special emphasis on the observables that are relevant to EW precision measurements. In Sects. 3.4.2–3.4.8, we present the impact of different subsets and combinations of higher-order corrections and if not stated otherwise express their effect using as a unit the results computed at NLO EW.

3.4.1 NLO EW corrections

At LO the DY CC and NC processes are purely of EW nature (the cross section is of $\mathcal{O}(G_{\mu}^2)$). The typical size of the impact of NLO EW corrections on the total cross section is of $\mathcal{O}(\alpha)$, i.e. at the per cent level. However, it is important to stress that the real radiation may have a much larger impact on the differential distributions, in particular in the presence of acceptance cuts. At NLO EW all the electrically charged particles may radiate a real photon. The distinction between initial state, final state and interference effects has been discussed not only in the NC, but also in the CC case [42]. It is important to stress that the potentially large effects due to initial state collinear emissions are re-absorbed in the definition of the physical proton PDFs, leaving a numerically small remnant. On the other hand the final state radiation effects are phenomenologically very important, because they modify the momenta of the final state leptons, affecting all the relevant distributions. We distinguish between observables whose line shape is relevant for the determination of the gauge boson masses and widths and other quantities whose normalization is important to constrain the proton PDFs or to correctly describe the background to new physics searches.

To the first group belongs the single lepton transverse momentum distributions and the lepton-pair transverse mass distributions around the W (Z) Jacobian peak, and, in the NC channel, at the Z resonance, the lepton-pair invariant mass distribution. In Fig. 24, we show the impact of NLO EW corrections relative to LO on these distributions. The largest, negative, corrections arise at the (Jacobian) peak of each distribution. The effect can be understood as a combination of the properties of the gauge boson production mechanism, which is peaked at the (W) Z boson mass, with the energy/momentum loss due to final state radiation; the latter reduces the actual value of the measured observables, depleting the peak and enhancing the left tail of the resonant shape. Since after QED mass factorization there are no large loga-

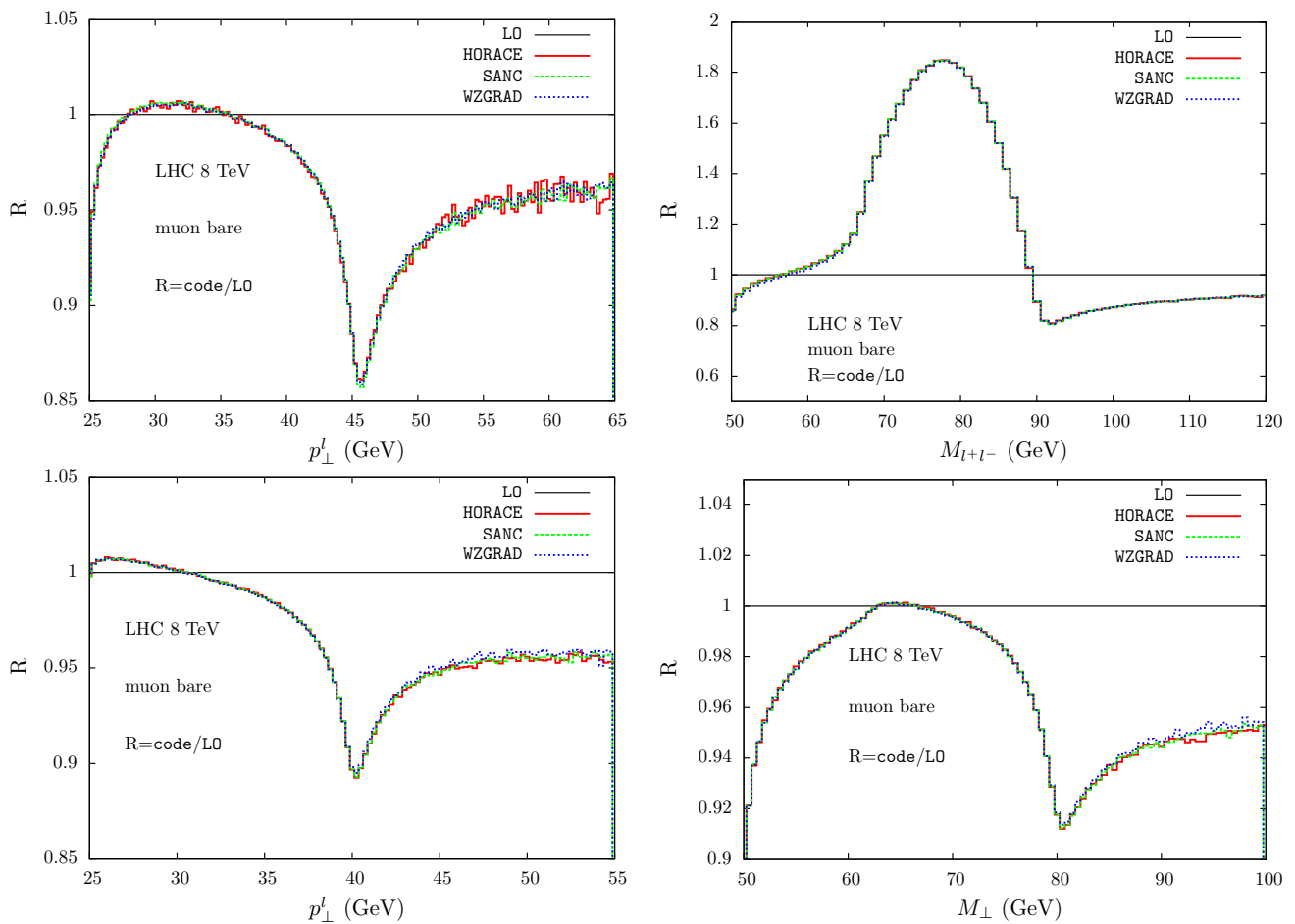


Fig. 24 Impact of NLO EW corrections in NC and CC DY processes with bare muon(s) at the 8 TeV LHC with ATLAS/CMS cuts, expressed in units of the corresponding LO, in the *benchmark* setup, evaluated with different codes. In the *upper panels*, for the $pp \rightarrow \mu^+ \mu^- + X$ process,

the lepton transverse momentum (*left*) and the lepton-pair invariant mass distributions are shown; in the *lower panels*, for the $pp \rightarrow \mu^+ \nu_\mu + X$ process, the lepton transverse momentum (*left*) and the lepton-pair transverse mass distributions are shown

rections due to ISR, the impact of initial state radiation on the lepton-pair and on the single lepton transverse momentum distributions is suppressed by the smaller coupling constant with respect to the QCD case; in the QED case the largest fraction of the corrections to these observables is due to final state radiation.

Among the observables which are sensitive to the absolute normalization of the process, we have the single lepton pseudo-rapidity and the lepton-pair rapidity distributions, and also the large-mass tail of the lepton-pair invariant mass distribution. The former receive a correction which is very close in size to the one of the total cross section, and which is quite flat along the whole (pseudo-)rapidity range (the FSR corrections and the redefinition of the couplings via renormalization do not modify the LO kinematics, yielding, in first approximation, a global rescaling of the distributions).

The NLO EW virtual corrections become large and negative in the tails of the single-lepton transverse momentum,

lepton-pair invariant and transverse-mass distributions, when at least one kinematical invariant becomes large, because of the contribution of the purely weak vertex and box corrections. This effect of the so-called EW Sudakov logarithms can not be re-absorbed in a redefinition of the couplings and is process dependent. A recent discussion of the DY processes in the Sudakov regime can be found, e.g., in Refs. [59,60].

The size of the effects due to the emission of real photons depends on the experimental definition of the lepton, i.e. on the recombination procedure of the momenta of the lepton with those of the surrounding photons. The radiation of photons collinear to the emitting lepton has a logarithmic enhancement, with a natural cut-off provided by the lepton mass. These mass logarithms cancel completely in the total inclusive cross section (Kinoshita–Lee–Nauenberg theorem), but leave an effect on the differential distributions. The recombination of the photons and lepton momenta effectively acts like the integration over the collinear corner of the

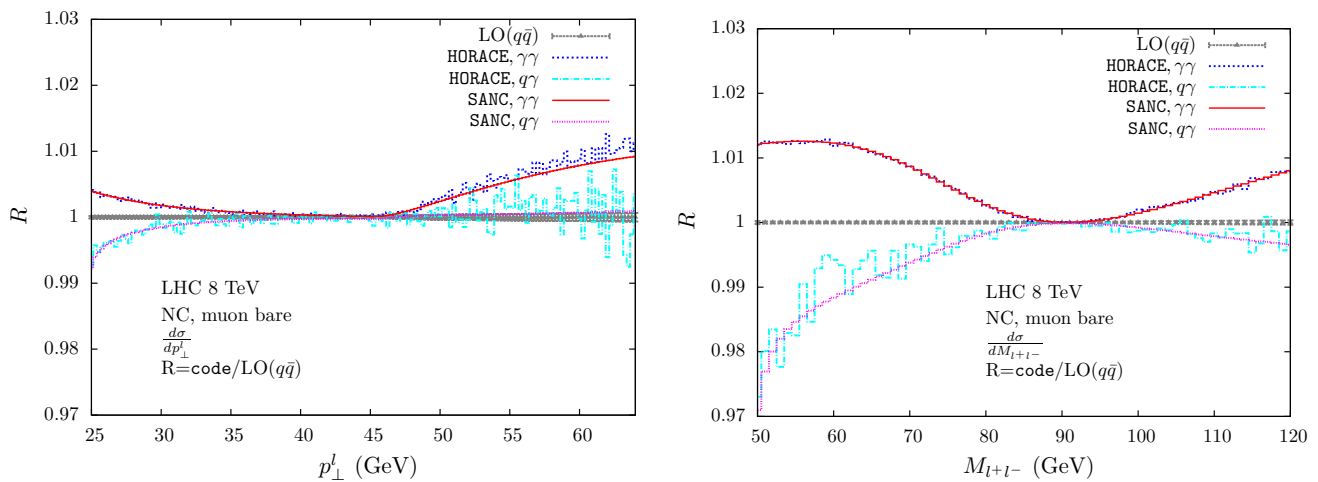


Fig. 25 Relative effect of photon-induced subprocesses in $pp \rightarrow \mu^+ \mu^- + X$, compared to the LO $q\bar{q}$ results in the G_μ scheme, both evaluated with the NNPDF23_lo_as_0130_qed PDF set at the 8 TeV LHC with ATLAS/CMS cuts. Results are shown for the lepton trans-

verse momentum (*left plot*) and the lepton-pair invariant mass (*right plot*) and are obtained with HORACE and SANC. Separately shown are the contributions of the LO $\gamma\gamma \rightarrow \mu^+ \mu^-$ subprocess and the $\mathcal{O}(\alpha)$ $\gamma q \rightarrow \mu^+ \mu^- q$ subprocesses

photon phase space, yielding a cancellation of the singular contribution from that region; as a consequence, the logarithmic enhancement of the corrections is reduced, as if the lepton had acquired a heavier effective mass.

3.4.2 Photon-induced processes

The $\mathcal{O}(\alpha)$ corrections develop initial-state QED collinear singularity, which have to be subtracted from the partonic cross section and can be re-absorbed in the definition and evolution of the proton PDFs, in close analogy to what is done in QCD. In turn, the QED terms present in the evolution kernel of these PDFs imply the existence of a photon density inside the proton, which allows the contribution of partonic subprocesses initiated by photons. The latter are present already at LO in the case of the NC DY process, $\gamma\gamma \rightarrow l^+ l^-$, or they appear at NLO in both the NC and CC DY processes, $\gamma q(\bar{q}) \rightarrow l^+ l^- q(\bar{q})$ and $\gamma q(\bar{q}) \rightarrow l\nu q'(\bar{q}')$.

In Fig. 25 we present the evaluation at hadron level of these contributions in the case of the NC DY process, done with the proton PDF set NNPDF2.3_lo_as_0130_qed, using the codes HORACE and SANC. We show the ratios $R = 1 + d\sigma(\gamma\gamma, \gamma q)/d\sigma(q\bar{q})$ to illustrate the relative effect of including the photon-induced processes in the LO prediction.

The reason for the contribution of the $\gamma q \rightarrow \mu^+ \mu^- q$ subprocess to be negative, i.e. values smaller than 1 in the plots, can be understood as being due to the presence of subtraction terms for the collinear divergences, which are necessary in a NLO calculation.

3.4.3 EW input scheme choices

The calculation of the NLO EW set of corrections to the DY processes, requires the renormalization of EW couplings and masses, which is typically done by imposing on-shell conditions on the relevant Green's functions. The choice of the set of physical observables necessary to evaluate the parameters (g, g', v) of the gauge sector of the Lagrangian is done following two main criteria: (1) the quantities which are best determined from the experimental point of view minimize the parametric uncertainties affecting all the predictions; (2) some observables automatically include in their definition important classes of radiative corrections, so that their use reduces the impact of the radiative corrections to the scattering process under study.

A convenient set of parameters that describes EW processes at hadron colliders is (G_μ, M_W, M_Z) , the so called G_μ scheme. The Fermi constant G_μ measured from muon decay naturally parameterize the CC interaction, while the W and Z masses fix the scale of EW phenomena and the mixing with the hyper-charge field. A drawback of this choice is the fact that the coupling of real photons to charged particles is computed from the inputs and in lowest order is equal to $\alpha_{G_\mu} = G_\mu \sqrt{2} M_W^2 (1 - M_W^2/M_Z^2)/\pi \sim 1/132$ much larger than the fine structure constant $\alpha(0) \sim 1/137$, which would be the natural value for an on-shell photon.

The alternative choice $(\alpha(0), M_W, M_Z)$, the so-called $\alpha(0)$ scheme, does not suffer of the problem with real photon radiation, but introduces: (i) a dependence on the unphysical quantities, light-quark masses, via the electric charge renor-

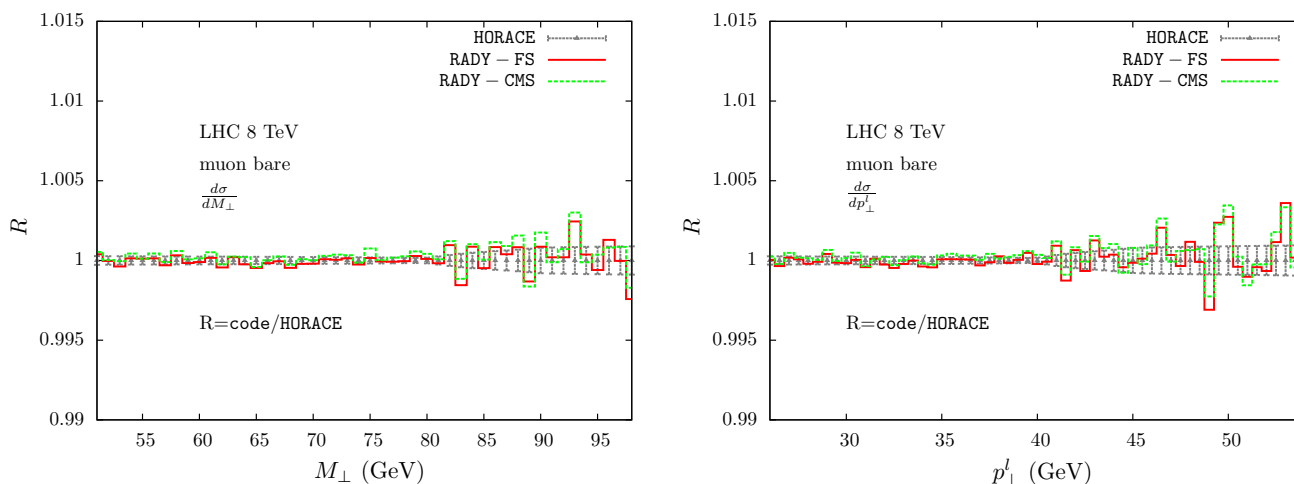


Fig. 26 Comparison of RADY NLO EW predictions when using different schemes for treating the W resonance. The plots show the transverse mass and momentum distribution of the final-state charged lepton

malization, and (ii) it leaves large radiative corrections at NLO and in higher orders.

These drawbacks of the two above mentioned schemes can be circumvented by a use of modified G_μ scheme when only LO couplings are re-expressed in terms of α_{G_μ}

$$\alpha \equiv \alpha(0) \rightarrow \alpha_{G_\mu} (1 - \Delta r) \tag{7}$$

and Sirlin’s parameter Δr [43], representing the complete NLO EW radiative corrections of $\mathcal{O}(\alpha)$ to the muon decay amplitude. Both real and virtual relative $\mathcal{O}(\alpha)$ corrections are calculated at the scale $\alpha(0)$, therefore such an approach may be referred as NLO at $\mathcal{O}(\alpha G_\mu^2)$. This choice is adopted in the *benchmark* setup of Sect. 3.1 both for NC and CC DY processes. In this scheme leading universal corrections due to the running of α and connected to the ρ parameter are absorbed in the LO couplings.

Further modifications may be considered. For NC DY the gauge invariant separation of complete EW radiative corrections into pure weak (PW) and QED corrections (involving virtual or real photons) is possible. Therefore, these two contributions may be considered at different scales, PW at $\mathcal{O}(G_\mu^3)$, and QED still at $\mathcal{O}(\alpha G_\mu^2)$. These different scales seem to be most natural for PW and QED contributions correspondingly. For CC DY PW and QED corrections are not separately gauge invariant, so that usually the complete NLO EW contribution (PW+QED) is considered using the same overall scale, either $\mathcal{O}(G_\mu^3)$ or $\mathcal{O}(\alpha G_\mu^2)$. More refined modifications may be considered, for instance based on defining gauge invariant subsets by using the Yennie–Frautschi–Suura approach [61]. The spread of predictions with different modifications of the G_μ scheme may be considered as an estimate for the uncertainty due to missing higher-order EW effects.

in $pp \rightarrow W^+ \rightarrow \mu^+ \nu_\mu + X$ at the 8 TeV LHC with ATLAS/CMS cuts in the *bare* setup. The definitions of the FS, CMS and PS schemes can be found in Ref. [18]

3.4.4 Impact of different gauge boson mass definitions

In Ref. [18] the evaluation of the LO and NLO EW cross sections for the NC DY process has been performed in different schemes for treating the Z -boson resonance, denoted as the factorization scheme (FS), complex-mass scheme (CMS) and pole scheme (PS). We refer to Ref. [18] for a detailed description of these various procedures. Here we provide in Figs. 26 and 27 a comparison of predictions for CC and NC Drell–Yan processes, respectively, obtained in these different schemes in the *tuned* comparison setup of Sect. 2.1. As also concluded in Ref. [18], the numerical differences between the CMS and FS/PS schemes are small. We observe that the predictions for the observables under study in this report obtained by using the FS, CMS and PS schemes agree within the statistical uncertainties of the MC integration.

3.4.5 Universal higher-order corrections in NC DY

In the following the starting point is the modified G_μ scheme (the *benchmark* scheme in this report) and we discuss two possible ways to include leading universal higher-order corrections, i.e. corrections beyond $\mathcal{O}(\alpha)$. In both cases the LO prediction is at $\mathcal{O}(G_\mu^2)$ and higher orders start at $\mathcal{O}(G_\mu^3) + \mathcal{O}(G_\mu^2 \alpha_s)$.

- Following Ref. [18], the leading $G_\mu m_t^2$ universal higher order corrections are taken into account via the replacements:

$$\begin{aligned} s_W^2 &\rightarrow \bar{s}_W^2 \equiv s_W^2 + \Delta\rho c_W^2, \\ c_W^2 &\rightarrow \bar{c}_W^2 \equiv 1 - \bar{s}_W^2 = (1 - \Delta\rho) \bar{c}_W^2 \end{aligned} \tag{8}$$

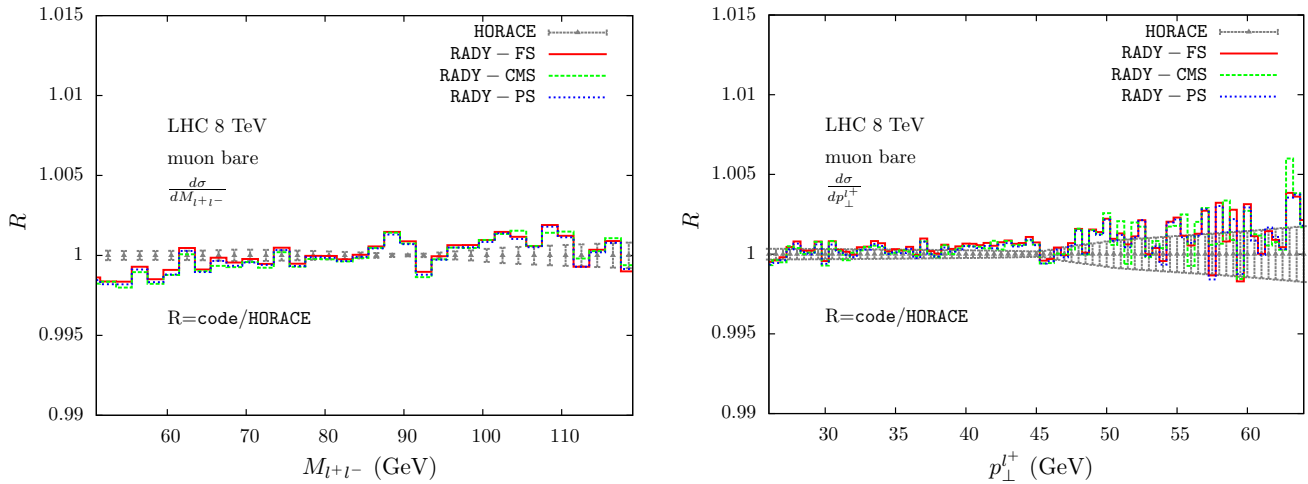


Fig. 27 Comparison of RADY NLO EW predictions when using different schemes for treating the Z resonance. The plots show the inverse mass and momentum distribution of the final-state lepton in

$pp \rightarrow \gamma, Z \rightarrow \mu^+ \mu^- + X$ at the 8 TeV LHC with ATLAS/CMS cuts in the *bare* setup. The definitions of the FS, CMS and PS schemes can be found in Ref. [18]

in the LO expression for the NC DY cross section. As was argued in Refs. [62,63], this approach correctly reproduces terms up to $\mathcal{O}(\Delta\rho^2)$.

The quantity $\Delta\rho$

$$\Delta\rho = 3x_t [1 + \rho^{(2)} (m_H^2/m_t^2) x_t] \left[1 - \frac{2\alpha_s(m_t^2)}{9\pi} (\pi^2 + 3) \right] \quad (9)$$

contains two contributions:

- (i) the two-loop EW part at $\mathcal{O}(G_\mu^2)$, second term in the first square brackets [64–67], with $\rho^{(2)}$ given in Eq. (12) of Refs. [66,67] (actually, after the discovery of the Higgs boson and the determination of its mass it became sufficient to use the low Higgs mass asymptotic, Eq. (15) of Refs. [66,67]);
- (ii) the mixed EW \otimes QCD at $\mathcal{O}(G_\mu\alpha_s)$, second term in the second square brackets [68,69].

The quantity $\Delta\rho^{(1)}$

$$\Delta\rho^{(1)} \Big|^{G_\mu} = 3x_t = \frac{3\sqrt{2}G_\mu m_t^2}{16\pi^2} \quad (10)$$

represents the leading NLO EW correction to $\Delta\rho$ at $\mathcal{O}(G_\mu)$ and should be subtracted from higher-order effects. Therefore, the contribution of higher-order effects has the following generic form:

$$\sum_i c_i [2(\Delta\rho - \Delta\rho^{(1)}) R_{1i} + \Delta\rho^2 R_{2i}], \quad (11)$$

where c_i and $R_{1i,2i}$ are combinations of $Z(\gamma) f \bar{f}$ couplings and the ratio c_W^2/s_W^2 , and their explicit form depends on the parametrization of the LO cross section where the replacements (8) are performed (cf. Eq. (3.49) of [18]).

This approach is implemented in RADY and SANC.

- As described in Ref. [26], the implementation of the NC DY in WZGRAD closely follows Refs. [70,71] for a careful treatment of higher-order corrections, which is important for a precise description of the Z resonance. The NLO differential parton cross section including weak $\mathcal{O}(\alpha)$ and leading $\mathcal{O}(\alpha^2)$ has the following form

$$d\hat{\sigma}^{(0+1)} = dP_{2f} \frac{1}{12} \sum |A_\gamma^{(0+1)} + A_Z^{(0+1)}|^2(\hat{s}, \hat{t}, \hat{u}) + d\hat{\sigma}_{\text{box}}(\hat{s}, \hat{t}, \hat{u}). \quad (12)$$

$d\hat{\sigma}_{\text{box}}$ describes the contribution of the box diagrams and the matrix elements $A_{\gamma,Z}^{(0+1)}$ comprise the Born matrix elements, $A_{\gamma,Z}^0$, the $\gamma, Z, \gamma Z$ self energy insertions, including a leading-log resummation of the terms involving the light fermions, and the one-loop vertex corrections. $A_{\gamma,Z}^{(0+1)}$ can be expressed in terms of effective vector and axial-vector couplings $g_{V,A}^{(\gamma,Z),f}$, $f = l, q$, including vertex corrections and self energy insertions. Moreover, the M_Z renormalization constant $\delta M_Z^2 = \text{Re}(\Sigma^Z(M_Z^2))$ is replaced by $\delta M_Z^2 = \text{Re}(\Sigma^Z(M_Z^2) - \frac{(\hat{\Sigma}^{\gamma Z}(M_Z^2))^2}{M_Z^2 + \hat{\Sigma}^\gamma(M_Z^2)})$ where Σ^V ($\hat{\Sigma}^V$) denotes the transverse part of the unrenormalized (renormalized) gauge boson self energy corrections. Higher-order (irreducible) corrections connected to the ρ parameter are taken into account by performing the replacement

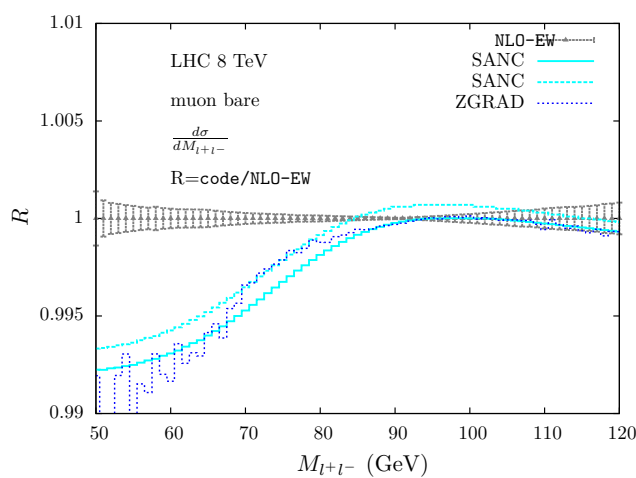
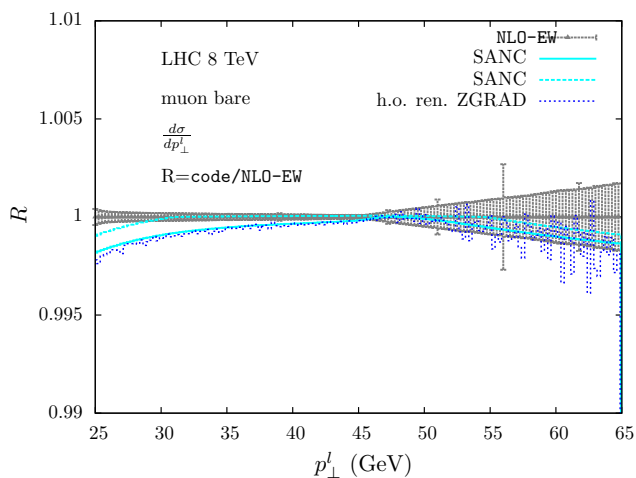


Fig. 28 Relative effects of higher-order ($\mathcal{O}(G_\mu^2)$) and higher) EW corrections in $pp \rightarrow \gamma, Z \rightarrow \mu^+\mu^-$, due to the inclusion of universal corrections using the ρ parameter as described in the text. Shown are the lepton transverse momentum (left) and lepton-pair invariant mass

(right) distributions, obtained for the 8 TeV LHC with ATLAS/CMS cuts. In blue the WZGRAD results; in light blue the SANC results obtained in a linear (solid) [first term of Eq. (11)] and quadratic (dashed) [both terms of Eq. (11)] implementation

$$\frac{\delta M_Z^2}{M_Z^2} - \frac{\delta M_W^2}{M_W^2} \rightarrow \frac{\delta M_Z^2}{M_Z^2} - \frac{\delta M_W^2}{M_W^2} - \Delta\rho^{h.o.} \quad (13)$$

where $\Delta\rho^{h.o.} = \Delta\rho - \Delta\rho^{(1)|G_\mu}$ with $\Delta\rho$ of Eq. (9) and $\Delta\rho^{(1)|G_\mu}$ of Eq. (10).

The impact of these universal higher-order EW corrections as implemented in SANC and WZGRAD is shown in Fig. 28.

3.4.6 Higher-order effects to all orders via running couplings in NC DY

The purely EW fixed-order results, in the case of the NC DY process, can be improved with the systematic inclusion of some classes of universal higher-order corrections. The strategy to achieve this result is given by the matching of an Improved Born Approximation (IBA) of the LO description of the process, together with the full $\mathcal{O}(\alpha)$ calculation, avoiding any double counting.

The IBA for reactions of the class $2f \rightarrow 2f$ has been extensively discussed at LEP [72]; here we discuss a specific implementation in the HORACE event generator. We can write the LO scattering amplitude in a symbolic compact form as

$$\begin{aligned} \mathcal{M}^{LO} = \mathcal{M}_\gamma + \mathcal{M}_Z = & \alpha(0) \frac{J_{q\bar{q}}^\gamma \cdot J_{l+l-}^\gamma}{q^2 + i\varepsilon} \\ & + \frac{g^2}{\cos\theta_W} \frac{J_{q\bar{q}}^Z \cdot J_{l+l-}^Z}{q^2 - M_Z^2 + i\Gamma_Z M_Z}, \end{aligned} \quad (14)$$

where $J_{f\bar{f}}^{\gamma,Z}$ are the fermionic currents coupling to photons and to Z bosons and $\cos\theta_W$ is the cosinus of the electroweak mixing angle. An improved expression of the amplitude \mathcal{M}_{IBA}^{LO} is obtained with the following replacement of the coupling constants:

$$\begin{aligned} \alpha(0) & \rightarrow \alpha(M_{ll}^2) && \text{photon-exchange} \\ \frac{g^2}{\cos\theta_W} & \rightarrow 4\sqrt{2}G_\mu M_Z^2 \frac{\rho_{fi}(M_{ll}^2)}{1 - \delta\rho_{irr}} && \text{Z-exchange}, \end{aligned} \quad (15)$$

where $\alpha(M_{ll}^2)$ is the on-shell running electromagnetic coupling constant, while $\delta\rho_{irr}$ represents universal corrections to the neutral current coupling and $\rho_{fi}(M_{ll}^2)$ is a compact notation for all those process dependent corrections that can be cast as an overall factor multiplying the Z-exchange amplitude (more details can be found in Refs. [11, 73]). The factors $\alpha(M_{ll}^2)$ and $\frac{1}{1 - \delta\rho_{irr}}$ include universal corrections to all orders while $\rho_{fi}(M_{ll}^2)$ is of $\mathcal{O}(\alpha)$.⁸

The use of the amplitudes in Eqs. (14)–(15) to compute the cross section represents an approximation of the exact NLO EW calculation for the non radiative part of the cross section; since they contain terms beyond NLO EW, one can also read a partial improvement over pure NLO. Their matching with the exact NLO EW expressions allows to recover this perturbative accuracy, but also to have a systematic inclusion of universal higher-order terms. Double counting is avoided by subtracting the $\mathcal{O}(\alpha)$ part of the effective couplings in Eq. (15), in that part of the virtual corrections where the UV counterterms are introduced.

⁸ For a discussion on the definition of an effective electromagnetic coupling at the 2-loop level see Ref. [74].

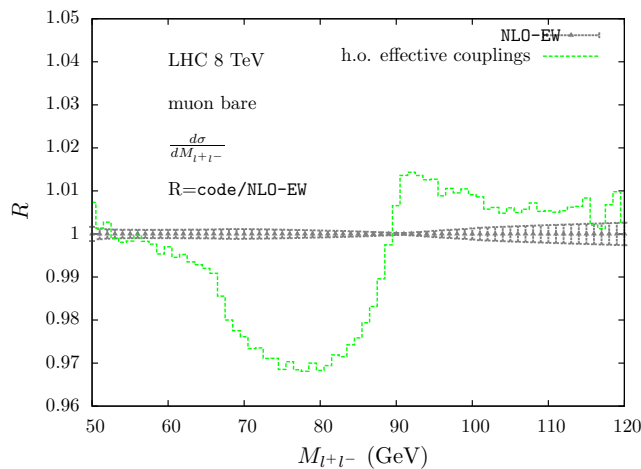
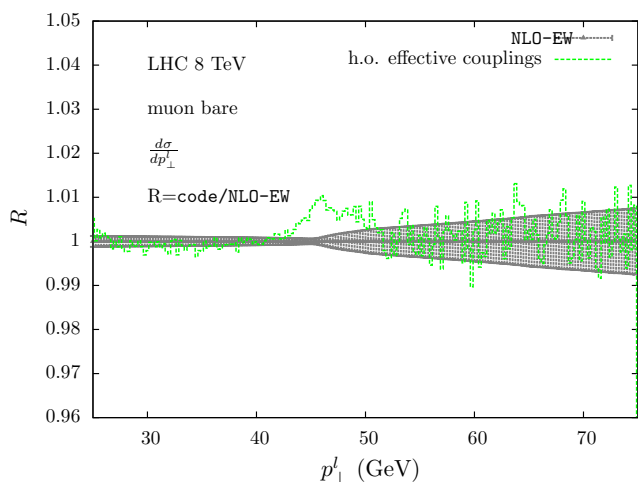


Fig. 29 Relative effect of higher-order ($\mathcal{O}(\alpha^2)$ and higher) EW corrections in $pp \rightarrow \mu^+\mu^- + X$ due to the inclusion of universal corrections via effective couplings. Shown are the lepton transverse momentum

(left), lepton-pair invariant mass (right) distributions for the 8 TeV LHC with ATLAS/CMS cuts. The results have been obtained with HORACE

The events are generated with the full NLO EW results computed with $(\alpha(0), M_W, M_Z)$ as input parameters, with a weight $d\sigma^{NLO-EW}$ for each phase space point. The latter is rescaled by the factor $K_{IBA}(\Phi_B) \equiv |\mathcal{M}_{IBA}^{LO}(\Phi_B)|^2 / |\mathcal{M}^{LO}(\Phi_B)|^2$, that accounts for all the higher-order effects and depends on the Born kinematical variables Φ_B .⁹

$$d\sigma_{IBA}^{NLO-EW} = K_{IBA}(\Phi_B)d\sigma^{NLO-EW} . \quad (16)$$

We remark that this rescaling is motivated by the factorization of the leading contributions due to soft and collinear QED radiation; in these phase-space regions the exact matrix element is well approximated by a factorized expression proportional to the underlying Born. The rescaling generates several factorizable terms of $\mathcal{O}(\alpha^2)$: among them, those due to the emission of a real photon enhanced by the effective couplings may have a sizeable impact on the differential distributions.

In the invariant mass region below the Z resonance the QED corrections increase the cross section by up to 100% of the fixed-coupling LO result. The introduction of the effective couplings yields a net effect at the few per cent level of the LO result. The impact of this redefinition of the LO couplings is demonstrated in Fig. 29, where we take the ratio of these improved predictions with those computed at NLO EW in the best setup of Sect. 3.1; the deviation from 1 is entirely due to terms of $\mathcal{O}(\alpha^2)$ or higher, present in the effective couplings.

The corrections described in this section are a reducible, gauge invariant subset, part of the full NNLO EW calculation of the NC DY process. They represent a sizeable contribution, due to the combination of two effects which, separately, are numerically leading on their own.

⁹ In the case of a radiative event, an effective Born configuration is computed to evaluate K_{IBA} .

3.4.7 QED shower matched to NLO EW matrix elements

The inclusion of multiple photon radiation in the presence of NLO EW matrix elements requires a matching procedure to avoid double counting. Several examples have been proposed in the literature following different algorithms, which have been implemented in the codes HORACE, POWHEG, and WINHAC, for instance. In Fig. 30 we use HORACE to illustrate the effect of all photon emissions beyond the first one in the NC (upper plots) and CC (lower plots) processes in the benchmark setup of Sect. 3.1 for the case of bare muons. The ratio shows the impact of the improved NLO EW prediction, when the NLO EW correction is matched to multiple photon radiation, over the NLO EW prediction; thus a deviation from 1 is entirely due to terms of $\mathcal{O}(\alpha^2)$ or higher. The impact of $\mathcal{O}(\alpha)$ corrections on the LO distributions shown in Fig. 24 is largely due to photon radiation and thus we also observe a non-negligible effect on the shape from higher-order multiple photon radiation in Fig. 30; the size of these effects, as expected, is in the 1% per cent ballpark, and depends on the shape of the observable. For example, while the $\mathcal{O}(\alpha)$ corrections to the lepton-pair transverse mass distribution can be as large as -8% of the LO prediction around the Jacobian peak, the $\mathcal{O}(\alpha^2)$ corrections of multiple photon radiation are $<0.5\%$ of the NLO EW prediction. The lepton-pair invariant mass is the only observable that significantly changes because of multiple photon radiation: in fact the $\mathcal{O}(\alpha)$ radiative effect is of $\mathcal{O}(85\%)$ below the Z resonance, while at $\mathcal{O}(\alpha^2)$ the effects are a fraction of the previous order correction and can be as large as 5%.

In Fig. 32 we study the impact of multiple-photon radiation in the CC DY process as described by WINHAC, which

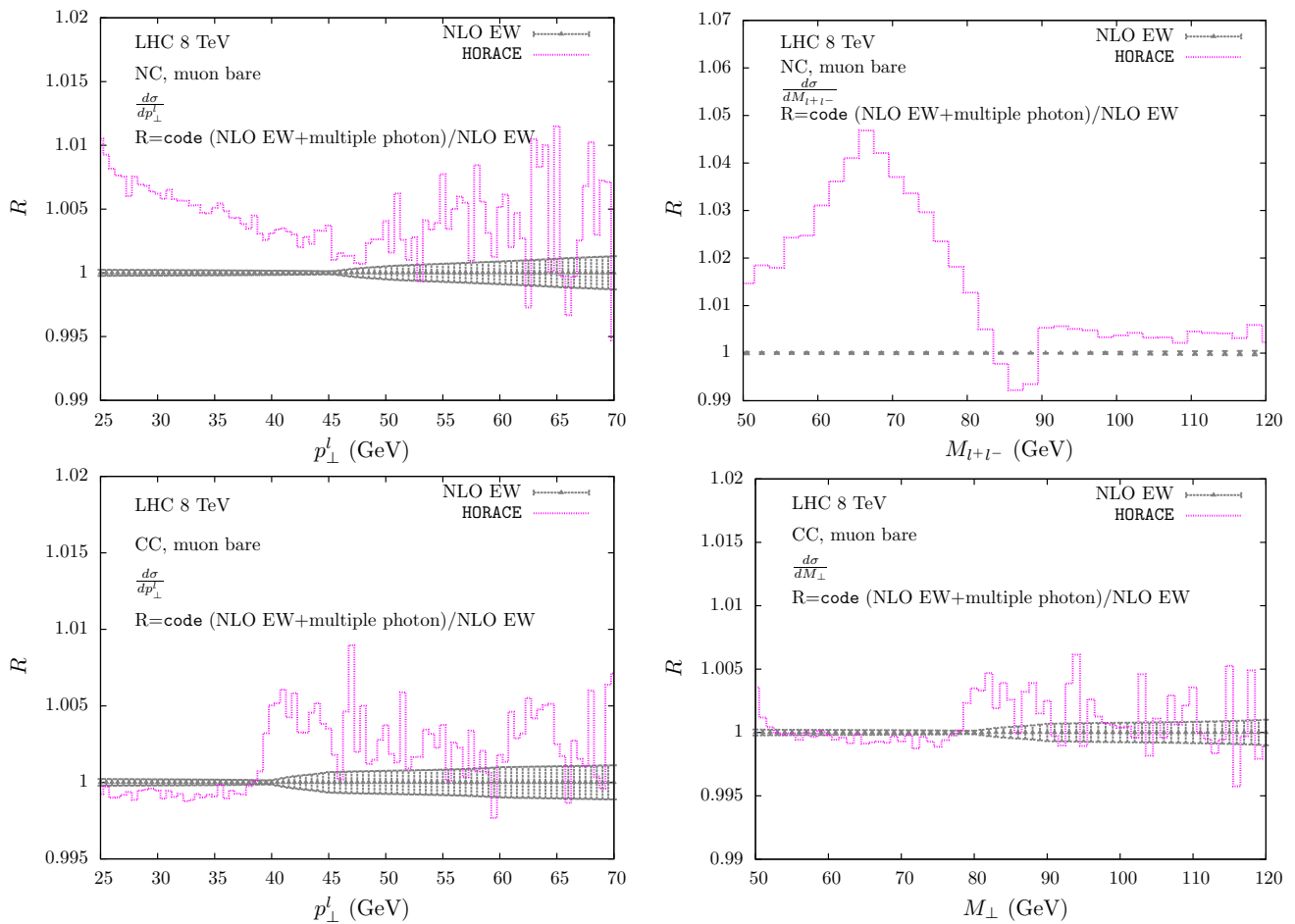


Fig. 30 Relative effect of higher-order ($\mathcal{O}(\alpha^2)$ and higher) EW corrections in $pp \rightarrow \mu^+\mu^- + X$ (upper plots) and $pp \rightarrow \mu^+\nu_\mu + X$ (lower plots), due to multiple-photon radiation matched to the NLO EW results, expressed in units of the pure NLO EW calculation evaluated in the *benchmark* setup for *bare* muons. Shown are the lepton transverse momentum in NC DY (upper left), lepton-pair invariant mass in

NC DY (upper right), lepton transverse momentum in CC DY (lower left), and lepton-pair transverse mass in CC DY (lower right) for the 8 TeV LHC with ATLAS/CMS cuts. The results are obtained in the HORACE formulation of matching NLO EW corrections to multiple-photon emission

is based on the Yennie–Frautschi–Suura (YFS) exponentiation scheme [61] matched to a NLO EW contribution, which leaves the generation of initial-state photon radiation (ISR) to a parton shower MC. This ISR-QED contribution is subtracted from the NLO EW prediction in a gauge-invariant way according to the YFS prescription, and the resulting prediction is denoted here as $\text{NLO EW}_{\text{sub}}$. As can be seen in Fig. 31, the resulting modified relative NLO EW prediction of WINHAC agrees with the corresponding modified relative NLO EW prediction of WZGRAD, WZGRAD-ISR in Fig. 31, in shape but differs in the normalization by a constant value of 0.01. This difference can be understood by comparing with the explicit expression for the ISR QED $\mathcal{O}(\alpha)$ correction of WZGRAD as defined in Ref. [42], but is left to a future study. The results for this comparison have been obtained in the setup of the *tuned comparison* of Sect. 2.1.

The *best* results of WINHAC for the CC DY process are obtained when interfaced with a parton shower MC (here: PYTHIA), which also handles the initial-state photon radiation, and when including multiple-photon radiation in the YFS scheme. The impact of the YFS exponentiation is shown in Fig. 32 on the example of the p_T distribution of the charged lepton and the transverse mass distribution of the $l\nu$ pair with and without taking into account the PYTHIA shower for initial-state photon and parton radiation.

The impact of YFS exponentiation observed in Fig. 32 is very similar to the multiple-photon radiation effects obtained with HORACE as shown in Fig. 30, i.e. also in the YFS exponentiation scheme of WINHAC the $\mathcal{O}(\alpha^2)$ corrections (and higher) amount to at most 0.5% of the $\text{NLO EW}_{\text{sub}}$ prediction. As expected, in the presence of the QCD PS the multiple-photon radiation effects are less pronounced in the lepton p_T

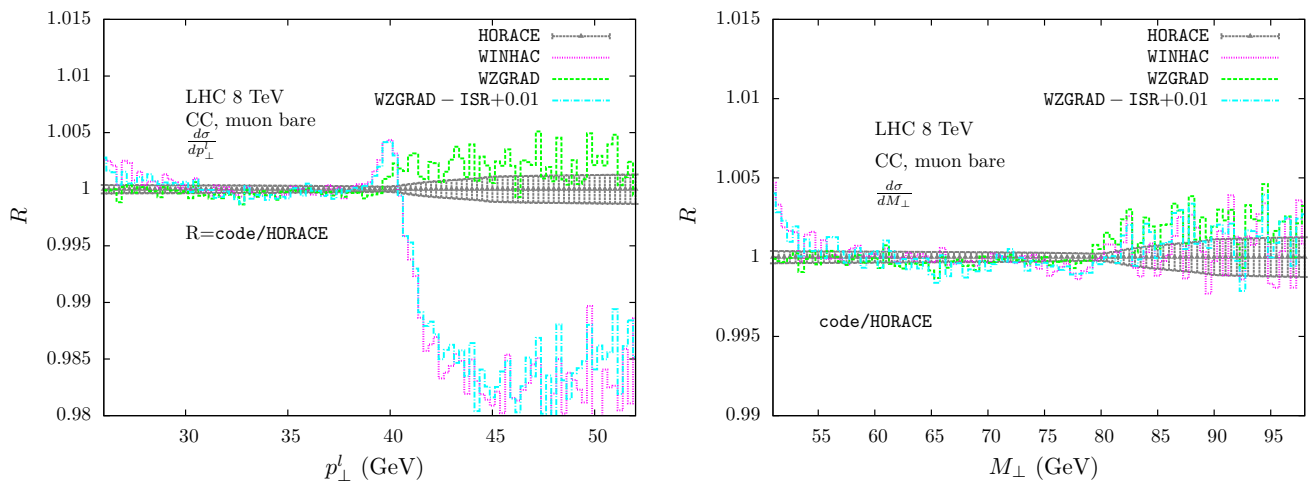


Fig. 31 Tuned comparison of the lepton transverse momentum (*left*) and lepton-pair transverse mass (*right*) distributions in $pp \rightarrow \mu^+ \nu_\mu + X$ for the 8 TeV LHC with ATLAS/CMS cuts in the *tuned compari-*

son setup for *bare* muons, including NLO EW corrections (HORACE , WZGRAD (*green curve*)) and ISR-QED subtracted NLO EW corrections by WINHAC (*pink curve*) and WZGRAD (*blue curve*)

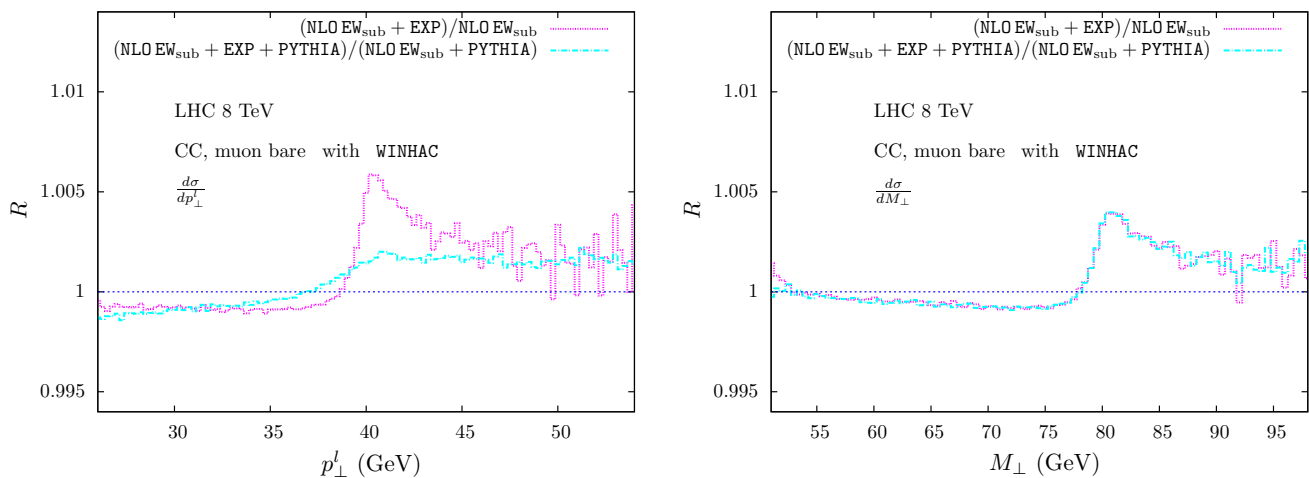


Fig. 32 Relative effect of higher-order ($\mathcal{O}(\alpha^2)$ and higher) EW corrections in $pp \rightarrow \mu^+ \nu_\mu + X$ due to multiple-photon radiation in the YFS exponentiation scheme (denoted as EXP) matched to the NLO EW_{sub} result, expressed in units of the pure NLO EW_{sub} calculation evaluated in the *benchmark* setup for *bare* muons, with and without taking into

account the PYTHIA parton shower for initial-state photon and parton radiation. Shown are the lepton transverse momentum (*left*), lepton-pair transverse mass (*right*) for the 8 TeV LHC with ATLAS/CMS cuts. The results are obtained in the WINHAC formulation of matching ISR-QED subtracted NLO EW corrections to multiple-photon emission

distribution but are unchanged in the lepton-pair transverse mass distribution (see also Sect. 4 for a discussion of the interplay of QCD and QED effects in these observables).

effect of additional light-fermion pair emission in the CC DY process has also been studied with the SANC code and was found to be less numerically important compared to the NC DY case.

3.4.8 Additional light-fermion-pair emission

We used the MC codes SANC and HORACE to study the impact of the emission of an additional light-fermion pair in the NC DY process. In Fig. 33 the relative effect with respect to the NLO EW result is shown for the lepton transverse mass and lepton-pair invariant mass distributions. The

4 Interplay of QCD and EW corrections

A precise description of DY observables requires the simultaneous inclusion of QCD and EW corrections and control over mixed QCD and EW effects, which is the topic of this

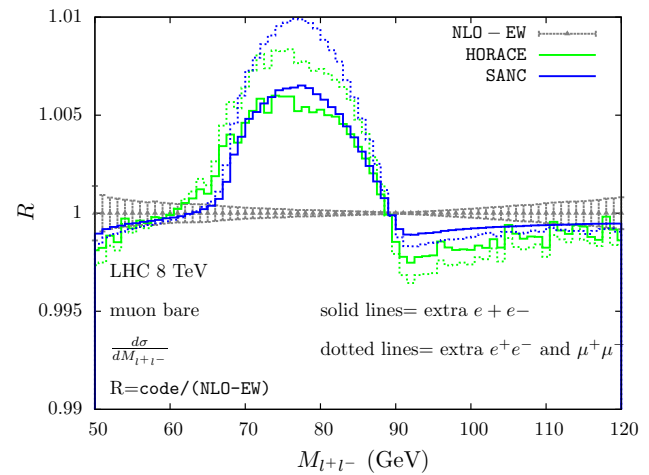
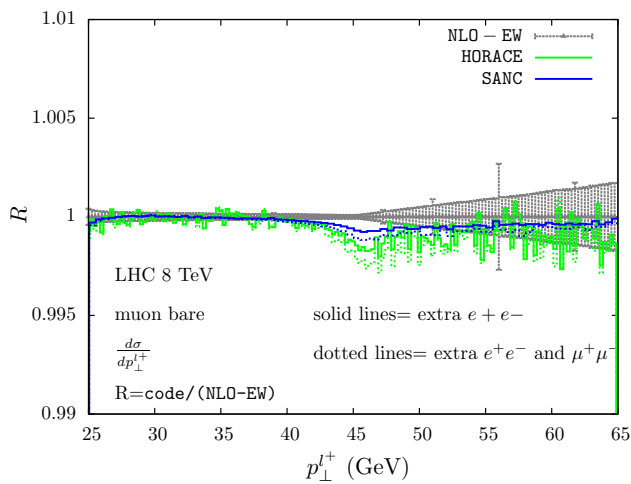


Fig. 33 Relative effect of the emission of an additional light-fermion pair in $pp \rightarrow \mu^+ \mu^- + X$, compared to the NLO EW cross section in the benchmark setup. The solid lines represent the effect of emitting an additional e^+e^- pair, while the dashed lines account for the possibility

of emitting a e^+e^- and a $\mu^+\mu^-$ pair. The HORACE results are shown in green and the SANC results in blue. The lepton transverse momentum (left) and the lepton-pair invariant mass (right) distributions are shown for the 8 TeV LHC with ATLAS/CMS cuts

section. To set the stage, we formally write a fixed-order double perturbative expansion for the fully differential DY cross section,¹⁰ in the strong and in the weak coupling constants, α_s and α , as follows:

$$d\sigma = d\sigma_{LO} + \alpha d\sigma_\alpha + \alpha^2 d\sigma_{\alpha^2} + \dots + \alpha_s d\sigma_{\alpha_s} + \alpha_s^2 d\sigma_{\alpha_s^2} + \dots + \alpha\alpha_s d\sigma_{\alpha\alpha_s} + \alpha\alpha_s^2 d\sigma_{\alpha\alpha_s^2} + \dots \quad (17)$$

We identify purely EW ($d\sigma_{\alpha,\alpha^2}$), purely QCD ($d\sigma_{\alpha_s,\alpha_s^2}$) and mixed QCDxEW corrections ($d\sigma_{\alpha\alpha_s,\alpha\alpha_s^2}$). The exact $\mathcal{O}(\alpha^2)$ and $\mathcal{O}(\alpha\alpha_s)$ results are not yet available, only some subsets are known (see Sect. 4.2 for a detailed discussion). In an effort to provide the most precise prediction including mixed EW and QCD effects, we identify two distinct problems that, to some extent, overlap:

1. As already discussed in the previous sections, many observables relevant for precision EW measurements require a formulation that goes beyond fixed-order perturbation theory and includes the resummation to all orders of some logarithmically enhanced terms, preserving with a matching procedure the (N)NLO accuracy on the total cross section. This problem, which was discussed separately for QCD and for EW corrections, is present also once we consider the effect of mixed QCDxEW terms: in other words we need a matching procedure that preserves the NLO-(QCD+EW) accuracy on the total cross section and that describes the emission of the hardest parton (gluon/quark/photon) with exact matrix elements,

leaving the remaining emissions to a Parton Shower algorithm.

2. As long as the exact $\mathcal{O}(\alpha\alpha_s)$ corrections to the four-fermion process are not fully known, we need to assess the accuracy of the recipes that combine QCD and EW effects available from independent calculations, e.g., the validity of an ansatz which factorizes QCD and EW terms.

In the Sects. 4.1 and 4.2 we will address both the above issues, in presence of a matching between fixed NLO and all-orders results.

In Sect. 4.3 we additionally show a comparison of different ways to simultaneously include QCD and QED/EW corrections to all orders on top of a LO description of the observables (with LO accuracy for the total cross section) and compare these results with the fixed order NLO predictions, in the case of calorimetric electrons in the final state.

4.1 Combination of QED/EW with QCD results in the POWHEG framework

The study of the DY observables that are relevant for high-precision measurements requires the inclusion of QED-FSR effects to all orders and of QCD-ISR effects to all orders, in order to obtain a description stable upon inclusion of further higher-order corrections.

The impact of multiple parton radiation has been discussed in Sects. 3.3 and 3.4, separately in the QCD and QED cases, in codes that match the PS algorithm with NLO fixed-order results.

PS codes are often used as stand-alone tools, since they provide a good approximation of the shape of the differen-

¹⁰ We understand that the phase-space factors are properly included in the definition of the various $d\sigma$ coefficients.

tial distributions. When QCD-PS and QED-PS are combined together, the resulting description has an exact treatment of the kinematics of each individual QCD/QED parton emission, but lacks the exact matrix element corrections and the normalization which are instead available in a fixed-order NLO-accurate calculation.

In the following we discuss in two steps the impact of the inclusion of different higher-order corrections, taking as representative examples the lepton-pair transverse mass (cfr. Fig. 34 left plots) and the lepton transverse momentum distributions (cfr. Fig. 34 right plots), in the process $pp \rightarrow \mu^+ \nu_\mu + X$ at the 14 TeV LHC with standard ATLAS/CMS cuts and bare muons. In Fig. 34 we show the normalized distributions, $d\sigma/dX/\sigma_{tot}$ ($X = m_T^{\mu\nu m\mu}, p_T^\mu$), in different perturbative approximations (upper plots), we expose the impact of QED-FSR corrections applied to different underlying hard processes (middle plots) and the impact of mixed QCD-EW effects in a simulation with full NLO-(QCD+EW) accuracy (lower plots).¹¹

We first start from the LO distributions of these two quantities, which show the sharply peaked behavior due to the jacobian factor. The QED-FSR emissions are simulated with the PHOTOS code and yield effects which are similar for the two observables, with a negative correction of $\mathcal{O}(-8\%)$ at the jacobian peak, as shown in the middle plots by the blue points.

We then consider the role of NLO-QCD corrections and of a QCD-PS in the POWHEG+PYTHIA code and remark (cfr. the upper plots) that, while the shape of the transverse mass distribution is preserved, to a large extent, by QCD corrections, the lepton transverse momentum distribution is instead strongly smeared, with a much broader shape around the jacobian peak. The inclusion of the PHOTOS corrections on top of the POWHEG+PYTHIA simulation has now a different fate, compared to the LO case (cfr. middle plots, red points): the shape and the size of the QED corrections are similar to the LO case for the transverse mass; in the lepton transverse momentum case instead the QED correction is reduced in size and flatter in shape, with respect to the LO case. The comparison of the percentage corrections due to QED-FSR in the two examples discussed above (blue and red points in the middle plots) shows a difference which is due to mixed QCDxQED corrections, since the set of pure QED corrections is common to the two simulations.

The code POWHEG- (QCD+EW) has been validated, separately in its QCD and EW components, in Sect. 2. Its use

¹¹ The treatment of FSR QED radiation present in POWHEG- (QCD+EW), up to svn version 3358, generates artificially enhanced $\mathcal{O}(\alpha\alpha_s)$ corrections, as pointed out in Refs. [75, 76], published after the completion of the present report. Concerning the POWHEG- (QCD+EW) code, an improved treatment which overcomes this problem is described in Ref. [75]. An alternative implementation is described in Ref. [76].

allows to reach the NLO-(QCD+EW) accuracy for the total cross section but it also has an impact on the differential distributions. In Fig. 34 (lower plots) we show the ratio of the distributions obtained with POWHEG- (QCD+EW) +PYTHIA + PHOTOS and with POWHEG + PYTHIA + PHOTOS. These ratios expose the size of mixed QCD-EW corrections present in the POWHEG- (QCD+EW) + PYTHIA + PHOTOS prediction but absent in POWHEG + PYTHIA + PHOTOS.

The impact on the M_W determination of the interplay between QCD and EW corrections in the POWHEG- (QCD+EW) framework has been presented in [75].

4.2 Towards exact $\mathcal{O}(\alpha\alpha_s)$: assessment of the accuracy of current approximations

As mentioned earlier, the question how to properly combine QCD and EW corrections in predictions will only be settled by a full NNLO calculation of the $\mathcal{O}(\alpha\alpha_s)$ corrections that is not yet available, although first steps in this direction have been taken by calculating two-loop contributions [77–81], the full $\mathcal{O}(\alpha\alpha_s)$ correction to the W/Z-decay widths [82, 83], and the full $\mathcal{O}(\alpha)$ EW corrections to W/Z+jet production including the W/Z decays [39, 40, 84].

Results for mixed EW-QCD $\mathcal{O}(\alpha\alpha_s)$ corrections to the charged- and neutral-current DY processes have been recently obtained in the so-called *pole approximation* (PA) [85–87]. This allows to assess the validity of simple prescriptions for the combination of EW and QCD corrections. The PA provides a systematic approximation of radiative corrections near the W- or Z-boson resonances, which is important for precision physics such as the M_W measurement. Applications of the PA to NLO EW corrections [17, 25, 42, 85] have been validated by a comparison to the complete EW NLO calculations and show excellent agreement at the order of some 0.1% in kinematic distributions dominated by the resonance region. Therefore the PA is expected to be a reliable tool for the calculation of the $\mathcal{O}(\alpha\alpha_s)$ corrections for resonant W/Z production. In the framework of the PA, radiative corrections are classified into factorizable corrections to W/Z production and decay sub-processes, and non-factorizable corrections that link production and decay by soft-photon exchange. The application to the $\mathcal{O}(\alpha\alpha_s)$ corrections results in four types of contributions illustrated in Fig. 35 for the case of the double-virtual corrections. The initial–initial factorizable corrections (a) are given by two-loop $\mathcal{O}(\alpha\alpha_s)$ corrections to on-shell W/Z production. The factorizable initial–final corrections (b) consist of one-loop QCD corrections to W/Z production multiplied by one-loop EW corrections to the decay. Factorizable final–final corrections (c) only arise from the vertex counterterm involving QCD corrections to the vector-boson self-energies, but are phenomenologically negligible [87]. In the non-factorizable two-loop corrections (d), the soft-photon corrections connecting the initial state, the intermediate vec-

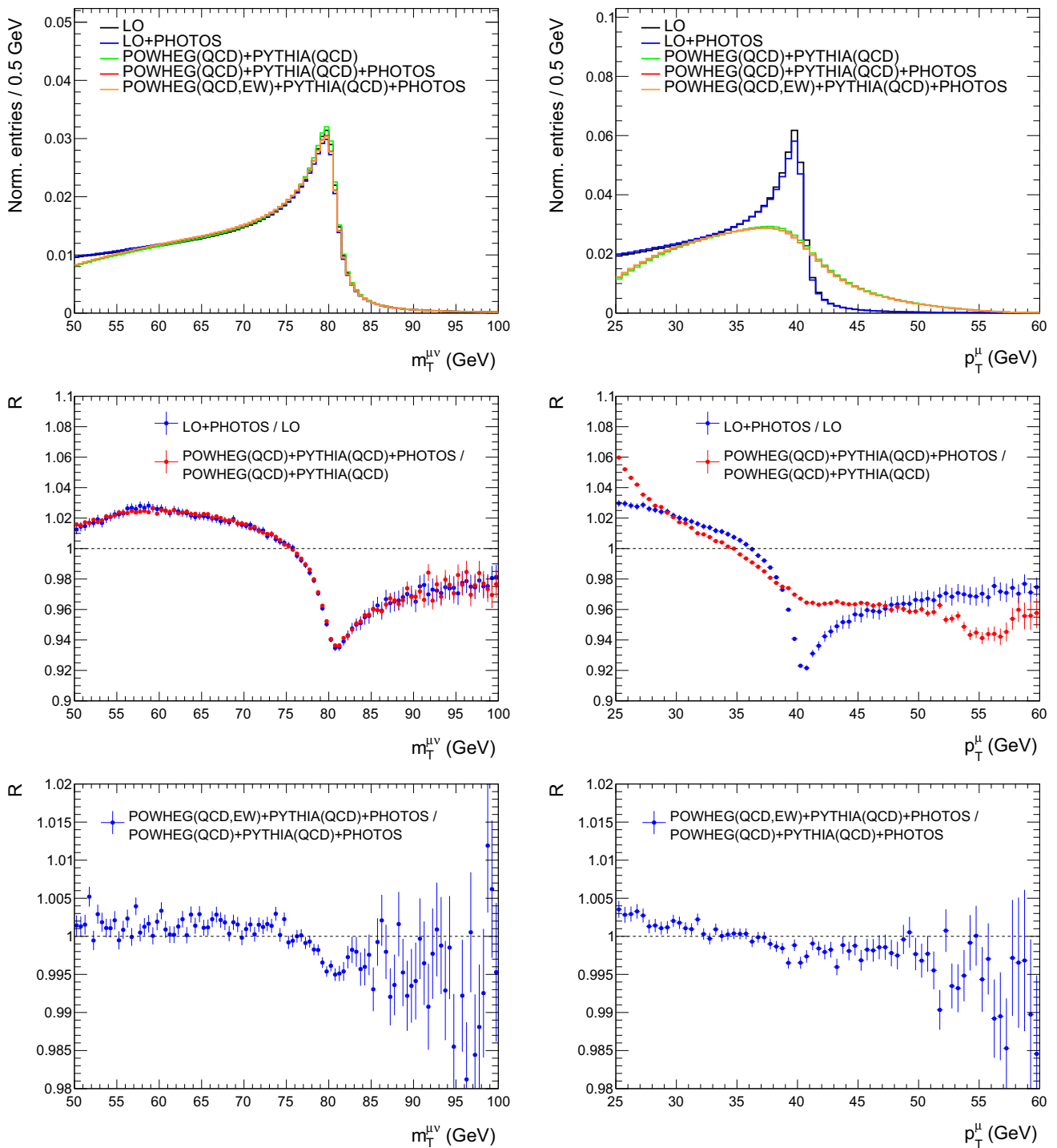


Fig. 34 Combination of QCD and EW corrections in the process $pp \rightarrow \mu^+ \nu_\mu + X$ at the 14 TeV LHC with standard ATLAS/CMS cuts for the lepton-pair transverse mass (*left plots*) and the charged lepton transverse momentum (*right plots*) distributions. The normalized distributions in different perturbative approximations are shown in the *upper plots*. The ratio of these distributions including a QED FSR PS and

the corresponding quantities where the QED shower has been switched off is shown in the *middle plots*. The ratio of distributions including full NLO-(QCD+EW) corrections matched with (QCD+QED)-PS and the corresponding quantities where only NLO-QCD + (QCD+QED)-PS has been retained is shown in the *lower plots*

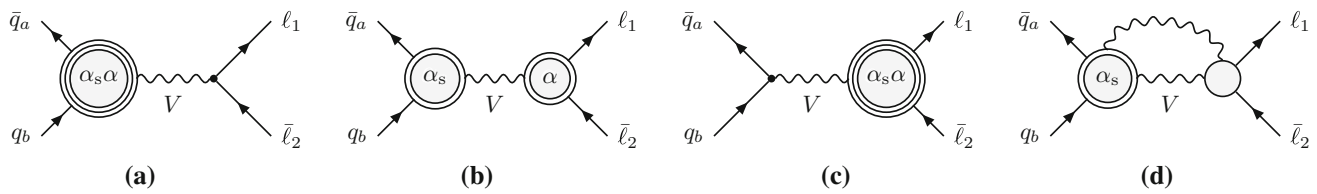


Fig. 35 Generic diagrams for the various contributions to the virtual factorizable (a–c) and non-factorizable (d) corrections of $\mathcal{O}(\alpha\alpha_s)$ in PA, with α_s , α , and $\alpha\alpha_s$ in the blobs indicating the order of the included loop corrections

tor boson, and the final-state leptons are dressed with gluon loop corrections to the initial quark–antiquark pair. For each class of contributions with the exception of the final–final corrections (c), also the associated real–virtual and double-real corrections have to be computed, obtained by replacing one or both of the labels α and α_s in the blobs in Fig. 35 by a real photon or gluon, including crossed partonic channels, e.g. with quark–gluon initial states. In Ref. [85] the non-factorizable $\mathcal{O}(\alpha\alpha_s)$ corrections to W/Z production have been computed in terms of soft-photon correction factors to squared tree-level or one-loop QCD matrix elements by using gauge-invariance arguments. The numerical impact of these corrections was found to be below the 0.1% level and is therefore phenomenologically negligible.

The $\mathcal{O}(\alpha\alpha_s)$ initial–final state corrections have been computed in Ref. [87]. Because of the large effect of real-photon emission off the final-state leptons at NLO, this class is expected to capture the dominant part of the full $\mathcal{O}(\alpha\alpha_s)$ corrections on kinematic distributions in the resonance region. Therefore the sum of the NLO QCD cross section σ_{NLO_s} and the NLO EW corrections can be improved by adding the initial–final-state corrections in the PA, $\sigma_{\alpha\alpha_s}^{\text{prod}\times\text{dec}}$:

$$\sigma_{\text{NNLO}_{s\otimes\text{ew}}} = \sigma_{\text{NLO}_s} + \alpha\sigma_\alpha + \alpha\alpha_s\sigma_{\alpha\alpha_s}^{\text{prod}\times\text{dec}}. \tag{18}$$

The last term in Eq. (18), in particular, includes the double-real contribution that is given in terms of the exact matrix elements for gluon or photon emission in vector-boson production and decay, respectively, treated without kinematic approximation on the photon or gluon momenta. In the POWHEG implementation discussed in Sect. 4.1, these effects are approximated by treating the first emission exactly and generating the second emission by a QCDxQED shower in the collinear approximation. On the other hand, this approach includes multiple collinear photon and gluon emissions which are not included in the fixed-order prediction (18).

In the numerical results shown below, all terms of Eq. (18) are consistently evaluated using the NNPDF2.3QED NLO set [32], which includes $\mathcal{O}(\alpha)$ corrections. We consider the case of “bare muons” without any photon recombination. Results obtained assuming a recombination of leptons with collinear photons can be found in Ref. [87] and show the same

overall features, with corrections that typically reduced by a factor of two.

Predictions for the transverse-mass and transverse-lepton-momentum distributions for W^+ production at the LHC with $\sqrt{s} = 14$ TeV are shown in Fig. 36. For Z production, Fig. 37 displays the results for the lepton-invariant-mass distribution and a transverse-lepton-momentum distribution. The red curves are given by the factorizable initial–final $\mathcal{O}(\alpha\alpha_s)$ corrections, normalized to the LO cross-section prediction,

$$\delta_{\alpha\alpha_s}^{\text{prod}\times\text{dec}} = \frac{\alpha\alpha_s\sigma_{\alpha\alpha_s}^{\text{prod}\times\text{dec}}}{\sigma_{\text{LO}}}, \tag{19}$$

where σ_{LO} is computed using the NNPDF2.3QED LO PDFs. One observes corrections beyond NLO of approximately -1.7% in the $M_{T, \nu l}$ distribution (left plot in Fig. 36). As can be anticipated from the size of the NLO QCD corrections, corrections to the transverse-lepton-momentum spectrum (right plots in Figs. 36, 37) can be much larger, rising to about 15% (20%) above the Jacobian peak for the case of the W^+ boson (Z boson) and dropping to almost -50% above. In fact, a realistic description of the $p_{T, l}$ spectrum near resonance requires the inclusion of higher-order gluon-emission effects. In case of the M_{l+l^-} distribution for Z production (left plot in Fig. 37), corrections up to 10% are observed below the resonance, consistent with the large EW NLO corrections from FSR in this region.

The result of the PA (19) allows to assess the validity of a naive product ansatz of the $\mathcal{O}(\alpha\alpha_s)$ correction,

$$\sigma_{\text{NNLO}_{s\otimes\text{ew}}}^{\text{naive fact}} = \sigma_{\text{NLO}_s}(1 + \delta_\alpha). \tag{20}$$

Here the relative EW correction factor $\delta_\alpha = \alpha\sigma_\alpha/\sigma_0$ is introduced as the ratio of the NLO EW correction and the LO contribution σ_0 to the NLO cross section, both evaluated with NLO PDFs, so that PDF effects cancel in this factor. The difference of the prediction (18) to the product ansatz (20), normalized to the LO cross section, reads

$$\frac{\sigma_{\text{NNLO}_{s\otimes\text{ew}}} - \sigma_{\text{NNLO}_{s\otimes\text{ew}}}^{\text{naive fact}}}{\sigma_{\text{LO}}} = \delta_{\alpha\alpha_s}^{\text{prod}\times\text{dec}} - \delta_\alpha\delta'_\alpha, \tag{21}$$

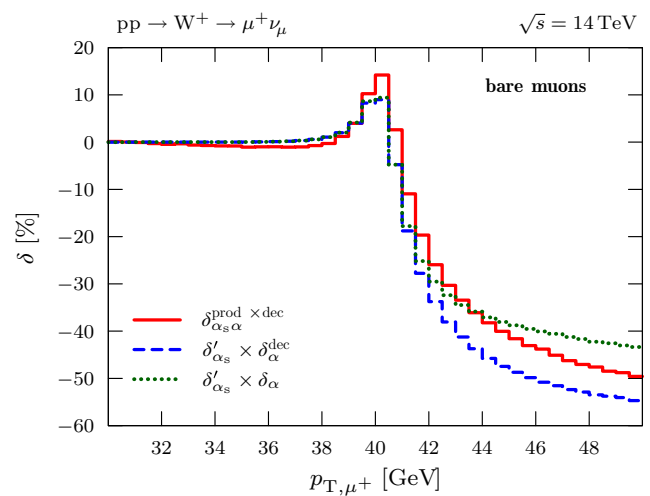
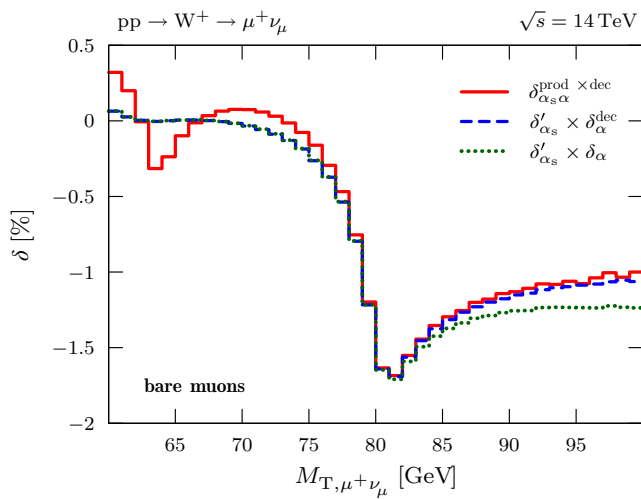


Fig. 36 Relative factorizable corrections (in red) of $\mathcal{O}(\alpha_s)$ induced by initial-state QCD and final-state EW contributions to the transverse-mass distribution (left) and the transverse-lepton-momentum distribu-

tion (right) for W^+ production at the LHC. The naive products of the NLO correction factors δ_α and δ'_{α_s} are shown for comparison (taken from Ref. [87])

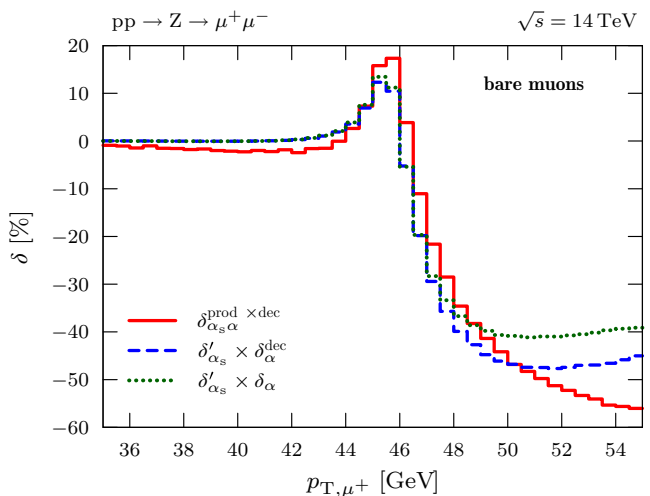
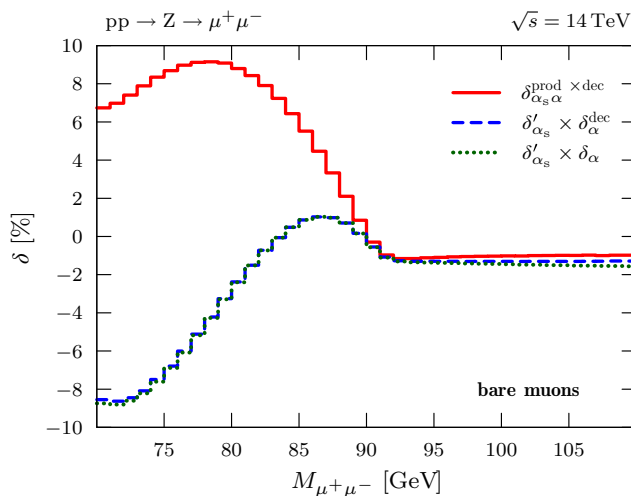


Fig. 37 Relative factorizable corrections (in red) of $\mathcal{O}(\alpha_s)$ induced by initial-state QCD and final-state EW contributions to the lepton-invariant-mass distribution (left) and a transverse-lepton-momentum

distribution (right) for Z production at the LHC. The naive products of the NLO correction factors δ'_{α_s} and δ_α are shown for comparison (taken from Ref. [87])

with the relative QCD correction factor $\delta'_{\alpha_s} = (\sigma_{\text{NLO}_s} - \sigma_0)/\sigma_{\text{LO}}$.¹² The agreement of the correction factor (19) with the product $\delta_\alpha \delta'_{\alpha_s}$ therefore provides an estimate for the accuracy of the naive product ansatz. In Figs. 36 and 37 two different versions of the EW correction factor are used for the product approximation, first based on the full NLO correction (δ_α , black curves), and second based on the dominant EW final-state correction of the PA ($\delta_\alpha^{\text{dec}}$, blue curves). The difference of these curves provides an estimate for the size of

the remaining as yet uncalculated $\mathcal{O}(\alpha_s)$ corrections beyond the initial-final corrections considered in the calculation of Refs. [85–87] and therefore also provides an error estimate of the PA, and in particular of the omission of the corrections of initial-initial type.

In the case of the M_{T,ν_l} distribution (left plot in Fig. 36), which is rather insensitive to W -boson recoil due to jet emission, both versions of the naive product ansatz approximate the PA prediction quite well near the Jacobian peak and below. Above the peak, the product $\delta'_{\alpha_s} \delta_\alpha$ based on the full NLO EW correction factor deviates from the other curves, which signals the growing importance of effects beyond the PA. In contrast, the product ansatz fails to provide a good

¹² Note that this correction factor differs from that in the standard QCD K factor $K_{\text{NLO}_s} = \sigma_{\text{NLO}_s}/\sigma_{\text{LO}} \equiv 1 + \delta_{\alpha_s}$ due to the use of different PDF sets in the Born contributions. See Ref. [86] for further discussion.

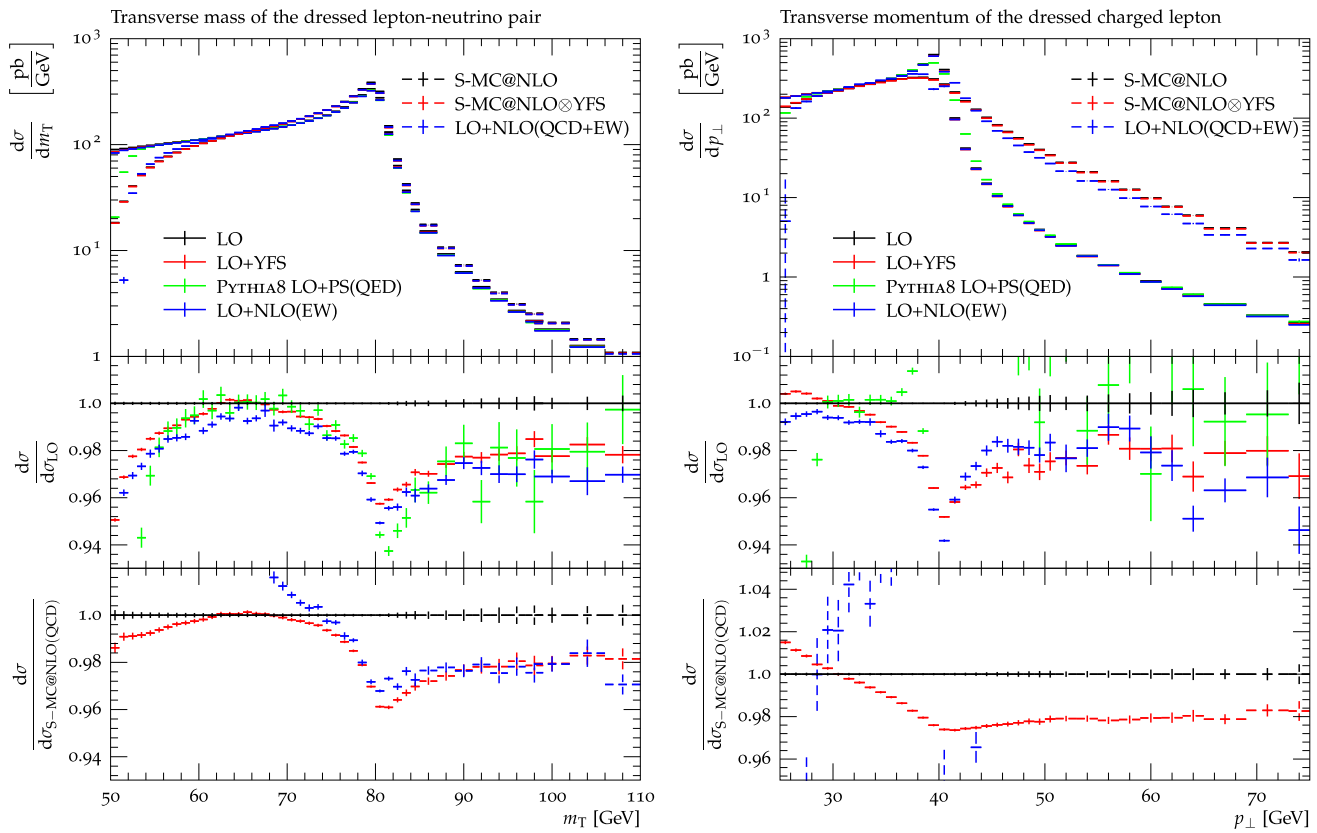


Fig. 38 Comparison of the description of the transverse mass of the dressed electron-neutrino pair (*left*) and the dressed electron transverse momentum (*right*) in electron-neutrino-pair production in the CC DY process with fiducial cuts (see text for more details)

description for the lepton $p_{T,l}$ distributions (right plots in Figs. 36, 37), which are sensitive to the interplay of QCD and photonic real-emission effects. In this case one also observes a larger discrepancy of the two different implementations of the naive product, which indicates a larger impact of the missing $\mathcal{O}(\alpha\alpha_s)$ initial-initial corrections of Fig. 35a, and in particular the real-emission counterparts. For the M_{l+l-} -distribution for Z production (left plot in Fig. 37), the naive products approximate the full initial-final corrections reasonably well for $M_{l+l-} \geq M_Z$, but completely fail already a little below the resonance where they do not even reproduce the sign of the full correction $\delta_{\alpha_s\alpha}^{\text{prod}\times\text{dec}}$. This failure can be understood from the fact that the naive product ansatz multiplies the corrections locally on a bin-by-bin basis, while a more appropriate treatment would apply the QCD correction factor at the resonance, $\delta'_{\alpha_s}(M_{l+l-} = M_Z) \approx 6.5\%$, for the events that are shifted below the resonance by photonic FSR. The observed mismatch is further enhanced by a sign change in the QCD correction δ'_{α_s} at $M_{l+l-} \approx 83$ GeV.

These examples show that a naive product approximation has to be used with care and does not hold for all distributions. The results are also sensitive to the precise definition of the correction factors δ_α and δ_{α_s} [86]. As shown in Ref. [87], a more suitable factorized approximation of

the dominant $\mathcal{O}(\alpha\alpha_s)$ effects can be obtained by combining the full NLO QCD corrections to vector-boson production with the leading-logarithmic approximation for FSR through a structure-function or a parton shower approach such as used in PHOTOS [12]. In this way the interplay of the recoil effects from jet and photon emission is properly taken into account, while certain non-universal, subleading, effects are neglected.

4.3 Comparing different ansatzes of higher-order QED/EW corrections combined with QCD parton showers

In this section we compare the higher-order QED corrections predicted by SHERPA's Yennie-Frautschi-Suura (YFS) soft-photon resummation [61, 88], the standard DGLAP collinear higher-order QED corrections as implemented in PYTHIA8 [89], and the exact NLO EW calculation performed by SHERPA using one-loop matrix elements from OPENLOOPS [90–92]. In Ref. [38], for the case of the NC DY process, the quality of the YFS implementation of SHERPA has been checked against the exact NLO EW $\mathcal{O}(\alpha)$ calculation and the NNLO QCD-EW mixed $\mathcal{O}(\alpha_s\alpha)$ calculation in the pole approximation of [85, 87]; we point to this reference for the quantitative results. In the following, the cal-

calculations including YFS exponentiation, standard DGLAP QED and fixed-order NLO-EW corrections have been performed also for the CC DY process and shall be compared among each other in a realistic scenario. We consider electrons dressed with the surrounding $\Delta R = 0.1$, which are required to have $p_T > 25$ GeV and $|y| < 2.4$, and a missing transverse momentum of at least 25 GeV.

Figure 38 (left) shows the comparison of the different calculations for the reconstructed transverse mass of the W boson. Besides the leading QCD higher-order corrections, the higher-order EW corrections between either the YFS resummation or the parton-shower approach agree well with the fixed-order result (see the central inset), only PYTHIA8's QED parton shower predicts a stronger correction around the peak and near the threshold. The differences with respect to the NLO EW correction can be traced to multi-photon emissions present in the all-order results and to genuine weak effects only present in the NLO EW calculation. The same findings were reported for the case of lepton pair production in Ref. [38]. Applying the YFS resummation in addition to higher-order QCD corrections, the implementation corresponds to a multiplicative combination of both effects and preserves these findings for the lepton-pair transverse mass distribution (lower inset), as already observed in Sect. 4.1. Again, subpercent level agreement is found with the fixed-order calculation in the peak region. At low transverse masses the resummation of QCD corrections is important and drives the difference to the fixed-order result.

Figure 38 (right) details the comparison of the different calculations for the transverse momentum of the dressed electron. Again, the exact $\mathcal{O}(\alpha)$ calculation is in subpercent level agreement with the YFS resummation, and again, the general offset can be attributed to both multiple photon emission corrections and genuine weak corrections (central inset). The PYTHIA8 QED parton shower shows a different behavior in the peak region. Once NLO QCD effects are also taken into account (lower inset), the importance of their resummation with respect to their simple fixed-order treatment, as already observed in Sect. 3.3.4, overwhelms the comparison between the YFS soft photon resummation and the fixed-order NLO EW calculation for this observable.

The investigation of the observed difference in the behavior of the QED parton shower in PYTHIA8 and the YFS soft-photon resummation is left to a future study.

5 Conclusions

What we did:

- In this report we compared several public codes which simulate the Drell–Yan processes in different perturbative approximations. All these codes are at least NLO accurate

in the description of inclusive observables in either the EW or strong interaction, or possibly with respect to both.

- This common level of accuracy allowed to consistently compare the codes, testing their respective numerical implementations and the resulting level of agreement (see Sect. 2).
- Relying on this NLO-accurate framework, it has been possible to define a way to quantify the impact of higher-order corrections, i.e. beyond NLO, which may differ from code to code (see Sect. 3). The study of the impact of different sets of corrections has been performed separately for the EW and strong interactions.
- Some codes provide, in the same implementation, QCD and EW corrections, which have been separately tested in Sects. 2 and 3. The interplay of both sets of corrections is discussed in Sect. 4.

What we computed and observed:

- The impact of all the higher-order corrections, which are available in some but not in all codes, is expressed as a percentage effect, using a common unit, namely the distribution obtained in the calculation which has NLO accuracy for the total cross section and uses the inputs of the *benchmark* setup.
- The distribution used as common unit may not be the most suitable choice for all the observables: in fact in some phase-space corners perturbation theory breaks down and the fixed-order distribution provides only a technical reference rather than a sensible estimate of the physical observable.
- The problem of a consistent matching of fixed- and all-orders results emerges in several cases discussed in Sect. 3, both in the EW and in the QCD sectors. Different matching procedures may agree on the accuracy on the observables inclusive over radiation (NLO or NNLO) but differ by the inclusion of higher-order subleading terms; the latter, despite their subleading classification, might nevertheless have a sizable impact on some differential distribution, sensitive to radiation effects.
- The analytical expression of the terms by which two matching procedures differ is not always available, leaving open only the possibility of a numerical comparison.

Comments on the numerical comparisons:

- In a tuned comparison at NLO, where all the input parameters and the simulation setup are identical and the matrix elements have the same accuracy for all the codes, we observe that the total cross sections agree at the 0.03% level both in the NLO EW and in the NLO QCD calculations; the differential distributions differ at most at the 0.5% level.

- The spread of the predictions at differential level reflects the impact of different choices in the numerical implementation of exactly the same calculation, in particular the handling of the subtraction of infrared and collinear divergences.
- In a tuned comparison of codes that share NNLO QCD accuracy for the observables inclusive over radiation (cfr. Sect. 3.3.2), the level of agreement for the total cross sections is at the 0.4% level and for the differential distributions is at the $\mathcal{O}(1\%)$ level, depending on the observable and on the range considered, but always with compatibility within the statistical error bands.

Comments on the hierarchy of the different higher-order effects:

- All the EW higher-order effects are of $\mathcal{O}(\alpha^2)$ or higher. Their size is in general at the few per mill level, with some exceptions like the lepton-pair invariant mass distribution, which receives corrections up to 5%. This particularly large size is due to the combination of two elements: on the one side to the steeply falling shape of the Z boson resonance; on the other side, to the fact that most of the events are produced at the Z peak, but final state radiation reduces the eventual invariant mass of the lepton pair, so that the lower-mass bins are populated. At $\mathcal{O}(\alpha)$ the effect is of $\mathcal{O}(100\%)$ and multiple photon radiation still yields an additional corrections of several per cent.
- In the absence of a full NNLO EW calculation, all the higher-order EW effects are necessarily subsets of the full result. They thus may not be representative of the full result, and care should be taken in using these partial results to estimate the effects of missing higher-order corrections.
- The size of the QCD radiative corrections strongly depends on the observable: the differential distributions which require a resummation to all orders in some phase-space corners should be discussed separately from those that are stable upon inclusion of radiative effects. Given our reference results obtained with codes that have NLO QCD accuracy for the total cross section, we studied higher-order effects due to NNLO QCD corrections, NLO QCD corrections matched with a QCD PS, and NNLO QCD corrections matched with a QCD PS. In case of the matched calculations we compared two different matching formulations.
- The NNLO QCD corrections to the invariant (transverse) mass distribution of the lepton pair are small in size, at the few per cent level over the whole spectrum. The same codes predict a large positive correction of $\mathcal{O}(40 - 50\%)$ of the lower-order result for the lepton-pair transverse momentum distribution,¹³ as the effect of having the exact description of two hard real parton emissions. The latter show to play an important role also in the description of the hard tail, above the Jacobian peak, of the single-lepton transverse momentum distribution, with effects again at the $\mathcal{O}(30-40\%)$ level.
- Matching fixed- and all-order results is necessary to obtain a sensible description of the Jacobian peak in the single lepton transverse momentum distribution or the low-momentum tail of the lepton-pair transverse momentum distribution. Even if this goal is achieved, nevertheless two codes that share the same accuracy for the total cross section (in the absence of acceptance cuts), i.e. NLO QCD or NNLO QCD, still exhibit sizable differences in the prediction of these same observables, in the intermediate ranges of the spectra. It should be stressed that these differences can be, in the NLO+PS matching, as large as few percent at the Jacobian peak or even several tens of percent for the lepton-pair transverse momentum distribution. The size of these differences is reduced, at the several per cent level, with the NNLO+PS matching. This kind of matching ambiguities should be added to the usual renormalization/factorization scale variations and deserves further investigation. An example of such a study of matching uncertainties can be found in Ref. [93], for the Higgs transverse momentum distribution in gluon fusion.
- QCD and EW effects are separately available at first perturbative order and have been extensively tested in Sect. 2. The possibility of combining the differential K-factors in a factorized ansatz has been shown to be accurate, compared to the $\mathcal{O}(\alpha\alpha_s)$ results available in pole approximation at the W (Z) resonance, for observables that are insensitive to a redistribution of events by QCD radiation, such as in the transverse-mass distribution of the W or Z bosons. Naive products fail to capture the dominant QCDxEW corrections in distributions such as in the transverse momentum of the lepton, which is sensitive to QCD initial-state radiation and photonic final-state radiation. For the invariant-mass distribution of the neutral-current process the naive product approach is insufficient as well because of large photonic final-state corrections and initial-state QCD corrections which depend on the reconstructed invariant mass in a non-trivial way.
- The POWHEG implementation of QCD+EW corrections shares with the other codes of the present report the NLO-

¹³ We remind the reader that the codes that have NNLO QCD accuracy for the total cross section are only NLO QCD accurate in the prediction of the large momentum tail of the lepton-pair transverse momentum distribution. For the same reason our reference results, which are NLO QCD accurate for the total cross section, are only LO accurate for this observable.

(QCD+EW) accuracy for the total cross section. On the other hand, it offers one possible solution to the matching of fixed- and all-orders results, both in QCD and in the EW sectors, and in turn it introduces mixed QCD \times EW factorizable corrections to all orders.

- The interplay between QCD and QED corrections is not trivial, as it can be checked in observables like the charged-lepton transverse momentum distribution, where one can appreciate the large size of mixed $\mathcal{O}(\alpha_s)$ and higher corrections. The impact, in the same QCD framework, of subleading effects due to weak radiative corrections and to the exact treatment of real radiation matrix elements is not negligible in view of precision EW measurements, e.g. being the correction at the several per mill level in the case of the lepton-pair transverse mass distribution.

Higher-order effects and theoretical uncertainties:

- The estimate of the accuracy available in the prediction of DY observables requires the distinction between: (1) higher-order corrections which have been computed and are available in at least one code and (2) missing higher-order terms which are unknown, whose effect can only be estimated.
- The present report provides, for item (1), guidance to assess the size of the corrections which are missing in one code, thanks to the analysis of Sect. 3, so that they can be treated as a theoretical systematic error, when they are not included in the simulation.
- On the other hand, item (2) requires a detailed, systematic discussion, which can start from the results of the present report, but goes beyond its scope. The estimate of the actual size of missing higher orders is an observable-dependent statement. In some specific cases the available fixed-order perturbative results may offer a handle to estimate the remaining missing corrections. On the other hand, the quantities which require matching of fixed- and all-order results are simultaneously affected by several sources of uncertainty whose systematic evaluation will require a dedicated effort (see, e.g., the discussion in Sect. 3.3.6).

Acknowledgements Work on this report was partially carried out at the *LHC Run II and the Precision Frontier* workshop at the Kavli Institute for Theoretical Physics (KITP), supported by NSF PHY11-25915, at the MIAPP workshop *Challenges, Innovations and Developments in Precision Calculations for the LHC*, supported by the Munich Institute for Astro- and Particle Physics (MIAPP) of the DFG cluster of excellence “Origin and Structure of the Universe”, and the *Prospects and precision at the Large Hadron Collider at 14 TeV* workshop at the Galileo Galilei Institute for Theoretical Physics (GGI). We are grateful to the CERN LPCC and Michelangelo Mangano for hosting workshops at the LPCC, which allowed for close interactions of members of this working group with members of the experimental collaborations involved in EW preci-

sion analysis. We thank the Department of Physics at the University of Milan and INFN for financial support for the kick-off meeting *W mass workshop*, and John Campbell and Fermilab for hosting the second *W mass workshop*.

Open Access This article is distributed under the terms of the Creative Commons Attribution 4.0 International License (<http://creativecommons.org/licenses/by/4.0/>), which permits unrestricted use, distribution, and reproduction in any medium, provided you give appropriate credit to the original author(s) and the source, provide a link to the Creative Commons license, and indicate if changes were made. Funded by SCOAP³.

Appendix A: Description of MC codes

In the following we provide a brief description of the MC codes used in this study. For details we refer to the relevant references which are also provided.

Appendix A.1: DYNNLO

DYNNLO [5] is a parton-level Monte Carlo program that computes the cross section for vector-boson production in pp and $p\bar{p}$ collisions. The calculation is performed up to NNLO in QCD perturbation theory. The program includes $\gamma - Z$ interference, finite-width effects, the leptonic decay of the vector boson and the corresponding spin correlations. The user is allowed to apply arbitrary (though infrared safe) cuts on the final state and to plot the corresponding distributions in the form of binned histograms. The program is available at <http://theory.fi.infn.it/grazzini/dy.html>, and more details can be found in the associated Ref. [5].

Appendix A.2: DYNNLOPS

DYNNLOPS [6] is a framework for matching fixed order NNLO-QCD predictions of Drell–Yan production to parton showers. The method is based on a reweighting procedure which uses events generated with the Bj-MiNLO generators of the POWHEG-BOX [50,51,94] and fixed order NNLO-QCD predictions obtained in DYNNLO [5]. Due to the MiNLO procedure the Bj generator is fully inclusive and NLO accurate for zero and one-jet phase space regions. By reweighting the events over the three dimensional phase space of the massive vector boson we acquire NNLO accurate events, which can be passed to a parton shower in the same way as usual POWHEG events. The MiNLO Sudakov form factor is constructed in such a way that the reweighting procedure does not introduce any spurious terms which could spoil the NNLO accuracy of the calculation. Although the MiNLO Sudakov form factor is not formally NNLL accurate, very good numerical agreement has been observed between dedicated resummation calculations of the vector boson transverse momentum and DYNNLOPS.

To date this procedure has been implemented for Higgs production [55], Drell–Yan production and associated Higgs production [95]. In all cases public codes exist and can be obtained through the POWHEG-BOX Version 2 by first checking out the repositories of the Zj and Wj generators. The code allows the user to set all relevant input parameters themselves and to apply cuts on the final state leptons and jets. An example analysis is also provided which the user can modify to their need. The code is provided with step-by-step instructions and requires only little more work to run compared to the Bj-MiNLO generators themselves.

Acknowledgements A. Karlberg is supported by the British Science and Technology Facilities Council and by the Buckee Scholarship at Merton College.

Appendix A.3: FEWZ

FEWZ calculates the fully differential production of dilepton pairs via the neutral-current (intermediate photons and Z-bosons) and charged-current processes. It is designed to make predictions for hadron-collider observables with realistic acceptance cuts at NNLO in the strong coupling constant. All spin correlations and finite-width effects are included. In the neutral-current case it allows for the computation of the NLO electroweak corrections as well. Technical details regarding several aspects of FEWZ relevant to users of the code are discussed below.

- All inputs, including cuts on leptons and jets, electroweak couplings, and other parameters which control run setting, are set in an external input file, allowing the user complete flexibility to customize FEWZ.
- Kinematic distributions are produced automatically during a run, with little overhead. The user can select which histograms to fill in an external input file. Most distributions of interest are included in the default version of FEWZ.
- When running with PDF sets that contain error eigenvectors, all eigenvectors are calculated automatically for each histogram bin. The resulting output can be combined using the included scripts to produce a final output file that contains the integration error as well as PDF error for both the total cross section and each histogram bin. FEWZ can be run using either LHAPDF, or with one of several PDF sets with native support.
- Shell scripts are provided for farming out the sectors in parallel either locally or on *Condor*, and a finishing script which combines the results of individual sectors. In addition to the basic operation of combining the sectors and computing PDF errors, the finishing script can perform operations such as addition, subtraction, multiplication, and division on different runs, all while treating the integration and PDF errors consistently.

- The user can either choose from two hard-coded schemes for the input parameters, the $\alpha(M_Z)$ or G_μ scheme, or specify each coupling manually. However, if the user decides to manually input the coupling parameters, only the QED corrections will be included in order to protect gauge invariance.

For more details on the usage or validation of FEWZ we refer the user to the publications [7, 8, 96] and the online documentation at <http://gate.hep.anl.gov/fpetriello/FEWZ.html>.

Appendix A.4: HORACE

HORACE is a parton-level Monte Carlo generator for precision simulations of charged-current and neutral-current Drell–Yan processes $pp \rightarrow W \rightarrow lv_l$ and $pp \rightarrow \gamma, Z \rightarrow l^+l^-, l = e, \mu$ at hadron colliders.

It is available at the web site <http://www2.pv.infn.it/~hepcomplex/horace.html>. It can be used to generate both weighted and unweighted events and to obtain predictions under realistic event selection conditions.

In a nutshell, the program includes the exact NLO electroweak (EW) radiative corrections matched with a QED Parton Shower (PS) to take into account higher-order QED leading logarithmic contributions due to multiple photon emission from any charged legs, according to the formulation described in detail in [10, 11]. Therefore, the code, on top of the exact EW NLO corrections, includes the leading effects due to initial and final state multiple photon radiation, as well as its interference. Thanks to the PS approach implemented in the code, the transverse degree of freedom of the emitted photons beyond $\mathcal{O}(\alpha)$ are kept under control. The generator can also run including only final-state-like QED corrections in a pure PS approach, as described in [4, 9]. Fixed-order or PS QCD contributions are not accounted for in the program.

As different classes of corrections are included in HORACE, it can be used to provide an estimate of higher-order effects and theoretical uncertainties, as documented in the report.

In detail, in HORACE the following EW contributions are taken into account

- Complete NLO EW corrections matched to multiple photon contributions.
- Leading universal EW effects beyond NLO (running α , ρ parameter).
- Different EW input parameter schemes (α_{G_μ} , $\alpha(0)$, $\alpha(M_Z)$)
- Photon-induced processes (γq and $\gamma\gamma$ contributions).
- Pair corrections in the leading logarithmic approximation.

Appendix A.5: PHOTOS

For a long time, the PHOTOS Monte Carlo program [97,98] was used for the generation of bremsstrahlung in the decay of particles and resonances. The core of the algorithm operates on elementary decays. Thanks to carefully studied properties of QED and investigation of several options for exact phase space parameterization, an algorithm could be constructed. With certain probability, PHOTOS algorithm replaces the kinematic configuration of the Born level decay with a new one, where a bremsstrahlung photon or photons are added and other particle momenta are modified. Over the years the program evolved into a high precision tool [99], for example it was found very useful in the interpretation of data for the precision measurement of the W mass by CDF and D0 [100,101]. In the 2005 program version 2.15 multi-photon radiation was introduced [12]. To gain flexibility of its application, the FORTRAN implementation is being replaced gradually by C++ and instead of HEPEVT, the C++ event structure HepMC [102] is used as the event record. Emission kernel based on complete first order matrix elements for QED final state bremsstrahlung was introduced, following papers [99,103] in [104].

Here we describe several initializations for PHOTOS, which may be of interest for the study of effects due to final state photonic bremsstrahlung in W or Z decays. We do not intent a detailed documentation, but we will rather point to parameters which need to be changed with respect to defaults and the code documented in [104].

In practical applications for detector response simulations PHOTOS in exponentiation mode will be certainly the best choice, both in case of Z and W decays. In case of C++ applications kernel featuring first order matrix element is then available as well. The initialization methods `Photos::setMeCorrectionWtForW(bool corr)`, `Photos::setMeCorrectionWtForZ(bool corr)` and `Photos::setExponentiation(bool expo)` should be all set true.

If matrix elements initialization is set false universal process independent kernel is used. This may be of interest to cross check the numerical importance of matrix element effect, which was missing for example in the FORTRAN implementation of PHOTOS. From our study [105] we conclude that the matrix element was necessary to improve precision from 0.3% of the FORTRAN version of PHOTOS to 0.2% precision level now. This uncertainty is for all QED final state emissions: photons, additional pairs and interference effect combined.

For the studies of bremsstrahlung systematic on observables relating W and Z decays one may be interested in degrading emission kernels to the level when the same formulae are used in W and Z decays. In case of the Z decays

kernel is applied for both outgoing leptons, but it is then the same as for the photon emission in W decay. Not only `Photos::setMeCorrectionWtForW(bool corr)`, `Photos::setMeCorrectionWtForZ(bool corr)` should be set to false, but also `Photos::setInterference(bool interference)` and `Photos::setCorrectionWtForW(bool corr)`. The size of this part of the bremsstrahlung effect, which is distinct for W and Z decays, can be then studied by comparison.

There are two other modes which are of importance. Single photon emission mode and double photon emission mode. Both of these modes are for the studies of theoretical effects.

Single photon mode, activated with `Photos::setExponentiation(bool expo)` and `Photos::setDoubleBrem(bool doub)` both set to false, is suitable to evaluate if definition of what is QED Final State Radiation (FSR) matrix element is the same in PHOTOS as in the calculation of complete electroweak corrections. This has to be verified, as we have done in case of studies with SANC. We have validated that indeed calculation of pure weak effects with contribution of final state QED bremsstrahlung removed can be used together with PHOTOS because QED bremsstrahlung is defined in both packages in the same way. The complete calculation resulting from use of pure weak calculator SANC and PHOTOS simultaneously has its systematic error under precise control. One should keep in mind that comparisons and studies of separating out pure EW from QED FSR are not straightforward. In the single photon mode, the so-called k_0 bias, resulting from the fact that below this threshold real photons are not generated by PHOTOS but their kinematic effect may be present in the part of QED FSR corrections removed from pure weak calculation.

Careful definition of separation between QED FSR and pure weak corrections is specially important in case of W , charged and relatively broad resonance, decay.

In case of the two photon mode, activated with `Photos::setDoubleBrem(bool doub)`, the k_0 bias is even stronger than in the single photon one. The purpose of this mode is to check how the iterative algorithm of PHOTOS works. Comparisons with the calculations faring exact double photon emission amplitudes can be performed that way as it was done in early time with tests using papers [106,107], a step in this direction is documented in [108] in context of the ϕ^* observable. General scheme for such studies of particular terms, such as interference corrections, or effects of second order QED matrix element embedded in exclusive exponentiation is now available for predictions for pp collisions as well, see Ref. [109].

To conclude, the PHOTOS Monte Carlo program is suitable now for applications at the 0.2% precision level for QED FSR emission and observables of single W or Z production

and decay. This result is valid for C++ HepMC applications including ϕ_η^* observable when kernels based on matrix element can be used. Otherwise precision of 0.3% should be assumed. Further improvement on precision is possible. Better test or implementation of pair emission is then needed as well as detailed discussion of interferences effect which may at certain moment need to be implemented as well with the help of correction weight added into PHOTOS and also initial state emission/parton shower algorithm. Finally let us point out that tests of Ref. [105] provide interesting technical tests of SANC as well.

Acknowledgements This project is financed in part from funds of Polish National Science Centre under decisions DEC-2011/03/B/ST2/00220 and DEC-2012/04/M/ST2/00240. Useful discussions with E. Richter-Was are acknowledged.

Appendix A.6: POWHEG_BMNNP and POWHEG_BMNNPV

Here we describe the simulation of Drell–Yan (DY) processes in the POWHEG BOX performed by means of the two separate packages: $W_{ew-BMNNP}$ [14] for the $pp \rightarrow W \rightarrow l\nu$ process and $Z_{ew-BMNNPV}$ [15] for $pp \rightarrow Z/\gamma^* \rightarrow l^+l^-$. They are available in the public repository of the POWHEG BOX [94] (Version 2) at the web site <http://powhegbox.mib.infn.it>.

The common feature of the two packages is the treatment of the hard matrix elements with NLO QCD and NLO Electroweak (EW) corrections, supplemented with QCD and QED higher order contributions within the POWHEG framework. The QCD virtual corrections and real radiation matrix elements are the same as the ones contained in POWHEG_W(Z) [13], while the expressions of the virtual EW corrections are the ones publicly available in Ref. [17] for the charged-current DY process and in Ref. [18] for the neutral-current DY process. The infrared and collinear singularities of EW origin in the loop integrals are regulated using a hybrid scheme: the singularities associated with the colored charged particles and the photon are regulated with dimensional regularization, while QED mass singularities are regulated by keeping finite lepton masses. The soft and collinear singularities of the real radiation matrix elements are subtracted using the FKS subtraction scheme [110], both for QCD radiation as well as for QED radiation described by the matrix elements associated to one-photon emission off quarks and leptons $q\bar{q}' \rightarrow W \rightarrow l\nu + \gamma$ and $q\bar{q} \rightarrow Z/\gamma^* \rightarrow l^+l^- + \gamma$. The singularities associated with the unstable nature of the W/Z vector bosons circulating in the loops are treated according to the factorization scheme [17, 18] and the complex mass scheme [111, 112]. The generation of the hardest radiation is performed by means of the product of Sudakov form factors associated with the singular regions

and defined in terms of the QCD and QED real radiation matrix elements. Thus the generation of a radiative event, i.e. containing an additional QCD parton or an additional photon,¹⁴ is the result of a competition between QCD and QED emission.

The NLO QCD and EW corrections are matched with Parton Shower (PS) contributions, according to the POWHEG method: once the configuration with the hardest (in transverse momentum) emission has been generated, the subsequent radiation process is handled by the PS (both for QCD and QED radiation) ordered in p_T , applying a veto technique. The multiple photon emission from external leptons is included by default by means of the package PHOTOS [12], switching off the contribution of QED radiation from the PS. Alternatively, it can be treated by the PS itself, and in this case also multiple QED radiation from initial state partons is simulated.

In summary, the POWHEG DY libraries $W_{ew-BMNNP}$ and $Z_{ew-BMNNPV}$ share the following features:

- normalization with QCD + EW corrections at NLO accuracy
- complete SM NLO corrections matched to a mixed QCD \otimes QED parton cascade, where the particles present in the shower are coloured particles or photons
- mixed $\mathcal{O}(\alpha\alpha_s)$ contributions partially taken into account (according to a factorized prescription, by construction)

The adopted input parameter schemes are the following ones:

- charged-current DY: G_μ scheme as default, where the input parameters are G_μ , M_W and M_Z . The user can also switch to the $\alpha(0)$ scheme (even if not recommended), where the input parameters are $\alpha(0)$, M_W and M_Z . In this scheme the masses of the light quarks in the fermionic corrections are taken finite and their values are chosen in such a way to reproduce the hadronic contribution to the hadronic vacuum polarization;
- neutral-current DY: in addition to the above two choices, also the scheme $\alpha(M_Z)$ can be switched on, where, instead of $\alpha(0)$, the value of $\alpha(M_Z)$ is used as input.

For user convenience, the contribution of QCD or EW corrections can be switched off by a proper flag.

Appendix A.7: POWHEG_BW

In POWHEG_BW the full EW $\mathcal{O}(\alpha)$ radiative corrections of Refs. [25, 27] contained in the public MC code WGRAD2 are added to the NLO QCD calculation of the $pp \rightarrow W \rightarrow l\nu$

¹⁴ In the present version the “photon-induced” processes are not considered.

process of POWHEG- W [13]. The resulting MC code, called in the following POWHEG- W_{EW} , is publicly available at the POWHEG_BOX web page and allows the simultaneous study of the effects of both QCD and NLO EW corrections and with both Pythia and Herwig. Note that the effects of photon-induced processes and of multiple photon radiation are not included and that QED corrections in Pythia need to be switched off to avoid double counting.

As default, POWHEG- W_{EW} produces results in the constant-width scheme and by using the fine structure constant, $\alpha(0)$, in both the LO and NLO EW calculation. More options can be found in subroutine `init_phys_EW` but should be used with care and under the advisement of the authors. Since QED radiation has the dominant effect on observables relevant to the W mass measurement, there is the possibility of only including resonant weak corrections by choosing `qnonr=0`, i.e. the weak box diagrams are neglected. Their impact is important in kinematic distributions away from the resonance region. The full weak 1-loop corrections are included with `qnonr=1`. The full set of QED contributions (QED=4) is included as default, i.e. initial-state and final-state radiation as well as interference contributions, but subsets can be studied separately by choosing the flag 'QED' accordingly. The QED factorization scheme can either chosen to be the DIS scheme (`lfc=1`) or the \overline{MS} scheme (`lfc=0`), and both schemes are defined in analogy to the corresponding QCD factorization schemes. A description of the QED factorization scheme as implemented in POWHEG- W_{EW} can be found in Ref. [25].

Fermion masses only enter to the EW gauge boson self-energies and as regulators of the collinear singularity. The mass of the charged lepton is included in the phase space generation of the final-state four-momenta and serves as a regulator of the singularity arising from collinear photon radiation off the charged lepton. Thus, no collinear cut needs to be applied (`collcut=0` in POWHEG- W_{EW}) on final-state photon radiation, allowing the study of finite lepton-mass effects. Note that the application of a collinear cut on final-state photon radiation (`collcut=1`) is only allowed in the electron case and only when a recombination of the electron and photon momenta is performed in the collinear region (usually defined by $\Delta R_{e\gamma} < R_{cut}$, see Ref. [25] for a detailed discussion).

Acknowledgements This research was supported by the National Science Foundation under award No. PHY-1118138 and a LHC Theory Initiative Graduate Fellowship, NSF Grant No. PHY-0705682.

Appendix A.8: RADY

RADY is a Monte Carlo program for the calculation of Radiative corrections to Drell-Yan processes, i.e. $pp/p\bar{p} \rightarrow W/Z \rightarrow l\nu_l/l^+l^-$. As a flexible Monte Carlo integrator, it supports all kinds of event definitions (any experimental cuts,

collinear-safe or non-collinear-safe treatment of photons, jet algorithms, etc.). A large variety of radiative corrections can be included in predictions, not only to achieve high precision, but also to allow for estimates of various scheme dependences and other theoretical uncertainties. In detail, RADY supports:

- Next-to-leading order (NLO) QCD and electroweak (EW) corrections within the SM. For Z production the individually gauge-invariant subsets of photonic final-state radiation, initial-state radiation, and initial-final interferences, as well as the genuine weak corrections can be investigated separately.
- NLO QCD and EW corrections within the Minimal Supersymmetric SM (MSSM). Genuine supersymmetric corrections can be investigated separately.
- Multi-photon radiation effects beyond NLO in the collinear approximation via structure functions.
- Leading universal EW effects beyond NLO (ρ -parameter, running α).
- Leading EW Sudakov logarithms beyond NLO.
- Corrections induced by initial-state photons (γq and $\gamma\gamma$ collisions).
- Different EW input-parameter schemes ($\alpha(0)$, $\alpha(M_Z)$, α_{G_μ}).
- Different gauge-invariant schemes for treating the W/Z resonances (complex-mass scheme, factorization scheme, pole scheme).
- Different technical treatments of soft and/or collinear photon/gluon emission (dipole subtraction and two variants of phase-space slicing). Note that, in particular, the treatment of collinear logarithms of the lepton masses is very efficient in the extended dipole subtraction scheme.
- Mixed NNLO QCD \times EW corrections of $\mathcal{O}(\alpha\alpha_s)$ based on the pole approximation worked out in Refs. [85,87].

Appendix A.9: SANC: mcsanc-v1.01 and mcsanc-v1.20

The SANC system (Support for Analytic and Numeric Calculations for experiments at colliders) [113] implements calculations of complete (real and virtual) NLO QCD and EW corrections for the Drell-Yan CC [19] and NC [20] processes, associative Higgs and gauge boson production [114], single top production [115,116] and several other processes at the partonic level. Here we give a brief summary of the main properties of this framework. For the complete list of SANC processes see [117]. All calculations are performed within the OMS (on-mass-shell) renormalization scheme in the R_ξ gauge [118], which allows an explicit control of the gauge invariance by examining the cancellation of the gauge parameters in analytical expression for matrix element. The use of the OMS scheme leads to running (s -dependent) width in vector boson propagators (cf. Eq. (2.10) of Ref. [18]).

The list of processes implemented in the `mcsanc-v1.01 Monte-Carlo integrator` [119, 120], is given in the Table 1 and the tree level diagrams are shown in Figure 1 of Ref. [120].

NLO corrections contain terms proportional to logarithms of the quark masses, $\log(\hat{s}/m_{u,q}^2)$. They come from the initial state radiation contributions including hard, soft and virtual photon or gluon emission. In the case of hadron collisions these logs have been already *effectively* taken into account in the parton density functions (PDF) and have to be consistently subtracted. The `mcsanc-v1.01` supports both $\overline{\text{MS}}$ and DIS subtraction schemes. A solution described in [121] allows to avoid the double counting of the initial quark mass singularities contained in the results for the corrections to the free quark cross section and the ones contained in the corresponding PDF. The latter should also be taken in the same scheme with the same factorization scale.

For example, the $\overline{\text{MS}}$ QED subtraction to the fixed (leading) order in α is given by:

$$\begin{aligned} \bar{q}(x, M^2) &= q(x, M^2) - \int_x^1 \frac{dz}{z} q\left(\frac{x}{z}, M^2\right) \frac{\alpha}{2\pi} \\ &\quad \times Q_q^2 \left[\frac{1+z^2}{1-z} \left\{ \ln\left(\frac{M^2}{m_q^2}\right) - 2 \ln(1-z) - 1 \right\} \right]_+ \\ &\equiv q(x, M^2) - \Delta q, \end{aligned}$$

where $q(x, M^2)$ is the parton density function in the $\overline{\text{MS}}$ scheme computed using the QED DGLAP evolution.

The differential hadronic cross section for DY processes with one-loop EW corrections is given by:

$$\begin{aligned} d\sigma^{pp \rightarrow \ell\ell' X} &= \sum_{q_1 q_2} \int_0^1 \int_0^1 dx_1 dx_2 \bar{q}_1(x_1, M^2) \\ &\quad \times \bar{q}_2(x_2, M^2) d\hat{\sigma}^{q_1 q_2 \rightarrow \ell\ell'}, \end{aligned} \quad (\text{A.1})$$

where $\bar{q}_1(x_1, M^2)$, $\bar{q}_2(x_2, M^2)$ are the parton density functions of the incoming quarks modified by the subtraction of the quark mass singularities and $d\hat{\sigma}^{q_1 q_2 \rightarrow \ell\ell'}$ is the partonic cross section of corresponding hard process. The sum is performed over all possible quark combinations for a given type of process ($q_1 q_2 = u\bar{d}, u\bar{s}, c\bar{d}, c\bar{s}$ for CC and $q_1 q_2 = u\bar{u}, d\bar{d}, s\bar{s}, c\bar{c}, b\bar{b}$ for NC). The expressions for other processes are similar.

The effect of applying different EW schemes in the SANC system is discussed in [20]. The SANC system supports $\alpha(0)$, G_μ , $\alpha(M_Z)$, of which the G_μ -scheme [122] can be preferable since it minimizes EW radiative corrections to the inclusive DY cross section.

The scheme of the SANC framework is shown on the Fig. 39. Analytical expressions are obtained for the formfactors and amplitudes of generalized processes $ffbb \rightarrow 0$ and $4f \rightarrow 0$ and stored as the FORM [123] language expressions [113, 114, 124, 125]. The latter are translated to the Fortran

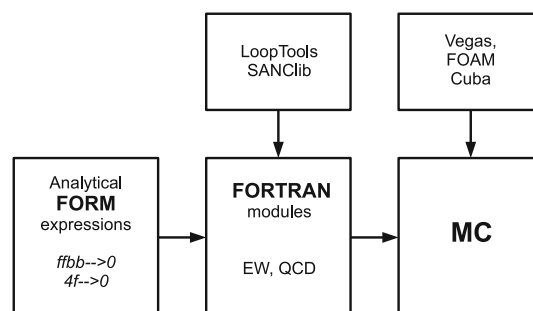


Fig. 39 The SANC framework scheme

modules [117] for specific parton level processes with an unified treatment QCD and EW NLO corrections. The modules are utilising Looptools [126] and SANCLib [127] packages for loop integrals evaluation. To build a Monte-Carlo code one convolutes the partonic cross sections from the modules with the parton density functions and feeds the result as an integrand to any Monte-Carlo algorithm implementation, e.g. FOAM [128] or Cuba [129].

Depending on the process and type of corrections, we subdivide the total NLO cross section at the partonic level into several terms: $d\sigma = \sum_{id=1}^{id=6} d\sigma_{id}$, differential over a generic observable which is a function of the final state momenta. The individual terms depend on auxiliary parameters $\bar{\omega}$ (photon energy which separates phase spaces associated with the soft and hard photon emission) and λ (photon mass which regularizes infrared divergences) which are introduced in the NLO calculations. They cancel out after summation in any physically observable differential NLO cross section. In general, NLO level hard sub-processes consist of: LO – leading order (id=0), *virt* – virtual (id=2), *real* brems(glue)-strahlung, $q\bar{q}$ -, gq -channels (id=3–4,6) and *subt* – subtraction (id=1,5); *real*, in turn, is subdivided into *soft* (id=3) and *hard* (id=4) contributions by the soft-hard separator parameter $\bar{\omega}$. (For description of id’s see Section 2.1 of [119].) The entire NLO sub-process cross section is independent of both unphysical parameters $\bar{\omega}$ and m_q .

The `mcsanc-v1.01` code [120] was thoroughly cross checked against another tools to provide reliable results. Many numerical comparisons with the well known MCFM [130] package are presented in Ref. [119]. The NLO QCD values are in agreement within statistical errors. To conclude, we note, that the “best what `mcsanc` can do at pure NLO level” i.e. the recommended approximation, is computation of distributions in the G_μ EW scheme with running widths.

The new `mcsanc-v1.20` version of integrator is published in [131]. The extensions concern implementation of Drell–Yan-like processes and include a systematic treatment of the photon-induced contribution in proton–proton collisions and electroweak corrections beyond NLO approximation. There are also technical improvements such as the calculation of the

forward-backward asymmetry for the neutral current Drell–Yan process. Results were compared to the ones presented in [18, 132]. The numbers illustrate good agreement within the statistical errors of the Monte Carlo integration.

Acknowledgements This work was supported in part by the RFBR grant 12-02-91526-CERN_a and by the Dynasty Foundation.

Appendix A.10: WINHAC

WINHAC [22–24] is a Monte Carlo event generator for Drell–Yan (DY) processes in proton–proton, proton–antiproton as well as nucleus–nucleus collisions. It features multiphoton radiation in the charge-current (W -boson mediated) DY processes within the Yennie–Frautschi–Suura (YFS) exclusive exponentiation scheme [61] and the $\mathcal{O}(\alpha)$ electroweak (EW) radiative corrections with initial-state photon radiation (ISR) subtracted in a gauge invariant way. The analytical formulae of the $\mathcal{O}(\alpha)$ virtual and soft-photon corrections have been obtained by the SANC group and provided in form of a numerical library [133]. They are implemented in WINHAC in two versions: (1) as the EW corrections to W -boson decays and (2) as the EW corrections to the full charged-current DY process. In the latter case the quark mass singularities of the ISR are subtracted in a gauge-invariant way. Two subtraction methods are implemented in the current version of WINHAC: (1) the “YFS-like scheme” described in [133] and (2) the “dipole-subtraction scheme”, similar to a recently developed method for matching NLO QCD effects with parton showers [134]. Generation of ISR photons is handed to the parton shower generators, such as Pythia or Herwig. Therefore, the predictions of WINHAC may differ slightly from the calculations based on the $\overline{\text{MS}}$ or DIS QED subtraction schemes.

The current version, 1.37, of WINHAC includes the Les Houches Accord (LHA) interface to parton shower generators, such as Pythia, Herwig, etc. This interface allows to write WINHAC generated events into a disk file or a named (FIFO) pipe, which can then be read in and processed further by an appropriate generator of QED/QCD parton showers and hadronisation. Using the FIFO pipe instead of an ordinary disk file has some advantages: programs run faster, one does not have to deal with huge data files, very large event statistics can be generated without overloading disk/quota capacity. We include a demo program in which events from WINHAC are sent to PYTHIA 6.4 for parton showering and hadronisation through one FIFO pipe and then sent back through another FIFO pipe to WINHAC for event analysis. In addition to the LHA interface, WINHAC includes also an internal interface to PYTHIA 6.4, in which appropriate PYTHIA routines are called directly from the WINHAC code. It is less universal but faster in CPU time and can be used for some dedicated studies, see e.g. Refs. [135–137]. Moreover, it includes options for correcting the PYTHIA 6 problem

of wrong charge asymmetries of the DY leptons transverse momenta, see Ref. [138].

In addition to unpolarized W -boson production, the program provides options for generation of polarized W -bosons in three different reference frames. WINHAC also includes the neutral-current (Z/γ) Drell–Yan process at the Born level and with the FSR QED corrections generated by PHOTOS [104] (through a dedicated interface). PHOTOS can also be used to generate QED FSR in the W -boson case, which might be useful for some studies.

WINHAC is interfaced with the LHAPDF package and provides the possibility to compute auxiliary weights corresponding to PDF errors; all these weights are calculated in a single MC run. In the case of nucleus–nucleus collisions, an option for switching on/off nuclear shadowing effects for PDFs is provided. Nuclear beams are defined through the input parameters by setting atomic numbers A , charge numbers Z and energies of two colliding nuclei. This collider option was applied to studies presented in Refs. [135, 139].

The QED FSR corrections in WINHAC were compared numerically with the ones implemented in the MC generator HORACE and a good agreement of the two programs for several observables was found [140]. Implementation of the $\mathcal{O}(\alpha)$ EW corrections was successfully cross-checked (to a high precision) with the SANC program [133].

Several options and steering parameters available in WINHAC make it a flexible Monte Carlo tool for various studies and tests related to the DY processes, particularly in the context of the Higgs-boson production at the LHC [141–143]. The original WINHAC program is written in Fortran, however rewriting it in C++ is already quite advanced [144]. A similar event generator for the neutral-current Drell–Yan process, called ZINHAC, is under development. We also work on the QCD NLO parton-shower algorithm and matching it with the QCD NLO hard process matrix elements, see [134, 145, 146].

Acknowledgements This research is supported in part by the programme of the French–Polish co-operation between IN2P3 and COPIN No. 05-116 and by the Polish National Centre of Science Grant No. DEC-2012/04/M/ST2/00240. We also thank the Galileo Galilei Institute for Theoretical Physics in Florence for the hospitality and the INFN for partial support during the GGI Workshop “Prospects and Precision at the Large Hadron Collider at 14 TeV” where some parts of this work were done.

Appendix A.11: WZGRAD

WZGRAD combines the Monte Carlo programs WGRAD2 [25, 27] and ZGRAD2 [26]. It is a parton-level Monte Carlo program that includes the complete $\mathcal{O}(\alpha)$ electroweak radiative corrections to $p p^{(-)} \rightarrow W^\pm \rightarrow \ell^\pm \nu X$ (WGRAD2) and

$p\bar{p} \rightarrow \gamma, Z \rightarrow \ell^+\ell^-X$ ($\ell = e, \mu$) (ZGRAD2). For the numerical evaluation, the Monte Carlo phase space slicing method for next-to-leading-order (NLO) calculations described in Refs. [147, 148] is used. Final-state charged lepton mass effects are included in the following approximation. The lepton mass regularizes the collinear singularity associated with final state photon radiation. The associated mass singular logarithms of the form $\ln(\hat{s}/m_\ell^2)$, where \hat{s} is the squared parton center of mass energy and m_ℓ is the charged lepton mass, are included in the calculation, but the very small terms of $\mathcal{O}(m_\ell^2/\hat{s})$ are neglected.

As a result of the absorption of the universal initial-state mass singularities by redefined (*renormalized*) PDFs [25, 149], the cross sections become dependent on the QED factorization scale μ_{QED} . In order to treat the $\mathcal{O}(\alpha)$ initial-state photonic corrections to W and Z production in hadronic collisions in a consistent way, the parton distribution functions should be used which include QED corrections such as NNPDF2.3QED [32]. Absorbing the collinear singularity into the PDFs introduces a QED factorization scheme dependence. The squared matrix elements for different QED factorization schemes differ by the finite $\mathcal{O}(\alpha)$ terms which are absorbed into the PDFs in addition to the singular terms. WZGRAD can be used both in the QED $\overline{\text{MS}}$ and DIS schemes, which are defined analogously to the usual $\overline{\text{MS}}$ [150] and DIS [31] schemes used in QCD calculations.

It is recommended that WZGRAD is used with a constant width and the G_μ input scheme, which corresponds to the EW input scheme used for producing the benchmark results in this report. Radiative corrections beyond $\mathcal{O}(\alpha)$ are partially implemented as described in Sect. 3.4.5.

Appendix B: Tuned comparison of total cross sections at NLO EW and NLO QCD for W^\pm and Z production with LHCb cuts

The results of the comparison of the total cross sections, computed with LHCb acceptance cuts, are presented in Tables 13, 14, 15, 16, 17 and 18.

Table 13 $pp \rightarrow W^+ \rightarrow l^+ \nu_l$ cross sections (in pb) at the 8 TeV LHC, with LHCb cuts and bare leptons

Code	LO	NLO QCD	NLO EW μ	NLO EW e
HORACE	841.82(3)	×	876.93(4)	862.99(5)
WZGRAD	841.820(7)	×	876.81(2)	862.86(3)
RADY	841.822(3)	928.61(9)	876.92(1)	862.96(1)
SANC	841.818(8)	928.8(1)	876.61(2)	862.59(2)
FEWZ	841.80(5)	928.8(1)	×	×
POWHEG-w	841.7(2)	928.67(4)	×	×

Table 14 $pp \rightarrow W^+ \rightarrow l^+ \nu_l$ cross sections (in pb) at the 8 TeV LHC, with LHCb cuts and “calorimetric” leptons

Code	LO	NLO-EW μ calo	NLO EW e calo
HORACE	841.82(3)	831.94(4)	876.33(5)
WZGRAD	841.820(7)	831.57(2)	875.97(3)
SANC	841.818(8)	831.36(2)	875.88(1)

Table 15 $pp \rightarrow W^- \rightarrow l^- \bar{\nu}_l$ cross sections (in pb) at the 8 TeV LHC, with LHCb cuts and bare leptons

Code	LO	NLO QCD	NLO EW μ	NLO EW e
HORACE	640.36(2)	×	664.81(3)	652.66(3)
WZGRAD	640.358(5)	×	664.79(1)	652.68(2)
RADY	640.353(2)	665.93(9)	664.828(8)	652.712(8)
SANC	640.357(2)	666.8(1)	664.784(6)	652.630(6)
FEWZ	640.35(2)	666.00(8)	×	×
POWHEG-w	640.36(2)	666.23(6)	×	×

Table 16 $pp \rightarrow W^- \rightarrow l^- \bar{\nu}_l$ cross sections (in pb) at the 8 TeV LHC, with LHCb cuts and “calorimetric” leptons

Code	LO	NLO-EW μ calo	NLO EW e calo
HORACE	640.36(2)	630.82(3)	665.24(4)
WZGRAD	640.358(5)	630.60(1)	665.16(2)
SANC	640.357(2)	630.597(6)	665.139(8)

Table 17 $pp \rightarrow \gamma, Z \rightarrow l^- l^+$ cross sections (in pb) at the 8 TeV LHC, with LHCb cuts and bare leptons

Code	LO	NLO QCD	NLO EW μ	NLO EW e
HORACE	75.009(2)	×	77.838(4)	76.053(4)
WZGRAD	75.0090(7)	×	77.931(2)	76.233(3)
RADY	75.0112(3)	87.173(8)	77.9518(9)	76.2523(9)
SANC	75.0087(4)	87.23(1)	77.881(4)	76.182(2)
FEWZ	75.001(3)	87.19(1)	(×)	(×)
POWHEG-z	75.04(2)	87.188(4)	×	×

Table 18 $pp \rightarrow \gamma, Z \rightarrow l^+ l^-$ cross sections (in pb) at the 8 TeV LHC, with LHCb cuts and “calorimetric” leptons

Code	LO	NLO-EW μ calo	NLO EW e calo
HORACE	75.009(2)	67.979(4)	77.142(4)
WZGRAD	75.0090(7)	67.961(2)	77.304(3)
SANC	75.0047(9)	67.9821(9)	77.245(2)

References

1. M.L. Mangano, Adv. Ser. Direct. High Energy Phys. **26**, 231 (2016). doi:[10.1142/9789814733519_0013](https://doi.org/10.1142/9789814733519_0013)

2. M. Baak, A. Blondel, A. Bodek, R. Caputo, T. Corbett et al., Working Group Report: Precision Study of Electroweak Interactions (2013). [arXiv:1310.6708](https://arxiv.org/abs/1310.6708)
3. J.R. Andersen et al., Les Houches 2013: Physics at TeV Colliders: Standard Model Working Group Report (2014). [arXiv:1405.1067](https://arxiv.org/abs/1405.1067)
4. C.M. Carloni Calame, G. Montagna, O. Nicrosini, M. Treccani, Phys. Rev. D **69**, 037301 (2004). doi:[10.1103/PhysRevD.69.037301](https://doi.org/10.1103/PhysRevD.69.037301)
5. S. Catani, L. Cieri, G. Ferrera, D. de Florian, M. Grazzini, Phys. Rev. Lett. **103**, 082001 (2009). doi:[10.1103/PhysRevLett.103.082001](https://doi.org/10.1103/PhysRevLett.103.082001)
6. A. Karlberg, E. Re, G. Zanderighi, JHEP **1409**, 134 (2014). doi:[10.1007/JHEP09\(2014\)134](https://doi.org/10.1007/JHEP09(2014)134)
7. R. Gavin, Y. Li, F. Petriello, S. Quackenbush, Comput. Phys. Commun. **184**, 208 (2013). doi:[10.1016/j.cpc.2012.09.005](https://doi.org/10.1016/j.cpc.2012.09.005)
8. Y. Li, F. Petriello, Phys. Rev. D **86**, 094034 (2012). doi:[10.1103/PhysRevD.86.094034](https://doi.org/10.1103/PhysRevD.86.094034)
9. C.M. Carloni Calame, G. Montagna, O. Nicrosini, M. Treccani, JHEP **05**, 019 (2005). doi:[10.1088/1126-6708/2005/05/019](https://doi.org/10.1088/1126-6708/2005/05/019)
10. C.M. Carloni Calame, G. Montagna, O. Nicrosini, A. Vicini, JHEP **0612**, 016 (2006). doi:[10.1088/1126-6708/2006/12/016](https://doi.org/10.1088/1126-6708/2006/12/016)
11. C. Carloni Calame, G. Montagna, O. Nicrosini, A. Vicini, JHEP **0710**, 109 (2007). doi:[10.1088/1126-6708/2007/10/109](https://doi.org/10.1088/1126-6708/2007/10/109)
12. P. Golonka, Z. Was, Eur. Phys. J. C **45**, 97 (2006). doi:[10.1140/epjc/s2005-02396-4](https://doi.org/10.1140/epjc/s2005-02396-4)
13. S. Alioli, P. Nason, C. Oleari, E. Re, JHEP **0807**, 060 (2008). doi:[10.1088/1126-6708/2008/07/060](https://doi.org/10.1088/1126-6708/2008/07/060)
14. L. Barze, G. Montagna, P. Nason, O. Nicrosini, F. Piccinini, JHEP **1204**, 037 (2012). doi:[10.1007/JHEP04\(2012\)037](https://doi.org/10.1007/JHEP04(2012)037)
15. L. Barze, G. Montagna, P. Nason, O. Nicrosini, F. Piccinini et al., Eur. Phys. J. C **73**(6), 2474 (2013). doi:[10.1140/epjc/s10052-013-2474-y](https://doi.org/10.1140/epjc/s10052-013-2474-y)
16. C. Bernaciak, D. Wackeroth, Phys. Rev. D **85**, 093003 (2012). doi:[10.1103/PhysRevD.85.093003](https://doi.org/10.1103/PhysRevD.85.093003)
17. S. Dittmaier, M. Kramer, Phys. Rev. D **65**, 073007 (2002). doi:[10.1103/PhysRevD.65.073007](https://doi.org/10.1103/PhysRevD.65.073007)
18. S. Dittmaier, M. Huber, JHEP **1001**, 060 (2010). doi:[10.1007/JHEP01\(2010\)060](https://doi.org/10.1007/JHEP01(2010)060)
19. A.B. Arbuzov, D.Y. Bardin, S. Bondarenko, P. Christova, L. Kalinovskaya, G.O. Nanava, R. Sadykov, Eur. Phys. J. C **46**, 407 (2006). doi:[10.1140/epjc/s2006-02505-y](https://doi.org/10.1140/epjc/s2006-02505-y). doi:[10.1140/epjc/s10052-007-0225-7](https://doi.org/10.1140/epjc/s10052-007-0225-7)
20. A. Arbuzov, D. Bardin, S. Bondarenko, P. Christova, L. Kalinovskaya et al., Eur. Phys. J. C **54**, 451 (2008). doi:[10.1140/epjc/s10052-008-0531-8](https://doi.org/10.1140/epjc/s10052-008-0531-8)
21. S. Höche, Y. Li, S. Prestel, Phys. Rev. D **91**(7), 074015 (2015). doi:[10.1103/PhysRevD.91.074015](https://doi.org/10.1103/PhysRevD.91.074015)
22. W. Placzek, S. Jadach, Eur. Phys. J. C **29**, 325 (2003). doi:[10.1140/epjc/s2003-01223-4](https://doi.org/10.1140/epjc/s2003-01223-4)
23. W. Placzek, PoS **EPS-HEP2009**, 340 (2009)
24. W. Placzek, S. Jadach, M.W. Krasny, Acta Phys. Pol. B **44**(11), 2171 (2013). doi:[10.5506/APhysPolB.44.2171](https://doi.org/10.5506/APhysPolB.44.2171)
25. U. Baur, S. Keller, D. Wackeroth, Phys. Rev. D **59**, 013002 (1999). doi:[10.1103/PhysRevD.59.013002](https://doi.org/10.1103/PhysRevD.59.013002)
26. U. Baur, O. Brein, W. Hollik, C. Schappacher, D. Wackeroth, Phys. Rev. D **65**, 033007 (2002). doi:[10.1103/PhysRevD.65.033007](https://doi.org/10.1103/PhysRevD.65.033007)
27. U. Baur, D. Wackeroth, Phys. Rev. D **70**, 073015 (2004). doi:[10.1103/PhysRevD.70.073015](https://doi.org/10.1103/PhysRevD.70.073015)
28. J. Beringer et al., Phys. Rev. D **86**, 010001 (2012). doi:[10.1103/PhysRevD.86.010001](https://doi.org/10.1103/PhysRevD.86.010001)
29. F. Jegerlehner, J. Phys. G **29**, 101 (2003). doi:[10.1088/0954-3899/29/1/311](https://doi.org/10.1088/0954-3899/29/1/311)
30. A. Martin, W. Stirling, R. Thorne, G. Watt, Eur. Phys. J. C **63**, 189 (2009). doi:[10.1140/epjc/s10052-009-1072-5](https://doi.org/10.1140/epjc/s10052-009-1072-5)
31. J.F. Owens, W.K. Tung, Annu. Rev. Nucl. Part. Sci. **42**, 291 (1992). doi:[10.1146/annurev.ns.42.120192.001451](https://doi.org/10.1146/annurev.ns.42.120192.001451)
32. R.D. Ball, V. Bertone, S. Carrazza, L. Del Debbio, S. Forte, A. Guffanti, N.P. Hartland, J. Rojo, Nucl. Phys. B **877**, 290 (2013). doi:[10.1016/j.nuclphysb.2013.10.010](https://doi.org/10.1016/j.nuclphysb.2013.10.010)
33. C. Schmidt, J. Pumplin, D. Stump, C.P. Yuan, Phys. Rev. D **93**(11), 114015 (2016). doi:[10.1103/PhysRevD.93.114015](https://doi.org/10.1103/PhysRevD.93.114015)
34. A. Denner, T. Sack, Nucl. Phys. B **347**, 203 (1990). doi:[10.1016/0550-3213\(90\)90557-T](https://doi.org/10.1016/0550-3213(90)90557-T)
35. A. Banfi, S. Redford, M. Vesterinen, P. Waller, T.R. Wyatt, Eur. Phys. J. C **71**, 1600 (2011). doi:[10.1140/epjc/s10052-011-1600-y](https://doi.org/10.1140/epjc/s10052-011-1600-y)
36. C. Buttar, S. Dittmaier, V. Drollinger, S. Frixione, A. Nikitenko et al., Les Houches Physics at TeV Colliders 2005, Standard Model and Higgs Working Group: Summary Report (2006). [arXiv:hep-ph/0604120](https://arxiv.org/abs/hep-ph/0604120)
37. C. Gerber et al., Tevatron-for-LHC Report: Top and Electroweak Physics (2007). [arXiv:0705.3251](https://arxiv.org/abs/0705.3251)
38. J.R. Andersen et al., in *9th Les Houches Workshop on Physics at TeV Colliders (PhysTeV 2015) Les Houches, France, June 1–19, 2015* (2016). [arXiv:1605.04692](https://arxiv.org/abs/1605.04692)
39. A. Denner, S. Dittmaier, T. Kasprzik, A. Mueck, JHEP **08**, 075 (2009). doi:[10.1088/1126-6708/2009/08/075](https://doi.org/10.1088/1126-6708/2009/08/075)
40. A. Denner, S. Dittmaier, T. Kasprzik, A. Mueck, JHEP **06**, 069 (2011). doi:[10.1007/JHEP06\(2011\)069](https://doi.org/10.1007/JHEP06(2011)069)
41. L. Barze, G. Montagna, P. Nason, O. Nicrosini, F. Piccinini et al., Eur. Phys. J. C **73**, 2474 (2013). doi:[10.1140/epjc/s10052-013-2474-y](https://doi.org/10.1140/epjc/s10052-013-2474-y)
42. D. Wackeroth, W. Hollik, Phys. Rev. D **55**, 6788 (1997). doi:[10.1103/PhysRevD.55.6788](https://doi.org/10.1103/PhysRevD.55.6788)
43. A. Sirlin, Phys. Rev. D **22**, 971 (1980). doi:[10.1103/PhysRevD.22.971](https://doi.org/10.1103/PhysRevD.22.971)
44. W.J. Marciano, A. Sirlin, Phys. Rev. D **22**(2695), 1980 (1985). doi:[10.1103/PhysRevD.22.2695](https://doi.org/10.1103/PhysRevD.22.2695) [Erratum: Phys. Rev. D **31**, 213, doi:[10.1103/PhysRevD.31.213](https://doi.org/10.1103/PhysRevD.31.213)]
45. R. Boughezal, J.M. Campbell, R.K. Ellis, C. Focke, W. Giele, X. Liu, F. Petriello, C. Williams, Eur. Phys. J. C **77**, 7 (2017). doi:[10.1140/epjc/s10052-016-4558-y](https://doi.org/10.1140/epjc/s10052-016-4558-y)
46. C. Anastasiou, L.J. Dixon, K. Melnikov, F. Petriello, Phys. Rev. Lett. **91**, 182002 (2003). doi:[10.1103/PhysRevLett.91.182002](https://doi.org/10.1103/PhysRevLett.91.182002)
47. S. Frixione, G. Ridolfi, Nucl. Phys. B **507**, 315 (1997). doi:[10.1016/S0550-3213\(97\)00575-0](https://doi.org/10.1016/S0550-3213(97)00575-0)
48. S. Frixione, B.R. Webber, JHEP **0206**, 029 (2002). doi:[10.1088/1126-6708/2002/06/029](https://doi.org/10.1088/1126-6708/2002/06/029)
49. P. Nason, JHEP **0411**, 040 (2004). doi:[10.1088/1126-6708/2004/11/040](https://doi.org/10.1088/1126-6708/2004/11/040)
50. K. Hamilton, P. Nason, G. Zanderighi, JHEP **1210**, 155 (2012). doi:[10.1007/JHEP10\(2012\)155](https://doi.org/10.1007/JHEP10(2012)155)
51. K. Hamilton, P. Nason, C. Oleari, G. Zanderighi, JHEP **1305**, 082 (2013). doi:[10.1007/JHEP05\(2013\)082](https://doi.org/10.1007/JHEP05(2013)082)
52. G.A. Ladinsky, C.P. Yuan, Phys. Rev. D **50**, 4239 (1994). doi:[10.1103/PhysRevD.50.R4239](https://doi.org/10.1103/PhysRevD.50.R4239)
53. C. Balazs, J.W. Qiu, C.P. Yuan, Phys. Lett. B **355**, 548 (1995). doi:[10.1016/0370-2693\(95\)00726-2](https://doi.org/10.1016/0370-2693(95)00726-2)
54. C. Balazs, C. Yuan, Phys. Rev. D **56**, 5558 (1997). doi:[10.1103/PhysRevD.56.5558](https://doi.org/10.1103/PhysRevD.56.5558)
55. K. Hamilton, P. Nason, E. Re, G. Zanderighi, JHEP **1310**, 222 (2013). doi:[10.1007/JHEP10\(2013\)222](https://doi.org/10.1007/JHEP10(2013)222)
56. S. Höche, Y. Li, S. Prestel, Phys. Rev. D **90**(5), 054011 (2014). doi:[10.1103/PhysRevD.90.054011](https://doi.org/10.1103/PhysRevD.90.054011)
57. L. Loennblad, S. Prestel, JHEP **1303**, 166 (2013). doi:[10.1007/JHEP03\(2013\)166](https://doi.org/10.1007/JHEP03(2013)166)
58. S. Alioli, C.W. Bauer, C. Berggren, F.J. Tackmann, J.R. Walsh, Phys. Rev. D **92**(9), 094020 (2015). doi:[10.1103/PhysRevD.92.094020](https://doi.org/10.1103/PhysRevD.92.094020)
59. M. Chiesa, G. Montagna, L. Barze, M. Moretti, O. Nicrosini et al., Phys. Rev. Lett. **111**(12), 121801 (2013). doi:[10.1103/PhysRevLett.111.121801](https://doi.org/10.1103/PhysRevLett.111.121801)

60. K. Mishra, L. Barzè, T. Becher, M. Chiesa, S. Dittmaier et al., Electroweak Corrections at High Energies (2013). [arXiv:1308.1430](https://arxiv.org/abs/1308.1430)
61. D.R. Yennie, S. Frautschi, H. Suura, *Ann. Phys. (NY)* **13**, 379 (1961)
62. M. Consoli, W. Hollik, F. Jegerlehner, in *In *Geneva 1989, Proceedings, Z physics at LEP I, vol. 1* 7-54 and CERN Geneva - TH. 5527 (89,rec.Nov.) 51 p* (1989)
63. M. Consoli, W. Hollik, F. Jegerlehner, *Phys. Lett. B* **227**, 167 (1989). doi:[10.1016/0370-2693\(89\)91301-4](https://doi.org/10.1016/0370-2693(89)91301-4)
64. R. Barbieri, M. Beccaria, P. Ciafaloni, G. Curci, A. Vicere, *Phys. Lett. B* **288**(95), 1992 (1993). doi:[10.1016/0370-2693\(92\)91960-H](https://doi.org/10.1016/0370-2693(92)91960-H) [Erratum: *Phys. Lett. B* **312**, 511]
65. R. Barbieri, M. Beccaria, P. Ciafaloni, G. Curci, A. Vicere, *Nucl. Phys. B* **409**, 105 (1993). doi:[10.1016/0550-3213\(93\)90448-X](https://doi.org/10.1016/0550-3213(93)90448-X)
66. J. Fleischer, O.V. Tarasov, F. Jegerlehner, *Phys. Lett. B* **319**, 249 (1993). doi:[10.1016/0370-2693\(93\)90810-5](https://doi.org/10.1016/0370-2693(93)90810-5)
67. J. Fleischer, O.V. Tarasov, F. Jegerlehner, *Phys. Rev. D* **51**, 3820 (1995). doi:[10.1103/PhysRevD.51.3820](https://doi.org/10.1103/PhysRevD.51.3820)
68. A. Djouadi, C. Verzegnassi, *Phys. Lett. B* **195**, 265 (1987). doi:[10.1016/0370-2693\(87\)91206-8](https://doi.org/10.1016/0370-2693(87)91206-8)
69. A. Djouadi, *Nuovo Cim. A* **100**, 357 (1988). doi:[10.1007/BF02812964](https://doi.org/10.1007/BF02812964)
70. D.Yu. Bardin et al., in *Workshop Group on Precision Calculations for the Z Resonance (2nd Meeting Held Mar 31, 3rd Meeting Held Jun 13) Geneva, Switzerland, January 14, 1994* (1997), pp. 7–162
71. W.F.L. Hollik, *Fortschr. Phys.* **38**, 165 (1990). doi:[10.1002/prop.2190380302](https://doi.org/10.1002/prop.2190380302)
72. G. Altarelli, R. Kleiss, C. Verzegnassi (eds.) in *Z Physics at LEP-1. Proceedings, Workshop, Geneva, Switzerland, September 4–5, 1989. Vol. 1: Standard Physics* (1989)
73. G. Degrassi, A. Sirlin, *Nucl. Phys. B* **352**, 342 (1991). doi:[10.1016/0550-3213\(91\)90446-5](https://doi.org/10.1016/0550-3213(91)90446-5)
74. G. Degrassi, A. Vicini, *Phys. Rev. D* **69**, 073007 (2004). doi:[10.1103/PhysRevD.69.073007](https://doi.org/10.1103/PhysRevD.69.073007)
75. C.M. Carloni Calame, M. Chiesa, H. Martinez, G. Montagna, O. Nicrosini, F. Piccinini, A. Vicini, *Precision Measurement of the W-Boson Mass: Theoretical Contributions and Uncertainties* (2016)
76. A. Mück, L. Oymanns, Resonance-improved parton-shower matching for the Drell–Yan process including electroweak corrections (2016)
77. A. Kotikov, J.H. Kuhn, O. Veretin, *Nucl. Phys. B* **788**, 47 (2008). doi:[10.1016/j.nuclphysb.2007.07.018](https://doi.org/10.1016/j.nuclphysb.2007.07.018)
78. R. Bonciani, *PoS EPS-HEP2011*, 365 (2011)
79. W.B. Kilgore, C. Sturm, *Phys. Rev. D* **85**, 033005 (2012). doi:[10.1103/PhysRevD.85.033005](https://doi.org/10.1103/PhysRevD.85.033005)
80. R. Bonciani, S. Di Vita, P. Mastrolia, U. Schubert, *JHEP* **09**, 091 (2016). doi:[10.1007/JHEP09\(2016\)091](https://doi.org/10.1007/JHEP09(2016)091)
81. R. Bonciani, F. Buccioni, R. Mondini, A. Vicini, *Eur. Phys. J. C* **77**(3), 187 (2017). doi:[10.1140/epjc/s10052-017-4728-6](https://doi.org/10.1140/epjc/s10052-017-4728-6)
82. A. Czarnecki, J.H. Kuhn, *Phys. Rev. Lett.* **77**, 3955 (1996). doi:[10.1103/PhysRevLett.77.3955](https://doi.org/10.1103/PhysRevLett.77.3955)
83. D. Kara, *Nucl. Phys. B* **877**, 683 (2013). doi:[10.1016/j.nuclphysb.2013.10.024](https://doi.org/10.1016/j.nuclphysb.2013.10.024)
84. A. Denner, S. Dittmaier, T. Kasprzik, A. Mueck, *Eur. Phys. J. C* **73**(2), 2297 (2013). doi:[10.1140/epjc/s10052-013-2297-x](https://doi.org/10.1140/epjc/s10052-013-2297-x)
85. S. Dittmaier, A. Huss, C. Schwinn, *Nucl. Phys. B* **885**, 318 (2014). doi:[10.1016/j.nuclphysb.2014.05.027](https://doi.org/10.1016/j.nuclphysb.2014.05.027)
86. S. Dittmaier, A. Huss, C. Schwinn, *PoS LL2014*, 045 (2014)
87. S. Dittmaier, A. Huss, C. Schwinn, *Nucl. Phys. B* **904**, 216 (2016). doi:[10.1016/j.nuclphysb.2016.01.006](https://doi.org/10.1016/j.nuclphysb.2016.01.006)
88. M. Schönherr, F. Krauss, *JHEP* **12**, 018 (2008). doi:[10.1088/1126-6708/2008/12/018](https://doi.org/10.1088/1126-6708/2008/12/018)
89. T. Sjöstrand, S. Ask, J.R. Christiansen, R. Corke, N. Desai, P. Ilten, S. Mrenna, S. Prestel, C.O. Rasmussen, P.Z. Skands, *Comput. Phys. Commun.* **191**, 159 (2015). doi:[10.1016/j.cpc.2015.01.024](https://doi.org/10.1016/j.cpc.2015.01.024)
90. S. Kallweit, J.M. Lindert, P. Maierhöfer, S. Pozzorini, M. Schönherr, *JHEP* **04**, 021 (2016). doi:[10.1007/JHEP04\(2016\)021](https://doi.org/10.1007/JHEP04(2016)021)
91. S. Kallweit, J.M. Lindert, P. Maierhöfer, S. Pozzorini, M. Schönherr, *JHEP* **04**, 012 (2015). doi:[10.1007/JHEP04\(2015\)012](https://doi.org/10.1007/JHEP04(2015)012)
92. F. Cascioli, P. Maierhofer, S. Pozzorini, *Phys. Rev. Lett.* **108**, 111601 (2012). doi:[10.1103/PhysRevLett.108.111601](https://doi.org/10.1103/PhysRevLett.108.111601)
93. E. Bagnaschi, R.V. Harlander, H. Mantler, A. Vicini, M. Wiesemann, *JHEP* **01**, 090 (2016). doi:[10.1007/JHEP01\(2016\)090](https://doi.org/10.1007/JHEP01(2016)090)
94. S. Alioli, P. Nason, C. Oleari, E. Re, *JHEP* **06**, 043 (2010). doi:[10.1007/JHEP06\(2010\)043](https://doi.org/10.1007/JHEP06(2010)043)
95. W. Astill, W. Bizon, E. Re, G. Zanderighi, *JHEP* **06**, 154 (2016). doi:[10.1007/JHEP06\(2016\)154](https://doi.org/10.1007/JHEP06(2016)154)
96. R. Gavin, Y. Li, F. Petriello, S. Quackenbush, *Comput. Phys. Commun.* **182**, 2388 (2011). doi:[10.1016/j.cpc.2011.06.008](https://doi.org/10.1016/j.cpc.2011.06.008)
97. E. Barberio, B. van Eijk, Z. Was, *Comput. Phys. Commun.* **66**, 115 (1991). doi:[10.1016/0010-4655\(91\)90012-A](https://doi.org/10.1016/0010-4655(91)90012-A)
98. E. Barberio, Z. Was, *Comput. Phys. Commun.* **79**, 291 (1994). doi:[10.1016/0010-4655\(94\)90074-4](https://doi.org/10.1016/0010-4655(94)90074-4)
99. P. Golonka, Z. Was, *Eur. Phys. J. C* **50**, 53 (2007). doi:[10.1140/epjc/s10052-006-0205-3](https://doi.org/10.1140/epjc/s10052-006-0205-3)
100. V.M. Abazov et al., *Phys. Rev. Lett.* **108**, 151804 (2012). doi:[10.1103/PhysRevLett.108.151804](https://doi.org/10.1103/PhysRevLett.108.151804)
101. T. Aaltonen et al., *Phys. Rev. Lett.* **108**, 151803 (2012). doi:[10.1103/PhysRevLett.108.151803](https://doi.org/10.1103/PhysRevLett.108.151803)
102. M. Dobbs, J.B. Hansen, *Comput. Phys. Commun.* **134**, 41 (2001). doi:[10.1016/S0010-4655\(00\)00189-2](https://doi.org/10.1016/S0010-4655(00)00189-2)
103. G. Nanava, Q. Xu, Z. Was, *Eur. Phys. J. C* **70**, 673 (2010). doi:[10.1140/epjc/s10052-010-1454-8](https://doi.org/10.1140/epjc/s10052-010-1454-8)
104. N. Davidson, T. Przedzinski, Z. Was, *Comput. Phys. Commun.* **199**, 86 (2016). doi:[10.1016/j.cpc.2015.09.013](https://doi.org/10.1016/j.cpc.2015.09.013)
105. A.B. Arbuzov, R.R. Sadykov, Z. Was, *Eur. Phys. J. C* **73**(11), 2625 (2013). doi:[10.1140/epjc/s10052-013-2625-1](https://doi.org/10.1140/epjc/s10052-013-2625-1)
106. E. Richter-Was, *Z. Phys. C* **61**, 323 (1994). doi:[10.1007/BF01413112](https://doi.org/10.1007/BF01413112)
107. E. Richter-Was, *Z. Phys. C* **64**, 227 (1994). doi:[10.1007/BF01557394](https://doi.org/10.1007/BF01557394)
108. T.K.O. Doan, W. Placzek, Z. Was, *Phys. Lett. B* **725**, 92 (2013). doi:[10.1016/j.physletb.2013.06.038](https://doi.org/10.1016/j.physletb.2013.06.038)
109. S. Jadach, B.F.L. Ward, Z. Was, *Phys. Rev. D* **88**(11), 114022 (2013). doi:[10.1103/PhysRevD.88.114022](https://doi.org/10.1103/PhysRevD.88.114022)
110. S. Frixione, Z. Kunszt, A. Signer, *Nucl. Phys. B* **467**, 399 (1996). doi:[10.1016/0550-3213\(96\)00110-1](https://doi.org/10.1016/0550-3213(96)00110-1)
111. A. Denner, S. Dittmaier, M. Roth, L. Wieders, *Nucl. Phys. B* **724**, 247 (2005). doi:[10.1016/j.nuclphysb.2011.09.001](https://doi.org/10.1016/j.nuclphysb.2011.09.001). doi:[10.1016/j.nuclphysb.2005.06.033](https://doi.org/10.1016/j.nuclphysb.2005.06.033)
112. A. Denner, S. Dittmaier, *Nucl. Phys. Proc. Suppl.* **160**, 22 (2006). doi:[10.1016/j.nuclphysbps.2006.09.025](https://doi.org/10.1016/j.nuclphysbps.2006.09.025)
113. A. Andonov, A. Arbuzov, D. Bardin, S. Bondarenko, P. Christova, L. Kalinovskaya, G. Nanava, W. von Schlippe, *Comput. Phys. Commun.* **174**(481), 2006 (2007). doi:[10.1016/j.cpc.2005.12.006](https://doi.org/10.1016/j.cpc.2005.12.006) [Erratum: *Comput. Phys. Commun.* **177**, 623. doi:[10.1016/j.cpc.2007.06.010](https://doi.org/10.1016/j.cpc.2007.06.010)]
114. D. Bardin, S. Bondarenko, L. Kalinovskaya, G. Nanava, L. Rummyantsev, W. von Schlippe, *Comput. Phys. Commun.* **177**, 738 (2007). doi:[10.1016/j.cpc.2007.06.006](https://doi.org/10.1016/j.cpc.2007.06.006)
115. D. Bardin, S. Bondarenko, L. Kalinovskaya, V. Kolesnikov, W. von Schlippe, *Eur. Phys. J. C* **71**, 1533 (2011). doi:[10.1140/epjc/s10052-010-1533-x](https://doi.org/10.1140/epjc/s10052-010-1533-x)
116. D. Bardin, S. Bondarenko, P. Christova, L. Kalinovskaya, V. Kolesnikov, W. von Schlippe, K. Yordanova, K. Yordanova, *Phys. Part. Nucl. Lett.* **9**, 472 (2012). doi:[10.1134/S1547477112060040](https://doi.org/10.1134/S1547477112060040)
117. A. Andonov, A. Arbuzov, D. Bardin, S. Bondarenko, P. Christova, L. Kalinovskaya, V. Kolesnikov, R. Sadykov, *Comput. Phys. Commun.* **181**, 305 (2010). doi:[10.1016/j.cpc.2009.10.004](https://doi.org/10.1016/j.cpc.2009.10.004)

118. DYu. Bardin, G. Passarino, *The Standard Model in the Making: Precision Study of the Electroweak Interactions* (Clarendon Press, Oxford, 1999)
119. D. Bardin, S. Bondarenko, P. Christova, L. Kalinovskaya, L. Romyantsev, A. Sapronov, W. von Schlippe, *JETP Lett.* **96**, 285 (2012). doi:[10.1134/S002136401217002X](https://doi.org/10.1134/S002136401217002X)
120. S.G. Bondarenko, A.A. Sapronov, *Comput. Phys. Commun.* **184**, 2343 (2013). doi:[10.1016/j.cpc.2013.05.010](https://doi.org/10.1016/j.cpc.2013.05.010)
121. K.P.O. Diener, S. Dittmaier, W. Hollik, *Phys. Rev. D* **72**, 093002 (2005). doi:[10.1103/PhysRevD.72.093002](https://doi.org/10.1103/PhysRevD.72.093002)
122. G. Degrossi, P. Gambino, A. Sirlin, *Phys. Lett. B* **394**, 188 (1997). doi:[10.1016/S0370-2693\(96\)01677-2](https://doi.org/10.1016/S0370-2693(96)01677-2)
123. J.A.M. Vermaseren, New features of FORM (2000). [arXiv:math-ph/0010025](https://arxiv.org/abs/math-ph/0010025)
124. A. Arbuzov, D. Bardin, S. Bondarenko, P. Christova, L. Kalinovskaya, G. Nanava, R. Sadykov, W. von Schlippe, *Eur. Phys. J. C* **51**, 585 (2007). doi:[10.1140/epjc/s10052-007-0327-2](https://doi.org/10.1140/epjc/s10052-007-0327-2)
125. A. Andonov, A. Arbuzov, S. Bondarenko, P. Christova, V. Kolesnikov, G. Nanava, R. Sadykov, *Phys. Atom. Nucl.* **73**, 1761 (2010). doi:[10.1134/S106377881010011X](https://doi.org/10.1134/S106377881010011X)
126. T. Hahn, M. Perez-Victoria, *Comput. Phys. Commun.* **118**, 153 (1999). doi:[10.1016/S0010-4655\(98\)00173-8](https://doi.org/10.1016/S0010-4655(98)00173-8)
127. D. Bardin, L. Kalinovskaya, V. Kolesnikov, W. von Schlippe, *Phys. Atom. Nucl.* **73**, 2048 (2010). doi:[10.1134/S1063778810120100](https://doi.org/10.1134/S1063778810120100)
128. S. Jadach, P. Sawicki, *Comput. Phys. Commun.* **177**, 441 (2007). doi:[10.1016/j.cpc.2007.02.112](https://doi.org/10.1016/j.cpc.2007.02.112)
129. T. Hahn, *Comput. Phys. Commun.* **168**, 78 (2005). doi:[10.1016/j.cpc.2005.01.010](https://doi.org/10.1016/j.cpc.2005.01.010)
130. J.M. Campbell, R. Ellis, *Nucl. Phys. Proc. Suppl.* **205–206**, 10 (2010). doi:[10.1016/j.nuclphysbps.2010.08.011](https://doi.org/10.1016/j.nuclphysbps.2010.08.011)
131. A. Arbuzov, D. Bardin, S. Bondarenko, P. Christova, L. Kalinovskaya, U. Klein, V. Kolesnikov, L. Romyantsev, R. Sadykov, A. Sapronov, *JETP Lett.* **103**(2), 131 (2016). doi:[10.1134/S0021364016020041](https://doi.org/10.1134/S0021364016020041)
132. S. Bremsing, S. Dittmaier, M. Kramer, A. Mueck, *Phys. Rev. D* **77**, 073006 (2008). doi:[10.1103/PhysRevD.77.073006](https://doi.org/10.1103/PhysRevD.77.073006)
133. D. Bardin, S. Bondarenko, S. Jadach, L. Kalinovskaya, W. Placzek, *Acta Phys. Pol. B* **40**, 75 (2009)
134. S. Jadach, W. Placzek, S. Sapeta, A. Siodmok, M. Skrzypek, *JHEP* **10**, 052 (2015). doi:[10.1007/JHEP10\(2015\)052](https://doi.org/10.1007/JHEP10(2015)052)
135. M.W. Krasny, F. Fayette, W. Placzek, A. Siodmok, *Eur. Phys. J. C* **51**, 607 (2007). doi:[10.1140/epjc/s10052-007-0321-8](https://doi.org/10.1140/epjc/s10052-007-0321-8)
136. F. Fayette, M.W. Krasny, W. Placzek, A. Siodmok, *Eur. Phys. J. C* **63**, 33 (2009). doi:[10.1140/epjc/s10052-009-1084-1](https://doi.org/10.1140/epjc/s10052-009-1084-1)
137. M.W. Krasny, F. Dydak, F. Fayette, W. Placzek, A. Siodmok, *Eur. Phys. J. C* **69**, 379 (2010). doi:[10.1140/epjc/s10052-010-1417-0](https://doi.org/10.1140/epjc/s10052-010-1417-0)
138. M.W. Krasny, W. Placzek, *Acta Phys. Pol. B* **43**, 1981 (2012). doi:[10.5506/APhysPolB.43.1981](https://doi.org/10.5506/APhysPolB.43.1981)
139. M.W. Krasny, S. Jadach, W. Placzek, *Eur. Phys. J. C* **44**, 333 (2005). doi:[10.1140/epjc/s2005-02398-2](https://doi.org/10.1140/epjc/s2005-02398-2)
140. C. Carloni Calame, S. Jadach, G. Montagna, O. Nicrosini, W. Placzek, *Acta Phys. Pol. B* **35**, 1643 (2004)
141. M.W. Krasny, W. Placzek, *Acta Phys. Pol. B* **45**(1), 71 (2014). doi:[10.5506/APhysPolB.45.71](https://doi.org/10.5506/APhysPolB.45.71)
142. M.W. Krasny, W. Placzek, *Acta Phys. Pol. B* **47**, 4 (2016)
143. M.W. Krasny, S. Jadach, W. Placzek, *Eur. Phys. J. C* **76**(4), 194 (2016). doi:[10.1140/epjc/s10052-016-4031-y](https://doi.org/10.1140/epjc/s10052-016-4031-y)
144. K. Sobol, *Acta Phys. Pol. B* **42**, 1605 (2011). doi:[10.5506/APhysPolB.42.1605](https://doi.org/10.5506/APhysPolB.42.1605)
145. S. Jadach, A. Kusina, W. Placzek, M. Skrzypek, M. Slawinska, *Phys. Rev. D* **87**(3), 034029 (2013). doi:[10.1103/PhysRevD.87.034029](https://doi.org/10.1103/PhysRevD.87.034029)
146. S. Jadach, M. Jezabek, A. Kusina, W. Placzek, M. Skrzypek, *Acta Phys. Pol. B* **43**, 2067 (2012). doi:[10.5506/APhysPolB.43.2067](https://doi.org/10.5506/APhysPolB.43.2067)
147. H. Baer, J. Ohnemus, J.F. Owens, *Phys. Rev. D* **42**, 61 (1990). doi:[10.1103/PhysRevD.42.61](https://doi.org/10.1103/PhysRevD.42.61)
148. B.W. Harris, J.F. Owens, *Phys. Rev. D* **65**, 094032 (2002). doi:[10.1103/PhysRevD.65.094032](https://doi.org/10.1103/PhysRevD.65.094032)
149. A. De Rujula, R. Petronzio, A. Savoy-Navarro, *Nucl. Phys. B* **154**, 394 (1979). doi:[10.1016/0550-3213\(79\)90039-7](https://doi.org/10.1016/0550-3213(79)90039-7)
150. W.A. Bardeen, A.J. Buras, D.W. Duke, T. Muta, *Phys. Rev. D* **18**, 3998 (1978). doi:[10.1103/PhysRevD.18.3998](https://doi.org/10.1103/PhysRevD.18.3998)